ALGOMA STEEL

The Algoma Steel Corporation, Limited
Sault Ste. Marie
Ontario, Canada
P6A 5P2

EVALUATION OF WELD ZONE CORROSION OF SHIPBUILDING STEEL PLATES FOR USE IN THE ARCTIC ENVIRONMENT

by

V.S. Donepudi, S. Santyr, L. Malik,
(AMCA International Limited)

A. Garner,
(Pulp and Paper Research Institute of Canada)

M. McLean,
(Algoma Steel Corporation, Limited)

Work on this Project was conducted under the auspices of the Canada Centre for Mineral and Energy Technology; Energy, Mines and Resources, Canada. Funding for this project was provided as a result of an Unsolicited Proposal.

DSS FILE NUMBER: 05SQ. 23440-4-9256
DSS CONTRACT SERIAL NUMBER: 1SQ84-00334
CANMET SCIENTIFIC AUTHORITY: R. BRIGHAM
JANUARY 1987

133 pp

MICROMEDIA

EXECUTIVE SUMMARY

When coatings on the hulls of ships operating in Arctic waters are abraded away, preferential corrosion in the weld zone is encountered. The objective of the program has been to assess the effects of base plate and weld metal chemistries, and weld heat input on the incidence of such weld zone corrosion using short term testing methods.

In successfully meeting the objectives of this contract, a comprehensive overview of weld zone corrosion with steels, welding consumables and welding practices relevant to North America, and particularly Canada, has been achieved. Data has been obtained on steels which varied from 235 to 515 MPa yield strength with particular emphasis on steels in the 350 MPa range (EH36 equivalent) with chemistry modifications for enhanced low temperature toughness. The commercial welding consumables with varying Cu and Ni contents which were chosen for this study have exhibited a meaningful range of corrosion properties in combination with the steels. The relative merits of selected electrochemical testing procedures have been demonstrated and when these data are combined with the complementary free corrosion data being performed at CANMET, a strategy for future weld-zone corrosion studies will be available.

Eleven different steels with varying Mn levels (0.54 to 1.45%) and alloying elements (Cu, Ni, Cr, V, Nb), along with four SMAW electrodes and four SAW wire/flux combinations were employed in the program. Each base plate/welding consumable combination was investigated at two heat input levels - 1.2 and 2.5 kJ/mm for SMAW and 2.5 and 4.0 kJ/mm for SAW.

Two types of accelerated electrochemical corrosion tests, namely galvanostatic anodic dissolution and potentiostatic anodic polarization tests were performed.

The galvanostatic anodic dissolution tests in 3.5% NaCl were performed on 172 butt welded specimens and 33 Noren weld hardening bars, the latter simulating the heat affected zones. The corrosion assessments were made by visual observations, depth profiling and macrophotography.

Potentiostatic anodic polarization tests in 3.5% NaCl were performed for the base steels, Gleeble simulated heat affected zones, undiluted weld metals and selected dilute weld metals. Current densities at -500 mV vs S.C.E. were used to rank various base steels, heat affected zones and weld metals. The results of these three tests have been used to predict the incidence of preferential HAZ or WM attack for each of the combinations examined.

The key findings include:

1. Increasing Mn levels in base plate above 1.1% increases susceptibility to HAZ preferential corrosion. Higher heat inputs may raise this limit to about 1.25% Mn.

   The presence of Ni and Cu in weld metal increases its resistance to preferential corrosion.

2. In heat affected zone, the coarse grained region is preferentially attacked to a greater extent than other regions of the HAZ.

3. In low C steels containing significant amounts of microalloying elements in conjunction with higher Mn levels, the subcritical region of the HAZ is attacked to almost the same extent as the coarse grained region. There was no relationship between preferential heat affected zone attack and carbon equivalent or hardness.

4. There was some evidence in the weld metal of preferential attack of the refined portion of the weld metal. The effect was most prevalent in C-Mn consumables with little or no alloying.

SOMMAIRE

L'objectif du programme a été évaluer, au contexte canadien, les effets des chimie du métal de base, de l'électrode et de l'énergie de soudage sur l'incidence de l'attaque corrosive du joint de soudure.

Le programme compris d'onze aciers avec un niveau de Mn divers (et les autre élements comme Cu, Ni, Cr, V, Nb) quatre électrodes enrobée et quatre combinaisons électrodes/flux à l'arc submergé. Chaque combinaison à été etudie à deux niveaux d'énergie; 1,7 et 2,5 kJ/mm pour l'arc manuel avec électrode enrobée, 2,5 et 4,0 kJ/mm pour l'arc submergé. Les aciers et les électrodes ont été choisi pour deux raisons. Ils ont donné un rang de l'attaque corrosive du joint de soudure et quelques combinaisons sont utilisées par l'industrie maritime canadienne.

Deux types d'épreuve électrochimique ont été completé. La première, l'épreuve de dissolution galvanostatique anodique dans une solution de 3,5% NaCl a été fait avec 172 spécimens de soudure bout à bout et 33 'Noren Weld Hardening Bars' qui a simulé la zone affecté de la chaleur (HAZ). L'évaluation de la corrosion, a été fait par observations visuel, mesurage du profil et la macrophotographie.

L'autre essai a été l'épreuve de polarization potentiostatique anodique dans une solution de 3,5% NaCl. Il a été fait pour les métaux de base, les zone affecté de la chaleur par simulation 'Gleeble' et le métal de soudure (dilué et non dilué). La densité de courant a -500 mV vs S.C.E. a été utilisé pour

classer les matériaux. Les résultats de ces épreuves ont été utilisé pour prédire l'incidence de corrosion de la HAZ ou le métal de soudure.

Les conclusions principales son comme tel:

1. L'augmentation de Mn ou métal de base plus qu'environ 1,1% augmente la susceptibilité de corrosion préférentiel de la HAZ. L'addition de Cu ou Ni ou l'augmentation de la chaleur de soudage monte la limite de Mn a environ 1,25%. L'addition de Ni et Cu au métal de soudure améliore sa résistance a la corrosion préférentiel.

2. La région à gros grain de la HAZ est plus susceptible à la corrosion préférentiel que les autres régions de la HAZ. Pour les acier avec un niveau significatif des éléments de microalliage et un niveau élevé de Mn, il n'y a pas de différence de corrosion entre la région à gros grain et la région subcritique.

3. Il n'y a pas de correlation entre la corrosion préférentiel de la HAZ et l'équivalent carbone ou la dureté de la HAZ.

TABLE OF CONTENTS

	Page
EXECUTIVE SUMMARY	
SOMMAIRE	
LIST OF TABLES	
LIST OF FIGURES	
INTRODUCTION	1
1.1 Summary of Corrosion Tests	3
OBJECTIVE	7
EXPERIMENTAL - MATERIALS AND METHODS	8
3.1 Materials	8
3.1.1 Steels	8
3.1.2 Consumables	9
3.1.3 Metallography of As-received Steels and Consumables	10
3.2 Fabrication of Tank Test Specimens	11
3.3 Fabrication of Butt Weld Specimens	11
3.4 Fabrication of Noren Weld Hardening (NWH) Bars	12
3.5 Fabrication of Gleeble-Cycled Specimens	13
3.6 Fabrication of Undilute Weld Specimens	13
3.7 Fabrication of Dilute Weld Specimens	14
3.8 Description of Anodic Dissolution Tests: NWH Bars and Butt Welds	14
3.9 Potentiostatic Anodic Polarization Tests	16
RESULTS AND OBSERVATIONS	19
4.1 Anodic Dissolution of Butt Welded Steels	19
4.1.1. Profilometry	19
4.1.2 Metallography of Butt-Welded Specimens	21
4.2 Anodic Dissolution of NWH Bars	22
4.2.1 Relative Corrosion Rates	22
4.2.2 Metallography of NWH Bar Specimens	22
4.3 Potentiostatic Anodic Polarization Tests	24
4.3.1 Base Materials	24
4.3.2 Simulated Heat Affected Zones - Gleeble Cycled Steels	25
4.3.3 Undilute and Dilute Weld Metals	26

TABLE OF CONTENTS...continued

	Page
DISCUSSION	29
SUMMARY AND CONCLUSIONS	33
ACKNOWLEDGEMENTS	37
REFERENCES	38

APPENDIX I

Table I Depth of Weld Metal Attack
Table II Depth of HAZ Attack

APPENDIX II

Optical macrographs of the as-corroded transverse sections of previously machined ends of butt weld specimens after anodic dissolution.

APPENDIX III

Regression analyses of current ratio data

A. Justification, method of regression analyses and results.

B. Table showing current ratios, ΔMn, ΔSi, ΔCr, ΔCu, and ΔNi values at low and high heat inputs.

C. Regression analyses plots - current ratio vs ΔMn, ΔSi, ΔCu, ΔNi and ΔCr at low and high heat inputs (two figures).

LIST OF TABLES

Table No.	Title
1	Chemical composition of base plate materials from Mill Test reports.
2	Chemical composition of weld metals.
3	Welding parameters
4	Current density data at -500 mV for shipbuilding grade steel plates and their corresponding simulated heat affected zones produced by Gleeble cycling.
5	Current density values for weld metal electrodes at -500 mV.
6	Current density values for dilute weld metals at -500 mV.
7.	Current ratios for various steels, consumables, and heat affected zones.
8	Heat affected zone or weld metal attack: predictions from potentiostatic data and comparison with butt weld corrosion assessments.

LIST OF FIGURES

Figure No.	Title
1	As-received microstructures of base plate steels and as-deposited weld metals.
2	Trapezoid tank test specimen.
3	Butt weld anodic dissolution test specimen.
4	Set up used for preparation of NWH bars.
5	The test cell showing a butt weld anode (left) and stainless steel cathode (right) with its polyethylene cathode compartment.
6	Two test cells on the left before the test and on the right during test, when copious ferrous and ferric corrosion products clouded the anolyte.
7	Twenty-two test cells in series with associated power supplies.
8	Composite representation of various test samples representing parent metal-weldment combination.
9	The test locations and specimen configuration.
10	A view of Model 351-1 EGG-PAR corrosion monitoring system, together with corrosion cell that was used for electrochemical tests.
11	Preferential attack of weld metal as judged by the depth-of-attack.
12	Preferential heat affected zone attack as judged by the depth of attack.
13	Photomicrograph of Stelco 350 WT butt weld specimen G41 (welded with OK 73.08 at 1.2 kJ/mm heat input) after anodic dissolution.
14	Photomicrograph of butt weld specimen G52 (Stelco 350 WT welded with L60/761 at 4.0 kJ/mm) after anodic dissolution test.

LIST OF FIGURES...continued

Figure No.	Title
15	Relative corrosion rate of NWH bar heat affected zones increased with manganese content and were higher at lower heat inputs.
16	NWH bar specimens for each base plate after anodic dissolution tests.
17	Microstructure of NWH bar for steel CR after anodic dissolution tests.
18	Microstructure of NWH bar for steel E after anodic dissolution tests.
19	Microstructure of NWH bar for steel K after anodic dissolution tests.
20	Microstructure of NWH bars for steel F after anodic dissolution tests.
21	Non-uniform attack of NWH bar for steel K (low heat input) after anodic dissolution test.
22a	Potentiostatic polarization curves of steels E, K, and F in 3.5% NaCl solution. Transverse cross sections were tested.
22b	Potentiostatic polarization curves of steels D, A, C, L and G in 3.5% NaCl solution. Transverse cross sections were tested.
23	Current densities at -500 mV vs. base plate manganese content. The current densities were measured at rolling planes, i.e., side surfaces of specimens.
24	Current densities at -500 mV vs. base plate manganese content. The current densities were measured at the cross-sectional surfaces.
25	Current densities of Gleeble simulated HAZ's at -500 mV vs % Mn in corresponding base plate steels. Heat inputs : o - 1.2 and Δ - 4.0 kJ/mm.
26	Current densities at -500 mV vs hardness of Gleeble simulated heat affected zones. Heat input 1.2 kJ/mm.

LIST OF FIGURES...continued

Figure No.	Title
27	Current densities at -500 mV vs hardness of Gleeble simulated heat affected zones. Heat input 4.0 kJ/mm.
28	Potentiostatic anodic polarization curves for SMAW (Shielded Metal Arc Welding) consumables deposited at 1.2 kJ/mm.
29	Potentiostatic anodic polarization curves for SMAW consumables deposited at 2.5 kJ/mm.
30	Potentiostatic anodic polarization curves for SAW consumables deposited at 2.5 kJ/mm.
31	Potentiostatic anodic polarization curves for SMAW consumables deposited at 4.0 kJ/mm.
32	Current density at -500 mV vs %Cu+Ni plots for SMAW consumables.
33	Current density at -500 mV vs %Cu+Ni plots for SAW consumables.

INTRODUCTION

The marine industry has long been confronted with the problem of hull corrosion in ships operating in icy seawater saturated with dissolved oxygen (approximately 20 p.p.m. at 0°C). The problem is accentuated when ice and abrasive particulates scrape the protective coatings or knock off the sacrificial anodes that are installed to afford cathodic protection to the hulls.

Under these circumstances, the preferential corrosion of the weld zone can be a severe problem. Finnish researchers have conducted extensive investigations to provide solutions to this problem[1-6] and have summarized their achievements in a recent paper[7]. A summary of these studies, together with a need for a corrosion testing program in Canada was provided in a review article by Gilmour[8]. Finnish researchers have primarily worked with high strength steels of up to 350 MPa yield strength and 490 MPa UTS. Recently, Japanese researchers have reported on weld zone corrosion studies of high strength (590 MPa minimum yield) steels containing varying alloying elements, such as manganese, copper, nickel, chromium, vanadium, niobium and molybdenum[9].

The early observation of corrosion in ice-breaking ships indicated that the preferential corrosion of the weld metal was the main problem. It was attributed primarily to the anodic nature of the weld metal relative to the parent plate in the Arctic environment. To minimize the relative anodicity of weld metal, ESAB, a Scandinavian electrode producer, developed an electrode which was alloyed with Cu and Ni to make it noble with respect to most

shipbuilding steels (OK 73.08 with nominally 0.6% Cu and 0.4% Ni, in weld deposit).

The use of a noble electrode, although quite successful in eliminating preferential weld metal corrosion transferred the problem to the heat-affected zone. Two types of corrosion attack have been reported as occuring in the heat-affected zone area; general corrosion of the heat-affected zone, and a knife line type of attack along the fusion boundary. The former has been attributed to the presence of low temperature transformation products as well as retained austenite. The occurrence of these phases depended on the parent steel composition and the weld heat input. Finnish researchers have reported that high heat inputs and parent steel with manganese content less than about 1% were found to reduce heat-affected zone corrosion. Lower carbon contents were marginally beneficial whereas the casting practice (ingot vs. continuous) was believed to be of little consequence. Further, a parent steel silicon content of 0.2% minimum had been suggested to reduce the weld metal corrosion rate.

The knife line type of fusion boundary attack has been related to the formation of low melting point sulfides in the heat-affected zone. In steels containing low sulfur and/or treated with calcium, zirconium, titanium, this is not a significant problem.

According to the recent empirical suggestions in Inoue et al's work[9] , it appears that the differences in base plate and weld metal nickel and copper compositions might also have some influence on the relative corrosion rate of heat affected zone and weld metal.

1.1 Summary of Corrosion Tests

The weld zone corrosion tests that have been done to date can be classified into the following two main categories:

i) free corrosion tests

ii) electrochemical tests

Belonging to the category of free corrosion tests are ESAB's tank test developed by Valanti[1] and the duct test[2]. In the tank test, weld bead on plate-type specimens are attached to a wheel that rotates continuously in a tank containing synthetic seawater. This has proven to reproduce the type of corrosion found on the hulls of ice breaking ships. However, this test must be run for a minimum of three months to identify the corrosion effects.

In the duct test, weld bead on plate-type specimens are laid at the bottom of a duct such that one surface is in contact with running seawater while all other surfaces are protected. Corrosion is very uneven in this type of test, but results correlate well with those obtained in the tank test. This test also requires at least three months of exposure time for meaningful results to be obtained.

Belonging to the category of electrochemical tests are the following:

i) electrochemical potential measurements;

ii) acquisition of full range polarization curves either by changing potential or current;

iii) constant current or constant potential tests.

The electrochemical potential measurements on a weld specimen will reveal the potential differences, if any, between different locations of the weldment, thus reflecting the relative corrosion rates of various regions of the weldment. The potentials of different locations can be measured by selective masking, or by moving the reference electrode probe over the weld surface. Unless the differences are significant, it is difficult to predict the areas of selective weld zone corrosion. This technique has been used to a limited extent.[10-12]

Potentiodynamic polarization curves[13] have been measured on samples from various areas in the weldment, however, the usefulness of this technique is restricted to regimes where there is no overlap or cross-over of the curves. Anodic potentials of -550mV or greater, were used by Strommen[13] to overcome this problem of "cross-over" in the polarization curves.

When the usefulness of anodic polarization curves is limited to one or two potentials only, comparable information can be obtained with constant potential or constant current anodic polarization tests at some selected currents corresponding to those potentials that simulate the surface condition of corroding weldment under field conditions. Raty, Hakala and Miekk-oja[3] performed current ratio tests, using a potential divider circuit to manipulate the current ratios of balancing arms of a four-electrode cell such that the two anodes, one of which was standard, were polarized to the same potential, viz., -500 or -550 mV vs S.C.E. in simulated seawater. The current ratios and their trends with various experimental variables (steel or weld metal composition, welding parameters, solutions) were used to evaluate the corrosion characteristics of the weldments. Later the potential divider system was

replaced by a potentiostat - using a conventional three electrode system where the solution oxygen level could be simulated by the level of applied potential. In several papers,[2-7] descriptions of the tests on the weldments or simulated heat affected zones at -500 and -550mV are given, but the results are not reported as a function of applied potential.

There is another electrochemical test, the anodic dissolution test, in which the test weldments are subjected to a small applied current, to polarize the anode to approximately -500 mV vs S.C.E. The tests are usually carried out in aerated 3% sodium chloride solutions for approximately 15 days. After the test, any region of preferential attack can be easily identified either visually and/or or with the aid of a profilometer.

The following summarizes the comparisons between the tank tests, anodic dissolution tests at constant current and potentiostatic polarization tests:

Tank Test	Anodic Dissolution Test	Potentiostatic Test
Closer to ship operating conditions; time consuming; test condition under oxygen diffusion control*	Accelerated - several specimens can be tested in two weeks; galvanostatic control is electrochemically similar to oxygen diffusion control*	Accelerated test (duration <1 hr/test); single specimen can be tested each time; test condition under activation control**; sensitive to surface preparation.

* transport of corrosive reactants and reaction products determine the corrosion rate.
**transport of electrons from and to the metal, determine the corrosion rate.

As outlined in the proposal to the Federal Government[14], various corrosion tests were undertaken to evaluate the heat affected zone and weld metal corrosion resistance of several steels (various compositions, both of Canadian

and offshore origins) in combination with shielded metal arc and submerged arc welding consumables. Potentiostatic tests were carried out on parent metals, simulated heat affected zones obtained by Gleeble cycling, "undilute" and "dilute" weld metal deposits. Comparative anodic dissolution tests were carried out on butt weld seams and the heat affected zones that were obtained by the Noren weld hardening procedure. Although not a part of this program, companion trapezoids for some of these steels and consumable combinations were provided to Dr. Brigham (CANMET) for tank tests.

OBJECTIVE

The objective of this program was to evaluate the relative corrosion resistance of the heat-affected zone and weld metal in shipbuilding steel plates as a function of:

(a) chemical compositions of the parent steels and weld metals, and

(b) weld heat input.

Specifically, the evaluation of the corrosion performance of the selected steels was to be studied using short term tests. The use of these short term tests, if shown to be reproducible and related to the tank test results, would allow any steel/consumable combination to be quickly and reliably evaluated as to its relative resistance to weld zone corrosion.

EXPERIMENTAL - MATERIALS AND METHODS

3.1 Materials

3.1.1 Steels

Eleven steels were examined in the program. These steels were predominantly of Canadian origin, with the exception of one American (ASTM A710 Gr A, Cl 3), one Japanese (Kawasaki EH36) and one Belgian (Shoralsim 355Z) steel.

These steels represent a wide range of chemical compositions and processing routes (Table 1). Steels A, D and K are essentially low strength (260-300 MPa minimum yield strength) C-Mn steels, typical of those which, in the past, have been traditionally used in ship and icebreaker fabrication. The Mn content of this group of steels is less than 1.1%.

Steels C, F, G, H, J and L are all microalloyed with varying amounts of niobium, vanadium or titanium, and represent a more recent generation of steels that possesses excellent notch toughness (equal to or better than EH grade requirements in ABS, DnV and Lloyds specifications) at 350 MPa minimum yield strength level. Two of these steels, F and G, were produced under 50/50 cost shared programs between the Federal Government, and Algoma Steel Co. and Stelco Inc., respectively. In general, these trial steels were designed to have excellent toughness at

low temperature and have higher Mn content (1.24 to 1.45%). They also contain small amounts of Ni and/or Cu.

Steel E (A710) having the lowest Mn content, and greatest amount of alloying elements, has been used for naval ships in the U.S., and steel B (350AT), containing Cu, Ni and Cr has improved resistance to atmospheric corrosion.

3.1.2 Consumables

Eight welding consumables, selected on the basis of expected deposit chemistry and toughness, were evaluated in the program. Four of the consumables were submerged arc welding wire/flux combinations and the other four were shielded metal arc welding electrodes. The undiluted weld metal deposit chemistries are shown in Table 2.

The ESAB OK 73.08 SMAW electrode was chosen because it was developed specifically for weld metal corrosion resistance. E8018-W, a North American weathering grade electrode, like the ESAB electrode gives a deposit alloyed with Cu and Ni. E7018-1 was chosen as a typical electrode which is presently used in shipbuilding applications and E8018-C1 was chosen for its high nickel content (2.15%).

Similarly the L60/761 SAW combination was chosen as a typical C-Mn consumable which is used in shipbuilding applications. Tibor 22/OP121TT was chosen on the basis of its good toughness properties at high heat

inputs which make it a candidate for use in shipbuilding applications. Thyssen S2-Ni 1/UV420TTR and SD2-3Ni/OP121TT also have excellent toughness properties resulting from varying levels of nickel.

3.1.3 Metallography of As-Received Steels and Consumables

Limited metallography was carried out in order to characterize the microstructures of the base steels and weld deposits resulting from differences in composition and in the case of steels, from processing routes.

Some typical baseplate and weld deposit microstructures are shown in Figure 1. Baseplate microstructures typically show ferrite and pearlite phases, with ferritic grain size depending on rolling history (as rolled, normalized, etc.) with the exception of A710 which is quenched and precipitation hardened yielding a fine equiaxed ferrite structure, with a uniform distribution of carbides.

The weld metals in general show columnar grains with grain boundary ferrite and intragranular acicular ferrite. The high nickel electrodes produce weld metals containing more "ferrite with non-aligned second phase (FS)".

3.2 Fabrication of Tank Test Specimens

Tank test specimens shown in Figure 2 were made by saw cutting trapezoids from each of the chosen base steels. Subsequent to cutting, two parallel grooves were machined for bead placement. For SAW welding, both grooves were 8mm deep for 2.5 and 4.0 kJ/mm welds, while for SMAW electrodes, one groove was 5mm deep and the other was 8mm deep for 1.2 and 2.5 kJ/mm welds, respectively. Welding parameters,selected through a series of procedure optimization trials, are listed in Table 3. Subsequent to welding, the trapezoids were sandblasted and then the narrow half of each trapezoid plate was machined flat. The completed trapezoids were delivered to CANMET/PMRL for tank testing.

3.3 Fabrication of Butt Weld Specimens

Anodic dissolution specimens were prepared by filling V-groove joints, using each combination of steel, consumable and heat input. Specimens for welding were 200 mm wide x 150 mm in length (i.e., 100mm wide for each half) to allow adequate material to be held in the jig grips as well as to allow for run on and run off weld material which was subsequently removed.

The welds were one-sided with a backing pass. Once welded, specimens 50mm x 150 mm x thickness (25mm max.) were sawcut from each weld. Again, specimens were sandblasted and then 25mm of the top face was machined flat as shown in Figure 3.

3.4 Fabrication of Noren Weld Hardening (NWH) Bars

NWH bars were prepared to simulate heat affected zone structures at various heat inputs. Three cylindrical specimens 10mm diameter x 150mm long, were machined from each base plate steel with the long axis parallel to the rolling direction. Three heat inputs (1.5, 2.5 and 4.0 kJ/mm) were simulated for each of the eleven steels in the following manner.

The specimens were individually heated at one end using a medium frequency induction coil, while the other end was immersed in water. An asbestos pad was placed between the coil and the water surface in order to avoid short circuiting due to boiling of the water near the surface. The "F" distance, as indicated in the schematic shown in Figure 4, was set at 10mm, 30mm and 50mm to simulate 1.5, 2.5 and 4.0 kJ/mm respectively. These values of F were determined by interpolating between the heat input equivalent (HIE) and corresponding F values reported by Saarinen and Onnela[2]. HIE values were calculated as follows:

$$HIE = \frac{60.I.V.}{v.k.\sqrt{d}}$$

where,

HIE: heat input equivalent (J/cm mm ½)
I: current (amps)
V: voltage (volts)
v: travel speed (cm/min)
d: plate thickness (mm)
k: shape coefficient

After heating in this manner, the specimens were smoothed using 600 grit SiC paper to remove any surface imperfections, such as scale, which might interfere with corrosion testing.

The completed specimens were tested using the galvanostatic anodic dissolution procedure.

3.5 Fabrication of Gleeble-Cycled Specimens

Heat affected zones were also simulated for potentiostatic anodic polarization tests using the computer controlled Gleeble 5000 unit at PMRL, CANMET. Specimens 10mm x 10mm x 80mm were machined from each steel with the rolling direction parallel to the 80 mm length. The heating and cooling cycles required to simulate each of the three heat inputs, (1.2, 2.5 and 4.0 kJ/mm), were determined by measuring the cooling curves for bead on plate welds. The time to cool from 800-500°C was measured for 1.2 and 2.5 kJ/mm welds deposited using SMAW electrodes (4.7s and 11.4s, respectively) and 2.5 and 4.0 kJ/mm welds deposited using SAW electrodes (24.0s and 65.0s, respectively). A peak temperature of 1350°C was used.

3.6 Fabrication of Undilute Weld Specimens

Undilute weld metal specimens were prepared for each electrode/heat input combination for potentiostatic polarization tests. These were obtained by building up a pad (approximately 20mm) of weld metal above the plate surface. A 10mm x 10mm x 50mm bar was removed from the top portion of the weld metal

pad. Two heat inputs were used; 1.2 and 2.5 kJ/mm for SMAW consumables, and, 2.5 and 4.0 kJ/mm for SAW consumables.

3.7 Fabrication of Dilute Weld Metal Specimens

Dilute weld metal specimens were prepared for the selected steel/heat input/weld metal combinations shown in Table 6.

These were made by depositing a two layer pad of weld metal onto the selected steels. After etching to establish the fusion line, the specimen was removed so that the first layer of the deposit could be examined in the potentiostatic test.

3.8 Anodic Dissolution Tests: NWH Bars and Butt Welds

NWH bars and butt weld specimens were corroded in galvanostatic tests to measure the relative susceptibility of weld metal and heat affected zone to preferential attack. Conditions were chosen so that important parameters such as chloride concentration and potential would be close to those which could exist under free-corrosion conditions in natural seawater. Galvanostatic testing was chosen because, of all the possible electrochemical test techniques, it closely approximates the cathodic-rate-controlled corrosion of a ship's carbon steel hull in oxygenated seawater.

Each of the 33 NWH bars (11 steels, 3 heat inputs) and 172 butt welds (11 steels, 8 consumables, each with 2 heat inputs, 4 samples not tested) were corroded at room temperature at a nominal current density of 0.88 mA/cm^2 for a period of 15 days. The solution for these tests was 8ℓ of distilled, deionized water containing 3.5% NaCl.

The tests were carried out in 10ℓ polypropylene containers, with intermixing of anolyte and catholyte prevented by a Saran membrane placed over the opening to the cathode compartment.

NWH bars were tested in a horizontal position with the heat affected end close to and below the membrane. Butt weld specimens were tested in a vertical position, held about 25mm off the bottom of the cell. The experimental set up is shown in Figures 5 and 6. Up to 15 cells were driven in series, with the test anode and cathode of adjacent cells connected by spot welded stainless steel wire (1.6mm 304L TIG welding wire, Figure 7).

Anolyte and catholyte pH was monitored daily, to ensure that the membrane was not leaking; anode, cathode and cell potentials were also monitored daily. Anolyte pH was in the range 6 to 8.5 units and anode potentials were generally in the range -600 to -560mV vs SCE, potentials typical of unprotected steel in seawater.

After the corrosion tests were completed, the anodes were carefully cleaned in inhibited HCl. Each anode was visually inspected and the severity and location of attack noted. Dimensional measurements were also taken: for NWH bars, bar diameters were determined to a precision of 25 μm with a vernier gauge, and for

the butt welds, corrosion depth profiles were traced perpendicular to the weld on an area which had been machined flat prior to testing. One location per sample was chosen for profilometry. A profilometer was used with a depth precision of ± 5 μm. Maximum depth of attack was also determined from enlarged photographs of the specimen ends (cross sectional view of the butt weld specimens). There was general agreement between the relative depth of attack assessed by these two approaches.

3.9 Potentiostatic Anodic Polarization Tests

In these tests, a sample that is representative of a given location of the weld zone is briefly polarized at a constant anodic potential (>15 minutes) and the current densities noted. The current densities are compared and expressed as current ratios in order to predict an incidence of heat affected zone or weld metal attack. The tested samples were classified into the following four categories:

1) parent metal steels
2) simulated heat affected zones - using Gleeble cycled specimens
3) undilute weld metal deposits at two different heat inputs
4) dilute weld metals

The specimens belonging to the categories were representative of the locations of a single weldment as shown in Figure 8.

Initially, the mid-length transverse cross-sections of all the Gleeble specimens were tested (Figure 9a). These results were reviewed, and further tests were performed on the rolling planes of the specimens in view of possible end-grain effects on the measured currents at a given potential. The specimen configuration is shown in Figure 9.

The samples were polished to 1 micron diamond and then ultrasonically cleaned in acetone. Masking with electroplaters' lacquer resulted in exposed areas of approximately 0.25 cm^2 for testing.

In a typical test, the polished specimen was pickled in 50% HCl at room temperature for 1 minute. Then the electrode was immersed in 3.5% NaCl solution which had been deaerated by bubbling with N_2 for 30 minutes. Potentials were then recorded for a period of 30 minutes. Polarization was done at room temperature using the following programme:

(i) held at -1.0V for 1 min. to reduce any previously formed film while the electrode was left on open circuit;

(ii) potential stepped from -1.0V to -0.6V;

(iii) potential increased from -0.6V to -0.45V in 50mV steps; at each applied potential, currents recorded and noted for a maximum of 15 minutes or until steady-state currents, were achieved;

(iv) every test was duplicated or triplicated as necessary.

The sample and solutions were contained in a 1000 ml EGG & PAR all-glass corrosion test vessel which had provisions for gas bubbling, counter, reference and working electrodes. A high density carbon and a saturated calomel electrode were used as counter and reference electrodes, respectively. As shown in Figure 10, the electrochemical test equipment was comprised of a microprocessor controlled PAR 351-1 potentiostat system including multivoltmeters for application, measurement and recording of potential and current.

All the potentials are measured and reported to saturated calomel electrode scale. The measured currents are expressed as milliamperes/sq. centimetre ($mA\text{-}cm^{-2}$) throughout the report. As was reported in the preliminary report[15], this test procedure gave current values that were reproducible to ± 10% of the average value.

RESULTS AND OBSERVATIONS

4.1 Anodic Dissolution of Butt Welded Steels

4.1.1 Profilometry

The maximum depth of attack, as measured by the profilometer, (Appendix I, Tables I & II) was used to classify the severity of attack of weld metal, and separately for heat affected zones. An as-measured depth-of-attack of 300 μm or more was taken as severe. It represents a corrosion rate equivalent to penetration of one-inch plate in three to four years. As-measured depths of 150 μm or less were judged not to be preferential attack. Measurements between these two depths were interpreted as slight preferential attack. All profilometric measurements were confirmed by visual assessments, and by estimates obtained from enlarged photographs of the as-corroded transverse-section of the previously machined end of the butt-welds, as shown in Figure 1 Appendix II.

Weld metal assessments are shown in Figure 11. It can be seen that E7018-1 and L60/761 weld metals were particularly susceptible to attack. Note that these weld deposits had no intentional additions of copper or nickel. In contrast, weld metals containing the greatest amounts of nickel (SD2-3Ni/OP121TT, E8018-C1) suffered no preferential attack. The remaining deposits also performed well, although it should be noted that the S2-Ni1/UV420TTR deposit was superior to the E8018-W deposit, even

though the former is leaner in Ni and Cu. This may be partially explained by different effective heat inputs (SAW vs SMAW).

Further, the Tibor 22/OP121TT performed well inspite of its negligible Ni content. Additional testing and analysis would be necessary to establish how the differences in chemistry (low Si and Mn, presence of Mo and Cu) from the other consumables influenced its performance.

Heat-affected-zone (HAZ) assessments are shown in Figure 12. As found by previous workers, preferential HAZ attack was more prevalent at lower heat inputs and higher manganese levels. This mode of attack was almost universally found in those steels with a nominal manganese content of 1.4%. Steels with less than 1% Mn showed no HAZ attack, and those with 1.0 to 1.2% Mn showed a slight propensity for HAZ corrosion at lower heat inputs. Although both welding processes have the same nominal heat inputs at 2.5 kJ/mm, because of arc efficiency, the actual heat input of the SMAW process is less than that of the SAW process. It was generally observed that the severe corrosion of the welds deposited using E7018-1 and L60/761, was associated with a lower tendency for preferential HAZ corrosion. Conversely, more noble weld metals (containing Ni) seemed to increase propensity for HAZ corrosion.

Fusion line corrosion, as reported by Rasanen and Relander[5], was found difficult to distinguish from general HAZ attack.

4.1.2 Metallography of Butt-welded Specimens

A number of butt-weld specimens were selected for metallographic examination on the basis of the anodic dissolution test results and profilometry measurements.

Based on this limited work, the only consistent observation was that the coarse-grained supercritical region of the HAZ seemed to be attacked more aggressively than other regions of the HAZ, such as the fine grained supercritical, intercritical and subcritical regions. One interesting anomaly was noted in the more highly micro-alloyed steels such as Algoma's LT60, and Stelco's 350 WT. In these specimens the subcritical region of the HAZ was a second region of particularly aggressive attack. This effect is shown in Figure 13.

Some of the weld metal deposits also showed preferential attack. The fine-grained reheated region of weld metal seemed to be more aggressively attacked than the as-deposited columnar regions. This was particularly true for the C-Mn electrodes with low alloy content. This effect is shown in Figure 14.

The relationship between specific microstructural constitutents such as martensite, ferrite with aligned second phase, or grain boundary ferrite, and extent of corrosion attack, was not clearly defined in this program. Although there did not appear to be any direct relationship between these constituents and preferential corrosion, more extensive analysis would be required to verify this.

4.2 Anodic Dissolution of NWH Bars

4.2.1 Relative Corrosion Rates

The relative corrosion rate of NWH bar HAZ's was determined by taking a ratio of the as-corroded base metal diameter to that of the HAZ measured 1mm above the A_1 - temperature zone. The approach to assess the relative corrosion rates employed here is the same as that used by Saarinen and Onnela[2].

When plotted against manganese content, it can be seen that heat-affected-zones corrode more readily at low heat inputs and higher manganese contents (Figure 15). It appears that for heat inputs equivalent to 2.5 kJ/mm and 4.0 kJ/mm, steels with Mn around 1.4% are particularly susceptible.

At a heat input of 1.5 kJ/mm, even with higher relative corrosion rates, a similar dramatic increase in susceptibility was found between 1.24% Mn and 1.39% Mn.

4.2.2 Metallography of NWH Bar Specimens

Close inspection of the tested NWH bars (Figure 16a through k) shows that in most steels with Mn >1.0% for 1.5 kJ/mm and with Mn ≅1.4% for 2.5 and 4.0 kJ/mm, a distinct shoulder occurred at the transition from HAZ to baseplate structures.

The minimum diameter generally occurred in what appeared to be the coarse grain supercritical region of the HAZ.

A second reduction in diameter was noted at the shoulder for steel F and particularly for steel G. This appeared to correspond to the subcritical region of the HAZ.

In order to verify which regions of the HAZ were most aggressively attacked, steels E, CR, F and K were sectioned and polished for further examination.

In each case the coarse grain supercritical region of the HAZ, was verified to be the region of greatest attack.

The attack in the subcritical region of the HAZ was verified for steel F although not to as great an extent as in the butt-weld specimens. The microstructures of the regions of most severe attack, i.e. the coarse grained HAZ for steels CR, E and K and both the coarse-grained and subcritical region of the HAZ for steel F, are shown in Figures 17 through 21. These figures also show the effects of heat input on the HAZ microstructures for these steels.

Some specimens (such as steels K and G) appeared to have more severe parent metal attack than others. This effect can be seen in the macrophotos shown in Figure 16. Steel K also showed deeper, non-uniform corrosive attack both in the HAZ (see Figure 21) as well as in base plate.

4.3 Potentiostatic Anodic Polarization Tests

The free corrosion potentials of all the steels examined and their corresponding simulated heat affected zones produced by Gleeble cycling, as well as weld metals, were measured prior to polarization. The potentials for all steels were in the -0.63 to -0.68V range, indicating that a high degree of deaeration had been achieved. The potentials of Gleeble cycled specimens and weld metals were also within this range.

Initially, attempts were made to develop complete anodic potentiostatic polarization curves using the potential programme already described. In the first few tests, the polarization curves for cross-sections of base materials E (A710), F (LT60) and K (A36) exhibited no crossover through the range of applied potentials, as shown in Figure 22a, and conformed to the following rankings in terms of corrosion resistance: A710 > LT 60 > A36.

However, with testing of the other base steels, there was a cross-over of polarization curves, see Figure 22b. Ranking on the basis of relative positioning of the polarization curves was therefore not possible and hence, all further comparisons were made on the basis of current densities that were measured at -500mV.

4.3.1 Base Materials

The current densities for different base steels at -500mV are shown in Table 4 for both the rolling plane as well as transverse cross-sections

of the steels, see Figures 23 and 24. The current densities for cross-sections of "B" steel were erratic and hence are not included in Figure 24. In general, the higher current densities at cross-section faces can be attributed to the higher density of MnS inclusions at the end-grains of the cross-sections of steels.

4.3.2 Simulated Heat Affected Zones: Gleeble Cycled Steels

In this set of tests, the heat affected zones were simulated by subjecting the base plate steels to differing heat inputs by Gleeble cycling. It was anticipated that an increase in heat input would decrease the corrosion rate i.e., decrease in the measured current density at constant potential. The current densities measured on the faces of the cross-sections did change with heat input, however, the direction of change of current density with heat input was not the same for all the steels. With increasing heat input, the current densities of the heat affected zones decreased for steels "F", "H" and "J", increased for steels "E", "A", "C", "L" and "G", and remained constant for steels "D" and "K".

In order to avoid possible end grain effects, additional tests at this potential (-500mV) were also performed on the rolling planes of the specimens that were Gleeble cycled at 1.2 and 4.0 kJ/mm. The current density measurements from these additional tests are shown in Table 4, and it can be seen that for majority of the steels (9 out of 11), the

HAZ at the higher heat input has lower current density i.e. increased corrosion resistance, as anticipated.

Attempts were made to seek relationships between HAZ current densities (corrosion resistance) vs %Mn and hardness (Figures 25, 26, 27). The data in Figure 25 is not consistent with earlier observations on anodic butt welds that an increase in Mn content of steel tends to increase the HAZ corrosion susceptibility since no clear relationship is shown.

As far as the influence of HAZ hardness on corrosion resistance is concerned (Figures 26 and 27), there is no relationship apparent at 1.2 kJ/mm. However, at 4 kJ/mm, there may be a trend that higher hardness improves HAZ corrosion resistance. It should be noted, however, that additional testing would be necessary to confirm any relationship between HAZ hardness, corrosion resistance and chemistry.

4.3.3 Undilute and Dilute Weld Metals

The potentiostatic polarization curves for the undiluted SMAW and SAW consumables are shown in Figures 28-31. The current densities at -500 mV are shown in Table 5. A weld deposit with the polarization curve to the left or with lowest current density was judged as the one with better corrosion resistance. Thus at -500 mV, the consumables with increasing weld deposit corrosion resistance can be arranged as:

1. SMAW's - low heat input - E8018C-1 > E8018W > OK 73.08 > E7018-1
2. SMAW's - high heat input - E8018C-1 > E8018W > OK 73.08 = E7018-1
3. SAW's - low heat input - SD2-3Ni/OP121TT = S2Ni1/UV420TTR > Tibor 22/OP121TTR > L60/761
4. SAW's - high heat input - SD2-3Ni/OP121TT > S2Ni1/UV420TTR = Tibor 22/OP121TT > L60/761.

However, it must be noted that as the applied potential shifts from -500 mV to -550 mV there may be some crossover with the polarization curves. As a result, the chemistry with the least resistance at -500 mV may be more resistant than other chemistries at -550 mV.

The current densities at -500mV, which were usually in the 2.5-15 mA/cm^2 range, are plotted as a function of (Ni+Cu) content of weld metal (Figures 32 and 33) and these figures indicate that Ni and Cu in weld metal improve its corrosion resistance. It should be added that if the data were plotted against Ni only, the same conclusions would be obtained.

The current densities for dilute weld metal zone were measured for selected "dilute" welds (Table 6). The base plates and consumables employed for these welds are also shown in Table 6. The heat inputs for welds were 2.5 kJ/mm and 4.0 kJ/mm for SMAW and SAW deposits, respectively. It was anticipated that the weld metal characteristics could be altered because of dilution from base plate. The dilution effects with SMAW-E8018W consumable are easily understood, at least

qualitatively, as dilution from leaner base steels (K,D,A) leads to reduction in weld metal corrosion resistance, and from richer base steel (E) leads to further improvements in corrosion resistance.

The results with SAW Tibor 22/OP121TT are not so easily explainable at first glance. However, it should be noted that greatest improvement in corrosion resistance occurred with K steel - the only semi killed (low Si) steel in the program. One could therefore infer that the unexpectedly good corrosion resistance of this weld deposit in butt weld anodic dissolution test was due to its low Si content rather than particular Mn, Cu or Mo contents.

DISCUSSION

The intent of this program has been to aid the development of reliable base plate, consumable and welding procedure combinations that are optimal to a reliable operation of ice-breaking ships in hostile environments such as ice infested Arctic seawaters. An attempt to define the susceptible combinations has been made by choosing two different accelerated electrochemical test procedures, i.e., galvanostatic anodic dissolution tests (for Butt Welds and NWH bars), and potentiostatic anodic polarization tests (current density measurements) for parent metals, Gleeble cycled heat affected zones, and weld metals, and comparing the results obtained by the two procedures. The results of these accelerated tests and field experience must be compared to the results of the tank testing ongoing at CANMET to establish their usefulness in predicting weld zone corrosion.

In the anodic dissolution test, it was possible to identify the particular location of weld zone that was more susceptible to corrosion. A comparable potentiostatic test would be to potentiostatically dissolve the entire weldment, assess the attack locations and correlate the potentiostatic dissolution and anodic dissolution observations. Since the potentiostatic tests in this study were conducted on base plates, HAZ's and weld metals separately, an attempt has been made to predict the preferential corrosion site for a given steel-weld metal combination by calculating appropriate current ratios. These are then compared with the observations in anodic dissolution tests. If it was found that the tank test results were modelled by the potentiostatic test, then it may be possible to develop empirical relationships

between current ratios, (i.e., susceptibility to preferential weld metal or HAZ corrosion) vs chemical compositional differences between base plates and weld metals. Such an approach, to design steel and weld deposit chemistries such that different regions of the weldment have matching corrosion resistance, and preferential corrosion is minimized, is demonstrated in Appendix III. It must be noted, however, that a relationship between the tank tests, anodic dissolution and potentiostatic test must be established.

The current densities at -500mV for parent metals, Gleeble cycled heat affected zones, and various consumables are shown in Tables 4 - 6. These current densities can be converted to current ratios and these form the basis for predictions of the incidence of weld metal or heat affected zone or base plate preferential attack.

The current ratios for various base-plate-consumable and heat affected zone combinations are shown in Table 7. For given steel and consumable combinations two different current ratios, R, were calculated. These are $R_{HAZ/WM}$ and $R_{HAZ/BP}$, described by:

i) $$R_{HAZ/WM} = \frac{(\text{Current density of coarse grain HAZ})_x}{(\text{Current density of weld deposit})_x} \quad (1)$$

and

ii) $$R_{HAZ/BP} = \frac{(\text{Current density of coarse grain HAZ})_x}{(\text{Current density of Base Plate})_x} \quad (2)$$

Where subscript x denotes the heat input at which the current densities are selected for ratio calculations.

The calculations are illustrated by the following example for E steel in combination with OK 73.08 at a heat input of 1.2 kJ/mm. Taking into account equation (1) $R_{HAZ/WM}$ can be calculated as 0.48 ($R_{HAZ/WM} = \frac{4.5\ mA/cm^2}{9.3\ mA/cm^2}$).

From equation (2) $R_{HAZ/BP}$ can be calculated as 1.88 ($R_{HAZ/BP} = \frac{4.5}{2.7}$).

From these ratios one could infer that in the weld zone, weld metal will be preferentially attacked with respect to the HAZ whereas with respect to the base plate the heat-affected zone would suffer preferential attack. A direct comparison of the absolute current densities for base plate E (2.7 mA/cm^2), heat affected zone (4.5 mA/cm^2) and weld metal (9.3 mA/cm^2) readily shows the weld metal (OK 73.08) to be the most susceptible to corrosion and the base plate to be the least susceptible.

In Table 7, it can be seen that the current ratios for all combinations except those involving SD2-3Ni weld metal covered the extremes of severe weld metal attack, ($R_{HAZ/WM} = 0.18$) to severe heat affected zone attack ($R_{HAZ/WM} = 2.8$). Since the current density for SD2-3Ni weld metal is given as a range, a single current ratio value could not be computed. Instead, a range for current ratio is shown, and where this led to ambiguity in predicting preferential corrosion site, a blank is shown in Table 8.

In principle, therefore, it is possible to predict the heat affected zone or weld metal attack using the following criteria:

i) $R_{HAZ/WM}$ >1 - HAZ attack

ii) $R_{HAZ/WM}$ <1 - weld metal attack

iii) slight attack when the ratios are 1 ±0.1

The predictions, based on current ratio calculations, are summarized in Table 8, together with the assessments from anodic dissolution experiments on butt-welded samples for comparison. By comparing the number of predictions based on current ratios that agreed with the anodic dissolution assessments, the agreement between the predictions and assessment is approximately 70%. The reasons for any disagreement between the test results was not identified. The authors understand that additional work will be done by CANMET to compare the results of this contract with the results obtained from the CANMET tank test program. Since the tank test has been recognized as simulating operating conditions, it will be necessary to compare results before any statement regarding the validity of the short term tests can be made.

SUMMARY AND CONCLUSIONS

In successfully meeting the objective of this contract, a comprehensive overview of weld zone corrosion with steels, welding consumables and welding practices relevant to North America, and particularly Canada, has been achieved. Data have been obtained on steels which varied from 235 to 515 MPa range (EH36 equivalent) with chemistry modifications for enhanced low temperature toughness. The commercial welding consumables, with varying Cu and Ni values, which were chosen for this study have exhibited a meaningful range of corrosion properties in combination with the steels. The relative merits of selected electrochemical testing procedures have been demonstrated and when these data are combined with the complementary free corrosion data being performed at CANMET, a strategy for future weld-zone corrosion studies will be available.

Specifically, anodic dissolution tests, under galvanostatic (applied constant current) conditions, were performed on 172 Butt Weld specimens and 33 NWH bars that were individually exposed to 3.5% NaCl solutions containing dissolved air (open to atmosphere), under stagnant conditions, at room temperature for 15 days. The butt welds were done in a variety of steels (11 in all), with varying Mn levels (0.54 - 1.45% range) and alloying additions such as Cu, Ni, Cr, Mo, V, Nb, Ti. They were made using four SMAW electrodes (E7018-1, OK73.08, E8018-C1, E8018W) and four SAW wire/flux combinations (L60/761, SD2-3Ni/OP121TT, Tibor 22/OP121TT and S2-Ni1/UV420TTR at low (1.2 kJ/mm for SMAW, 2.5 kJ/mm for SAW) and high (2.5 kJ/mm for SMAW, 4.0 kJ/mm for SAW) heat input levels. The NWH bars tested, included the same 11 steels at three heat

input equivalents corresponding to 1.2, 2.5 and 4.0 kJ/mm. After testing, the samples were cleaned, and visually and metallographically examined. As well, corrosion depth profiling was carried out by profilometry for butt weld specimens.

Potentiostatic tests were performed on the same parent metals and weld metals as well as heat affected zones produced by Gleeble cycling. The test solution was the same as that used in anodic dissolution test, but was N_2-bubbled and stirred. Potentiostatic, anodic polarization curves (-1.0V - 1 min, -600 to -400mV @ 50mV step/15 min) were developed for the parent plates and weld metals. The current density data at -500mV vs S.C.E. were used to rank parent metals and weld metals and to assess the effects of heat input. Current ratios were calculated and the predictions of weld metal or heat affected zone attack were made. These predictions were compared with Butt weld assessments.

Based on data collected from the short term tests conducted, it was possible to assess the corrosion performance of both the HAZ and weld metal.

1. Heat Affected Zone

i) The anodic dissolution testing demonstrated that the HAZ corrosion resistance decreased with an increase in manganese content in the parent plate and higher heat input. A careful selection of heat input and consumable would be necessary to minimize preferential HAZ corrosion for those steels containing more than 1% Mn. This selection process is even more important when the manganese content in the parent plate approaches 1.4%.

The measured current densities from the potentiostatic polarization tests confirmed the trend of increasing corrosion resistance (current density) with decreasing Mn content and higher heat inputs.

ii) Metallographic examination showed that in general, the coarse-grained heat affected zone is preferentially atacked to a greater extent than other regions of the heat affected zone. In addition, the subcritical region of the heat affected zone was attacked almost to the same extent as the coarse grained region in low carbon steels containing large amounts of micro-alloying elements.

iii) There was no relationship between preferential heat affected zone corrosion and either carbon equivalent or hardness.

2. Weld Metal

i) The corrosion rate of weld metal has been shown by means of anodic dissolution tests on butt welds and potentiostatic polarization experiments on undiluted and diluted weld deposits to vary with weld metal chemistry - particularly Ni or Ni and Cu in combination. The SMAW E7018-1 and the SAW L60/761 which are commonly used in ship construction are not intentionally alloyed with Cu and/or Ni and were found to be most prone to attack. On the other hand, E8018-C1 (2.15% Ni) and SD2-3Ni/OP121TT (2.79% Ni) showed no preferential weld metal attack. In general, other weld metals with intermediate chemistries were attacked at intermediate rates although some anomalies (e.g. Tibor 22) have been identified where

corrosion behaviour is the result of more subtle changes in chemistry. It should be noted, however, that the Scandinavian electrode ESAB OK73.08 (0.35% Cu, 0.55% Ni) is not unique in exhibiting enhanced weld metal corrosion resistance.

ii) The current densities of "dilute weld metal" specimens suggest that low Si in weld metal is also conducive to increased weld metal corrosion resistance.

iii) The limited metallography done indicated that there was some evidence in the weld metal of preferential attack of the refined portion of the weld metal. This effect was most prevalent in the C-Mn consumables (i.e. little or no alloying).

3. Correlation of Test Methods

From current ratio calculations, it was possible to predict the likely incidence of weld metal or heat affected zone attack. The variation of current ratios, R, from which the possible incidence of preferential corrosion in heat affected zone ($R > 1$) or weld metal ($R < 1$) could be predicted. The predictions were then compared to the results of the butt weld anodic dissolution testing although not totally comparable to the butt weld testing, there was agreement in approximately 70% of the tests.

ACKNOWLEDGEMENTS

We would like to gratefully thank the following:

1. Messrs. M. Chambers (AMCA) and A. Menard (PAPRICAN) for patiently performing numerous electrochemical - potentiostatic and galvanostatic experiments.

2. Dr. R.J. Brigham of CANMET for organizing corrosion depth profiles, chemical analyses and valuable comments throughout this program.

3. Dr. J. Bowker and Mr. M. Letts of CANMET for permitting the use of Gleeble cycling equipment and assistance.

4. Dr. K. Davies of CANMET for permitting use of induction coil equipment and assistance.

5. Mr. M.J. Pates and his workshop colleagues in timely fabrication of welded specimens.

6. Mr. A. Morgan for multiple linear regression analyses of the current ratio *vs* composition data.

7. Mrs. S. Jackson, D. Baker, F. Haakman, and D. Perrin for typing and processing of reports as well as related papers through this program.

8. D.S.S.; for 50% funding of this program through the unsolicited proposals program.

9. Algoma Steel Corp. Ltd. for providing six of the steels investigated and for 50% funding of this program.

10. Stelco Inc., Fabrique de Fer de Charleroi, and Burrard Yarrows Shipyard for providing additional steels investigated in the program.

REFERENCES

1. Valanti, V.O., "Uber Galvanische Korrosion von Schweissnahten au Geschwerssten Wasserfahrzeugen". Schiff und Haffen, H8, 1961, pp. 695-709.

2.. Saarinen, A. and Onnela, K. "A Method for Testing Corrodibility of Heat-Affected Zones in Steel". Corrosion Science, Vol. 10, 1970, pp. 809-815.

3. Raty, R., Hakala, J., and Miekk-oja, H.M., "Current Ratio Test and Its Application to the Examination of the Zone Corrosion Occurring in Welded High Strength Structural Steels when Used in Seawater". Jernkont. Ann. 154, 1970, pp. 397-411.

4. Relander, K. and Onnela, K., "Corrosion Behaviour of Heat-Affected Zones in Welded Ships", Jernkont. Ann. 154, 1970, pp. 173-180.

5. Rasanen, E., Relander, K., "Development of Shipbuilding Steel Plates for Use on Arctic Seas. Scand. J. Metallurgy 7, 1978, pp. 11-17.

6. Uusitalo, E., "Effect of Flow Rate on the Galvanic Corrosion of Low Carbon Steels in Sea Water", Corrosion, Vol.17, 1961, pp. 67t-70t.

7. Rasanen, E.O., "Steel Selection for Welded Structures with Particular Reference to Weld Corrosion". Paper No. 23.1 Presented at 23rd Annual CIM Conference of Metallurgists, Quebec City, August 19-22, 1984.

8. Gilmour, J.B., "The Corrosion of Welds in Ice Breaking Ships - A Review". Canmet Report 80-14E; Energy, Mines and Resources Canada; April 1980.

9. Inoue et al, "Local Corrosion of Welds of High Strength Steels in Seawater". Paper presented at Electrochemical Society Symposium on Corrosion and Applied Electrochemistry, Oct. 9-11 (1985).

10. Bradley, J.N., and Rowlands, J.C., "Corrosion of Unprotected and Painted Weldments in Seawater". British Welding Journal, 476-481 (1962).

11. Lundin, S., "Erfharungen bei Korrosion, sprufungen von Schweipnahten and verschiedenen Schiffbaustahlen in Seewasser". Schiff and Hafen, 24, No. 3, 185-195 (1972).

12. Steffens, H.D., "Corrosion Phenomena in Welded Joints of Structural Steel". Annual Assembly, International Institute of Welding, Israel (1975).

13. Strommen, R., "Determination of Localized Corrosion of Heat Affected Zones of High Tensile C-Mn Steels in Seawater". Annual Assembly, International Institute of Welding, Israel (1975).

REFERENCES...continued

14. McLean, M., "Evaluation of Weld Zone Corrosion of Shipbuilding Steel Plates for Use in the Arctic Environment". Project Proposal A.S.C. MR-84-1 Submitted to Supply and Services Canada by Algoma Steel Corporation.

15. V.S. Donepudi and S. Santyr, "Evaluation of the Corrosion of Welds in Shipbuilding Steel Plates for Use in the Arctic Environment" - Task 5 Progress Report - Report No. 7-184-119/1 (1985).

TABLE 1: CHEMICAL COMPOSITION OF BASEPLATE MATERIALS FROM MILL TEST REPORTS

Steel Code Designation	Condition	C	Mn	Si	P	S	Cu	Ni	Cr	Mo	V	Ti	Nb	Al
A(300W)	AR	.16	1.10	.19	.014	.012	.01	.01	.01	--	--	--	--	.033
B(350AT)	CR	.16	1.08	.32	.013	.006	.30	.57	.38	--	--	--	--	.051
C(350WT)	CR/TE	.10	1.24	.23	.012	.010	.05	.07	.04	.02	.044	--	.039	.051
D(260WT)	N	.16	1.01	.23	.023	.019	.01	.01	.02	.01	--	--	--	.042
E(A710 Gr.A,C13	PH	.06	.54	.29	.005	.005	1.20	.89	.70	.21	--	--	.037	--
F(Algoma LT60)	N	.12	1.39	.28	.017	.011	.15	.15	.17	--	.053	--	.041	.027
G(Stelco 350WT)	CR	.07	1.40	.29	.003	.004	--	.25	.25	--	.08	.012	.02	*
H(Stelco S)	CR	.15	1.40	.29	.009	.005	--	.27	--	--	.07	.011	--	*
J(EH36)	*	.15	1.45	.45	.016	.006	.14	.02	.01	--	.031	.001	--	.022
K(A36)	AR	.17	.75	.045	.013	.014	.03	.02	.02	.01	--	--	--	--
L(Shoralsim 355Z	N	.114	1.24	.417	.011	.005	.297	.164	.084	.024	--	--	.001	.030

AR = as-rolled; CR = controlled-rolled; TE = tellurium treated -0.006% TE;
N = normalized; PH = quenched precipitation hardened;
* - information not available.

TABLE 2: CHEMICAL COMPOSITION OF UNDILUTED WELD METALS (SPECTROCHEMICAL ANALYSIS)

	C	Mn	Si	P	S	Cu	Ni	Cr	Mo	V	Ti	Al	B
SMAW OK.73.08 (1.2kJ/mm)	.055	1.16	.37	.01	.010	.35	.55	.065	--	.030	.015	<.005	.0002
SMAW E7018-1 (1.2kJ/mm)	.050	1.40	.37	.01	.013	.035	.05	.04	--	.010	.012	<.005	.0002
SMAW E8018-C1 (1.2kJ/mm)	.035	0.81	.30	.008	.015	.026	2.15	.025	.007	.015	.012	<.005	.0002
SMAW E8018-W (1.2kJ/mm)	.040	.96	.38	.01	.012	.185	1.40	.245	<.025	.015	.014	<.005	.0002
SAW L60/761 (2.5kJ/mm)	.035	1.85	1.12	.025	.020	.065	.02	.045	--	<.005	.01	<.005	.0004
SAW SD2-3Ni/OP121TT (2.5kJ/mm)	.060	.95	.27	.01	.005	.085	2.79	.125	.11	.005	.005	.015	.0002
SAW Tibor 22/OP121TT (2.5kJ/mm)	.055	1.01	.17	.02	.005	.165	.06	.095	.24	.005	.01	.013	.0007
SAW Thyssen S2Ni1/ UV420TTR (2.5kJ/mm)	.085	1.16	.22	.013	.010	.065	1.23	.035	--	.010	.01	.015	.0002

TABLE 3: WELDING PARAMETERS

Desired Heat Input (kJ/mm)	Electrode Diameter (mm)	Current (Amps)	Voltage (Volts)	Travel Speed (mm/s)	Cooling Time (800-500°C)
1.2 (SMAW)	3.2	150	22	2.8	4.7
2.5 (SMAW)	4.0	230	27	2.5	11.3
2.5 (SAW)	4.0	600	32	7.7	24.0
4.0 (SAW)	4.0	650	32	5.2	65.6

TABLE 4

CURRENT DENSITY DATA AT -500mV FOR SHIPBUILDING GRADE STEEL PLATES AND THEIR CORRESPONDING SIMULATED HEAT AFFECTED ZONES PRODUCED BY GLEEBLE CYCLING

Tests in N_2-saturated, stirred 3.5% NaCl solutions at room temperature. The current densities against a given steel designation are expressed in mA/cm^{-2} *read from graphs; A - current densities at cross-sections; B - current densities at rolling planes.

Steel Designation and Code		Parent Metal		B-Gleeble Cycled Steels (Heat Input kJ/mm)			% Mn
		A	B	1.2	2.5*	4.0	
A-710	E	6.4	2.7	4.5	3.4	2.3	0.54
ASTM A-36	K	10.8	9.2	18.0	16.0	13.8	0.75
CSA G40.21 260T	D	12.0	7.7	7.0	8.9	11.0	1.01
CSA G40.21 350AT	B	2.5	7.5	7.5	6.6	6.0	1.08
CSA G40.21 300W	A	13.0	10.7	15.0	12.0	8.4	1.10
CSA G40.21 350WT	C	14.2	9.9	14.0	12.3	10.3	1.24
Shoralsim 355Z	L	6.2	6.9	12.5	11.4	10.1	1.24
Algoma LT60	F	11.1	6.4	11.5	10.2	8.7	1.39
Stelco 350WT	G	15.0	8.1	14.0	13.2	12.6	1.40
Stelco	H	12.1	12.8	18.0	15.5	12.1	1.40
Kawasaki EH36	J	11.6	10.9	12.0	12.4	13.2	1.45

TABLE 5

CURRENT DENSITY VALUES FOR WELD METAL ELECTRODES
AT -500 mV

Potentiostatic tests in N_2-bubbled, stirred, 3.5% sodium chloride solutions at room temperature. Ref. Figs. 28-31.

Heat Inputs: 1) SMAW Consumables - Low - 1.2 } kJ/mm
High - 2.5 }

2) SAW Consumables - Low - 2.5 } kJ/mm
High - 4.0 }

CONSUMABLE	Current Density/mA.cm^{-2}	
	Low Heat Input	High Heat Input
SMAW		
1. OK73.08	9.3	11.0
2. E7018-1	14.0	11.0
3. E8018-W	7.8	7.8
4. 8018-C1	6.4	6.6
SAW		
1. L60/761	15.0	14.8
2. SD2-3 Ni	2.7-8.9	2.8-8.5
3. Tibor 22/OP121TT	10.4	12.2
4. Thyssen S2Ni1/UV420TTR	6.7	12.7

TABLE 6

CURRENT DENSITIES FOR DILUTE WELD METALS AT -500 mV VS S.C.E.

Test conditions as in Table 4. Heat inputs for SMAW and SAW consumables, respectively, are 2.5 and 4.0 kJ/mm.

*Current densities (mA/cm^2) for undilute welds for comparison.

Steel Designation and code	SMAW E8018W 8.0*	SAW Tibor 22/OP121TT 10.4*
E (A710)	2	9
K (ASTM A-36)	12	8
D (CSA G40.21 260WT)	19	10
B (CSA G40.21 350AT)	7	12
A (CSA G40.21 300W)	16	-
C (CSA G40.21 300WT)	9	11
F (Algoma LT60)	9	10
G (Stelco 350WT)	Erratic	Erratic
J (Kawasaki EH 36)	7	11

TABLE 7

CURRENT RATIOS AT -500mV FOR HEAT AFFECTED ZONE
WELD METAL AND BASE PLATE COMBINATIONS

I = current density in mA/cm². Ratios are calculated from data in Tables 4 and 5.

$R_{HAZ/WM} = I_{HAZ}/I_{BP}$ $\qquad$ $R_{HAZ/BP} = \frac{I_{HAZ}}{I_{BP}}$

	SMAW								SAW										
STEEL DESIG-NATION	OK 73.08		E7018-1		E8018-C1		E8018-W		L60/761		SD2-3/Ni		TIBOR 22		THYSSEN		i_{HAZ}/i_{BP}		
	1.2	2.5	1.2	2.5	1.2	2.5	1.2	2.5	2.5	4.0	2.5	4.0	2.5	4.0	2.5	4.0	$\frac{i_{1.2}}{i_{B.P.}}$	$\frac{i_{2/5}}{i_{B.P.}}$	$\frac{i_{4.0}}{i_{B.P.}}$
E	0.48	0.31	0.32	0.31	0.70	0.52	0.58	0.44	0.23	0.16	1.2-0.42	0.82-0.27	0.33	0.19	0.51	0.18	1.88	1.26	1.26
K	1.93	1.45	1.29	1.45	2.81	2.40	2.31	2.05	1.10	0.93	5.9-1.88	4.90-1.62	1.54	1.13	2.40	1.09	2.00	1.73	1.50
D	0.73	0.81	0.50	0.81	1.09	1.35	0.90	1.14	0.60	0.74	3.3-1.0	3.92-1.29	1.16	0.90	1.33	0.87	1.70	1.42	0.90
B	0.81	0.60	0.54	0.60	1.17	1.00	0.96	0.85	0.44	0.41	2.44-0.74	2.14-0.33	0.63	0.49	0.99	0.47	1.00	0.88	0.73
A	1.61	1.10	1.07	1.10	2.34	1.82	1.92	1.54	1.20	0.57	4.44-1.34	3.11-0.99	1.15	0.69	1.79	0.66	1.40	1.12	0.79
C	1.51	1.12	1.00	1.12	2.19	1.86	1.78	1.58	0.82	0.70	4.63-1.38	3.68-1.21	1.18	0.84	1.84	0.81	1.40	1.24	1.03
L	1.34	1.04	0.89	1.04	1.95	1.73	1.54	1.46	0.74	0.68	4.11-1.25	3.61-1.19	1.07	0.83	1.66	0.80	1.80	1.65	1.46
F	1.24	0.93	0.82	0.93	1.80	1.55	1.47	1.31	0.68	0.59	3.78-1.15	3.11-1.02	0.98	0.71	1.52	0.69	1.80	1.59	1.36
G	1.51	1.20	1.00	1.20	2.19	2.00	1.79	1.69	0.88	0.85	4.89-1.48	4.5-1.48	1.27	1.03	1.97	1.00	1.73	1.63	1.64
H	1.94	1.41	1.29	1.41	2.81	2.35	2.31	1.99	1.03	0.82	5.74-1.74	4.32-1.42	1.49	0.99	2.31	0.95	1.40	1.21	0.95
J	1.34	1.13	0.86	1.13	1.88	1.88	1.54	1.59	0.83	0.93	4.59-1.39	4.93-1.62	1.19	1.13	1.85	1.09	1.31	1.18	1.21

TABLE 8

HEAT AFFECTED ZONE OR WELD METAL ATTACK
POTENTIOSTATIC PREDICTIONS AND BUTT WELD DATA

P = Predicted from current ratios $R_{HAZ/WM}$ (Table 5); A = From Butt Weld Anodic Dissolution Assessments
W = Weld Metal Attack; H = Heat Affected Zone Attack; BP = Base Plate Attack; S = Slight
The numerical values 1.2, 2.5 and 4.0 are heat inputs (kJ/mm).

		SMAW								SAW							
STEEL DESIG-NATION		OK 73.08		E7018-1		E8018-C1		E8018-W		L60/761		SD2-3/Ni		TIBOR 22		THYSSEN	
		1.2	2.5	1.2	2.5	1.2	2.5	1.2	2.5	2.5	4.0	2.5	4.0	2.5	4.0	2.5	4.0
E	P	<---------- W ---------->															
	A	W	W	W	W	SW	SH	SW	W	W	W	SH	SH	SW			
K	P	H	H	SH	H	H	H	H	H	SH	SW	H	H	H	SH	H	SH
	A	W	W	W	W	SH	SH/BP	SW	SW	W	W	SH/BP	SH/BP	SH/BP	SH/BP	SH/BP	SH/BP
D	P	W	W	W	W	SH	H	SW	SH	W	W	H/SH	H	SH	SW	H	SW
	A	SH	SH	W	W	H	H	BP/H	H	W	W	SH/BP	SH/BP	SH/BP	H/BP	H/BP	H/BP
B	P	SW	W	W	W	SH	-	SW	SW	W	W	-	-	SW	W	-	W
	A	SW	SW	W	W	SW	SW	SW	SW	W	W	H	H	H	H	SH/BP	SH/BP
A	P	H	SH	SH	SH	H	H	H	H	W	W	H	SH	SH	SW	H	W
	A	H	H	W	W	H	H	SH	SH	W	W	H/BP	H/BP	SH/BP	SH/BP	SH/BP	H/BP
C	P	H	H	SH	H	H	H	H	H	W	SW	H	H	H	SW	H	SW
	A	H	H	W	W	H	H	H	H	W	W	SH	SH	SH	SH	SH	SH
L	P	H	SH	SW	SH	H	H	H	H	W	W	H	H	SH	SW	H	SW
	A	SH	SH	W	W	H	H	H	H	W	-	H	-	SW	-	SH	-
F	P	H	SW	W	SW	H	H	H	H	W	W	H	SH	SW	W	H	W
	A	H	H	W	W	H	H	H	H	W	W	SH	SH	H	H	H	SH
G	P	H	H	-	SH	H	H	H	H	W	SW	H	H	SH	H	H	SH
	A	H	H	W	W	H	H	H	H	W	SH	H	H	H	H	H	H
H	P	H	H	H	H	H	H	H	H	SW	W	H	H	H	-	H	-
	A	H	H	H	W	H	H	H	H	W	W	H	H	H	H	SH	H
J	P	H	H	W	H	H	H	H	H	W	SW	H	H	H	H	H	SH
	A	H	H	W	W-H	H	H	H	H	W	W	H	H	H	H	H	H

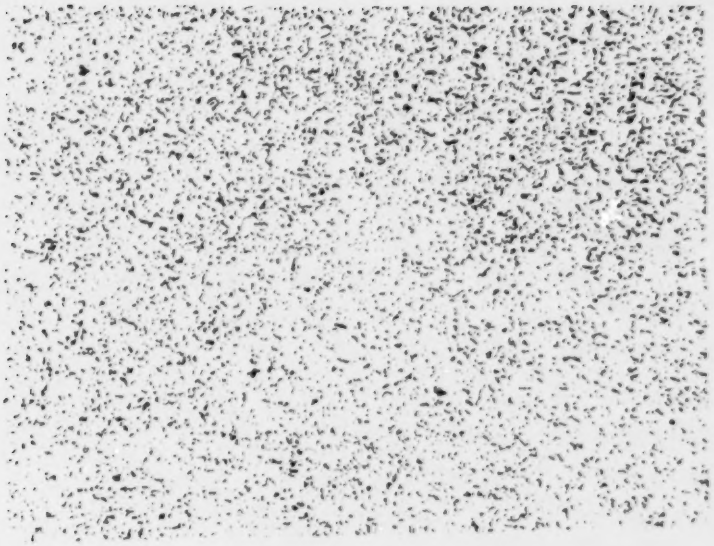

Figure 1a) Steel E (A710 Gr. A Cl 3) as-received microstructure, quenched and precipitation hardened
Neg.9091; Mag.x200; Etch 2% nital.

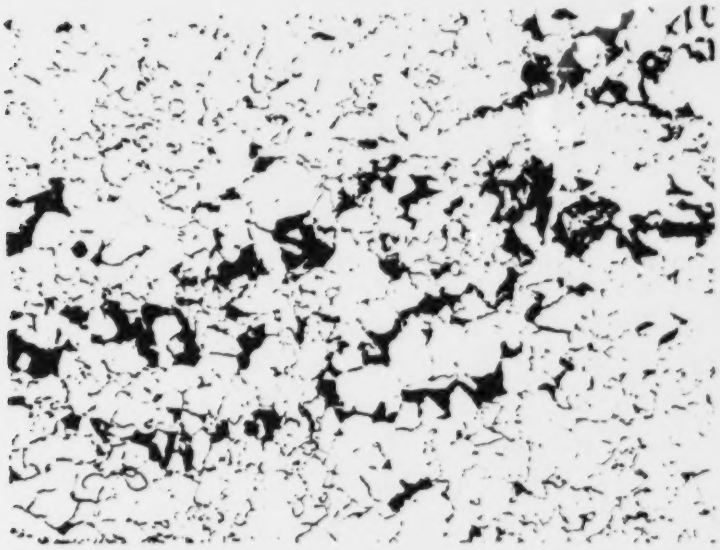

Figure 1b) Steel CR (G40.21 Gr.350 WT) as-received microstructure, controlled rolled, Te treated
Neg.9090; Mag.x200; Etch 2% nital.

Figure 1: As-received microstructures of as-received base plate steels and as-deposited weld metals.

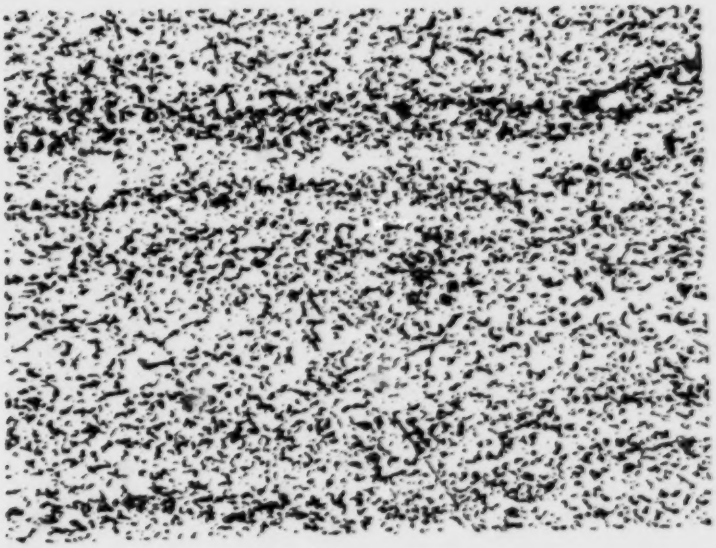

Figure 1c) Steel F (Algoma LT60) as-received microstructure; Neg.9093; Magx200; Etch 2% nital.

Figure 1d) Steel K (A36) as-received microstructure; semi-killed ingot cast, as-rolled.
Neg.9092; Magx200; Etch 2% nital.

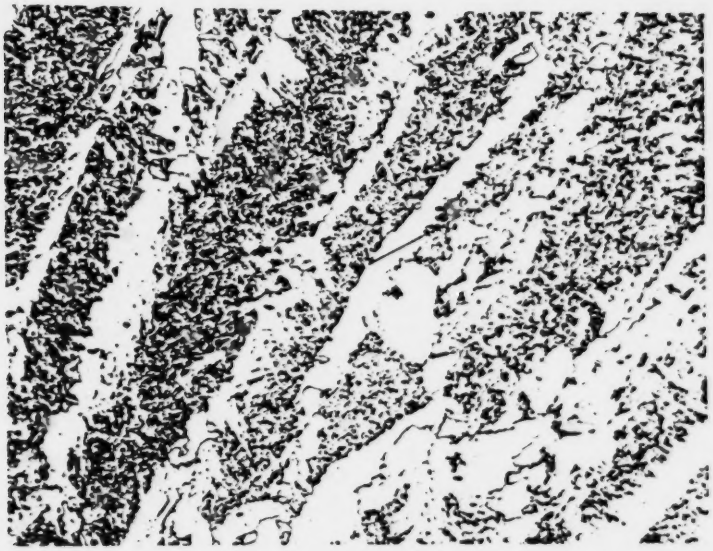

Figure 1e) E7018-1 - heat input 1.2 kJ/mm as-deposited microstructure.
Neg 9212; Magx200; Etch 2% nital.

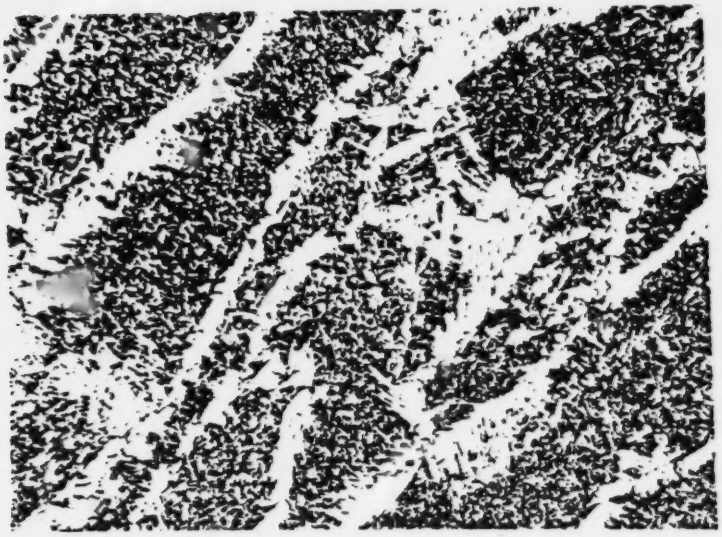

Figure 1f) E7018-1 - heat input 2.5 kJ/mm as-deposited microstructure.
Neg 9213; Magx200, Etch 2% nital.

Figure 1g) E8018-C1 - heat input 1.2 kJ/mm as-deposited microstructure.
Neg 9214; Magx200; Etch 2% nital.

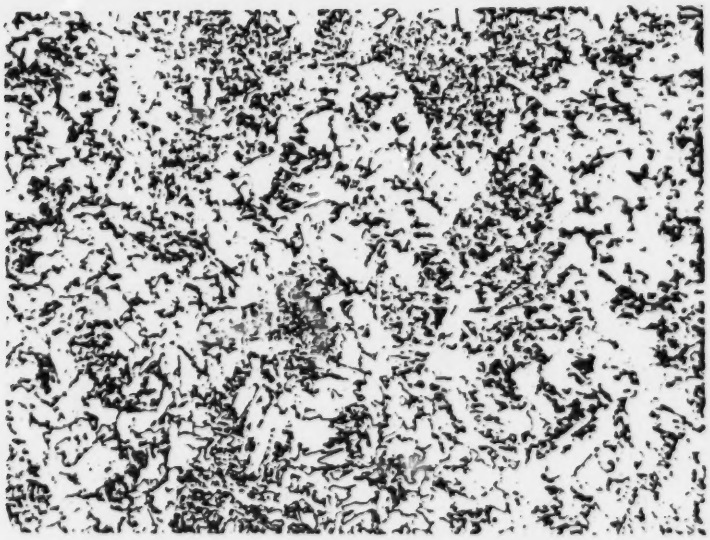

Figure 1h) E8018-C1 - heat input 2.5 kJ/mm as-deposited microstructure.
Neg 9215; Magx200, Etch 2% nital.

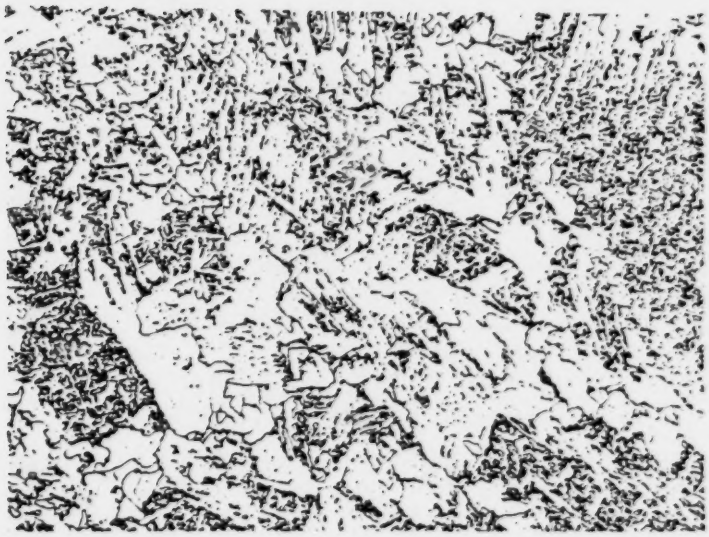

Figure 1i) L60/761 - heat input 2.5 kJ/mm as-deposited microstructure.
Neg 9208; Magx200; Etch 2% nital.

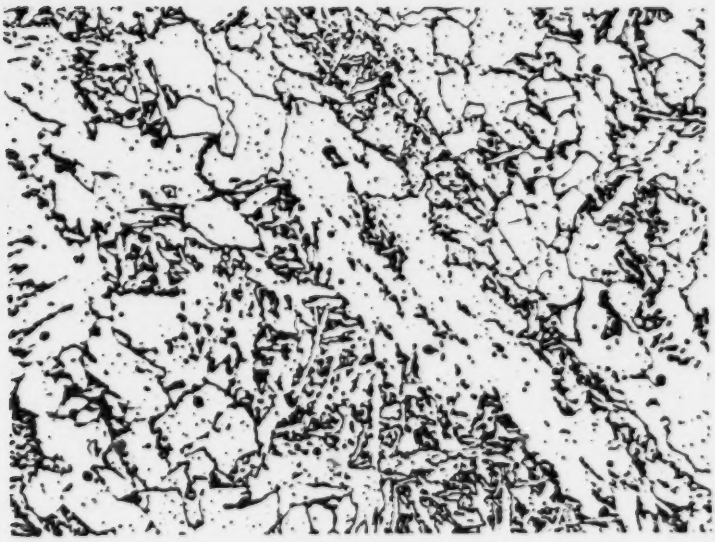

Figure 1j) L60/761 - heat input 4.0 kJ/mm as-deposited microstructure.
Neg 9211; Magx200, Etch 2% nital.

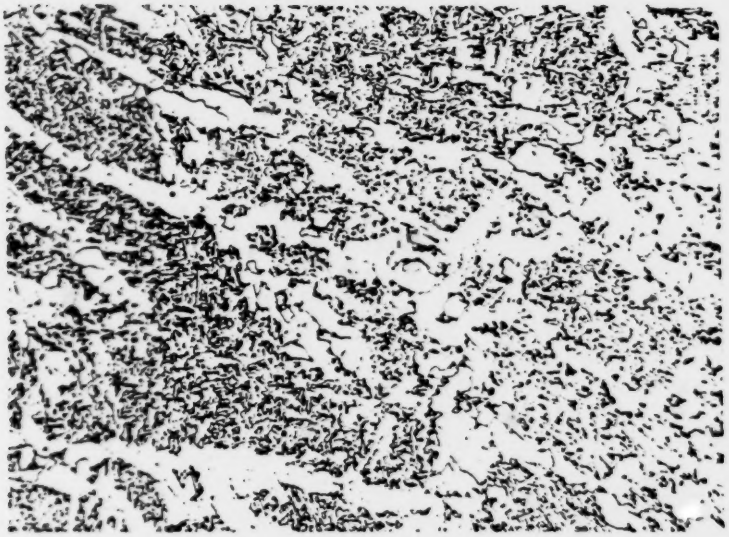

Figure 1k) Tibor 22/OP121TT - heat input 2.5 kJ/mm
as-deposited microstructure.
Neg 9209; Magx200; Etch 2% nital.

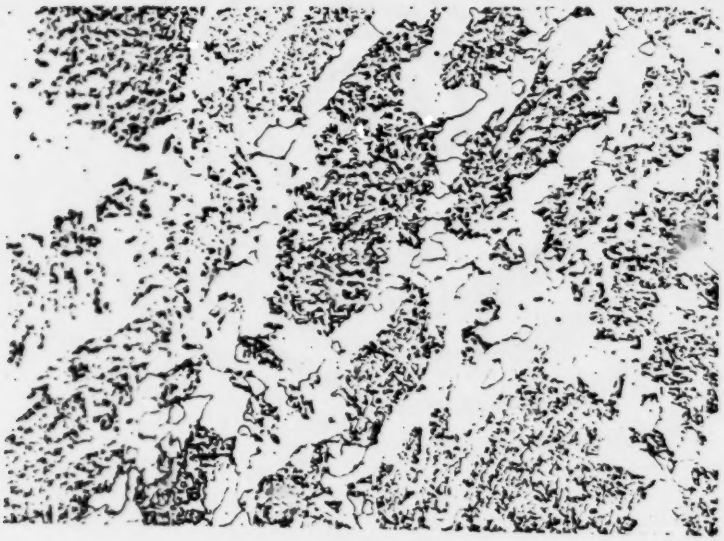

Figure 1l) Tibor 22/OP121TT - heat input 4.0 kJ/mm
as-deposited microstructure.
Neg 9210; Magx200, Etch 2% nital.

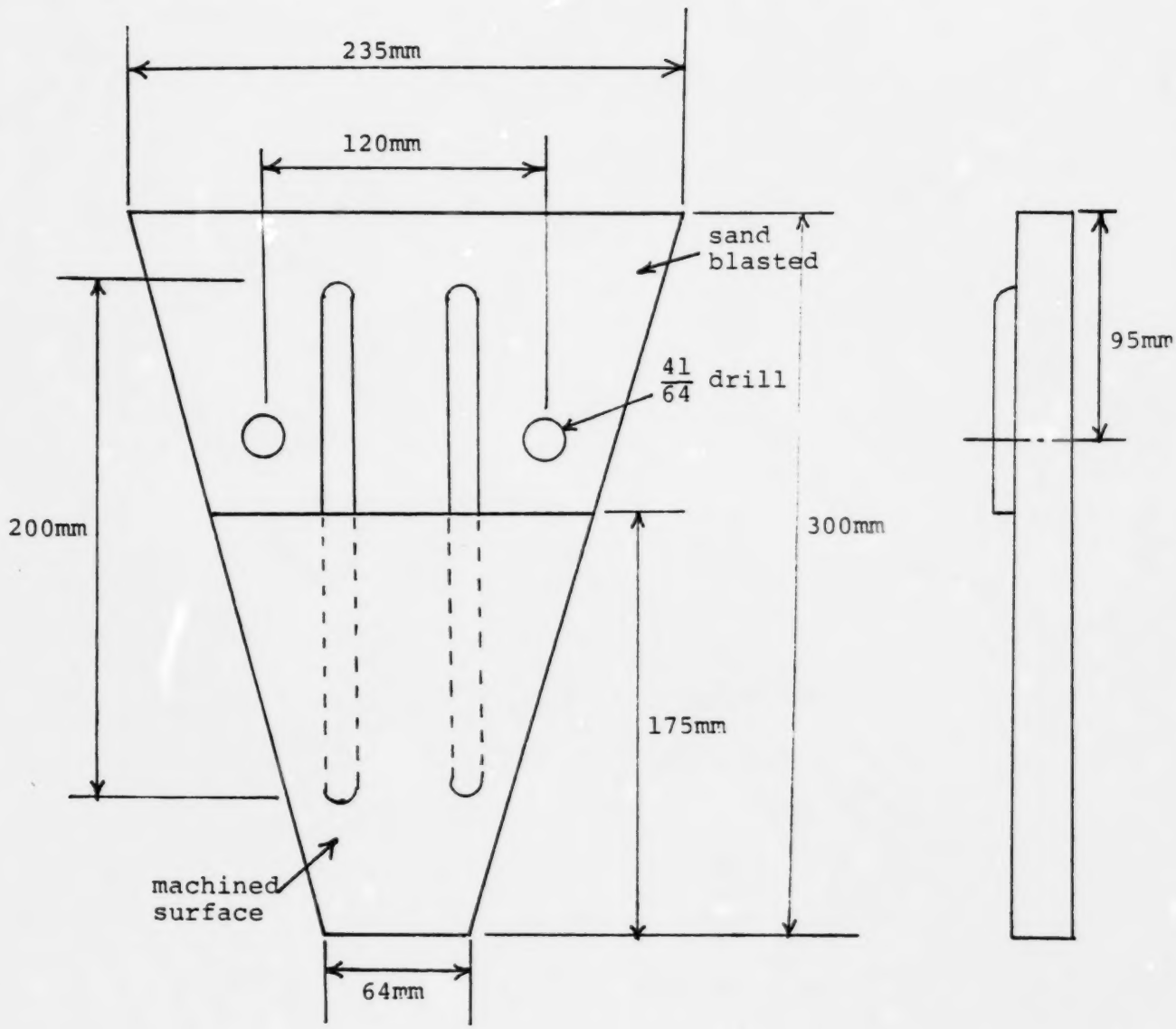

Figure 2: Trapezoid Tank Test Specimen

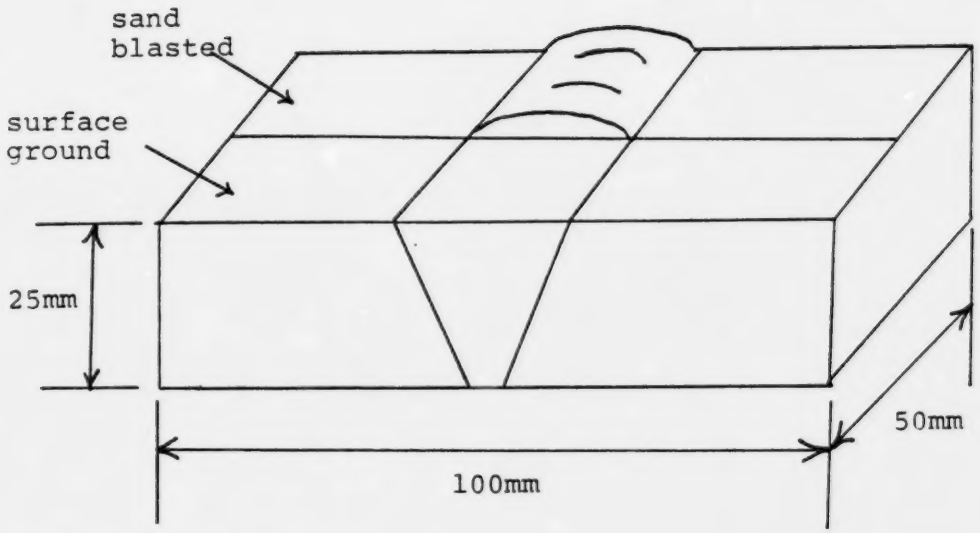

Figure 3: Butt Weld Anodic Dissolution Test Specimen

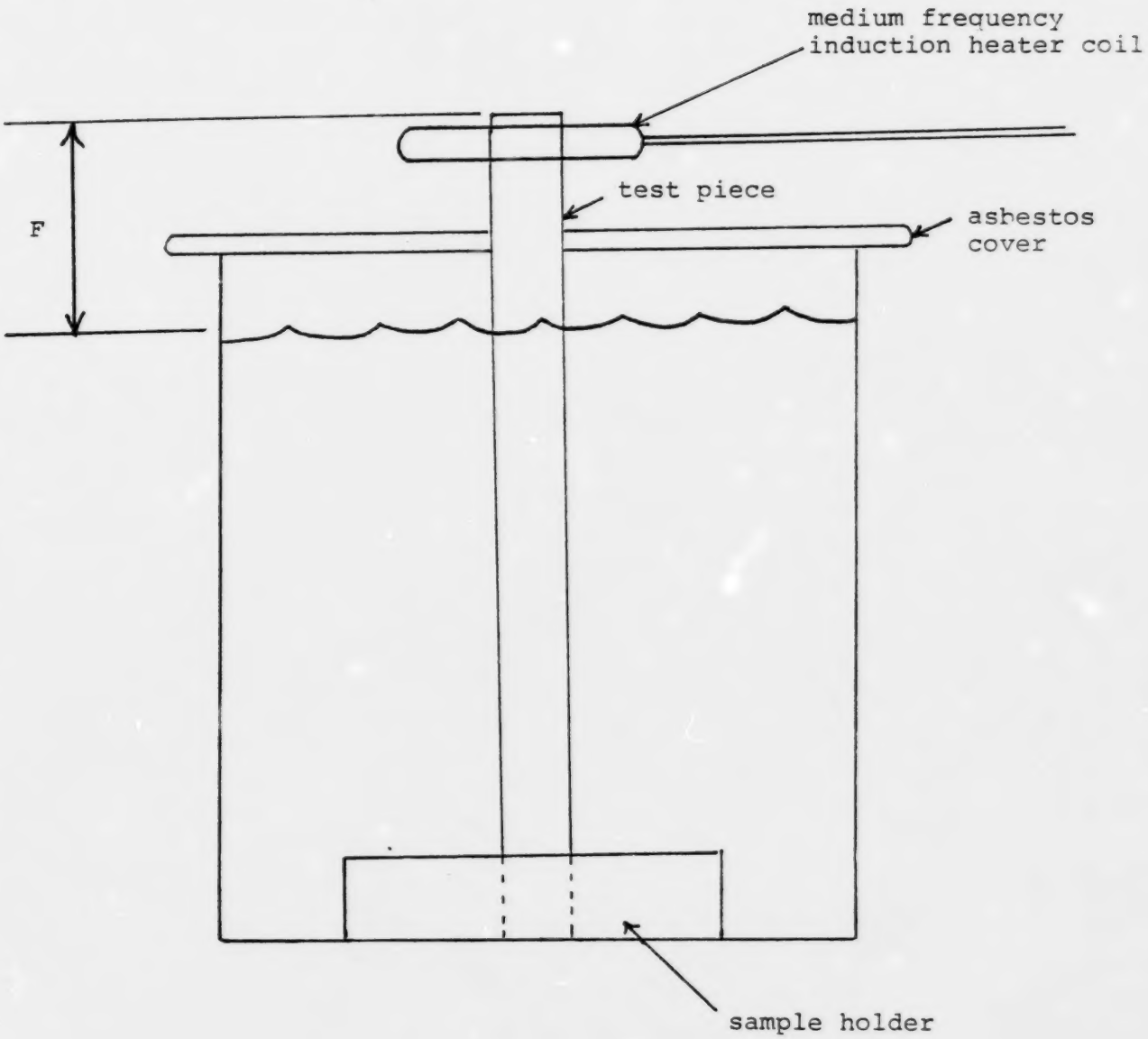

Figure 4: Set Up Used for Preparation of NWH Bars

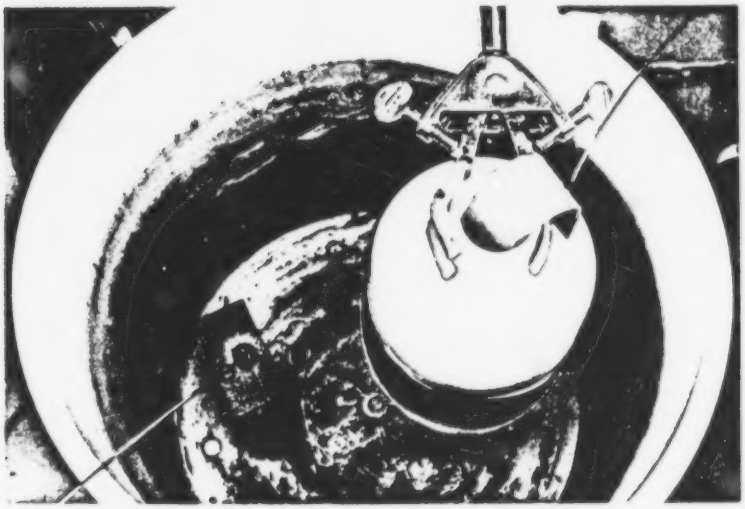

Figure 5: The test cell showing a butt weld test anode (left) and stainless steel cathode (right) with its polyethelene cathode compartment. A Saran membrane covers the bottom of the cathode compartment to prevent anolyte and catholyte mixing.

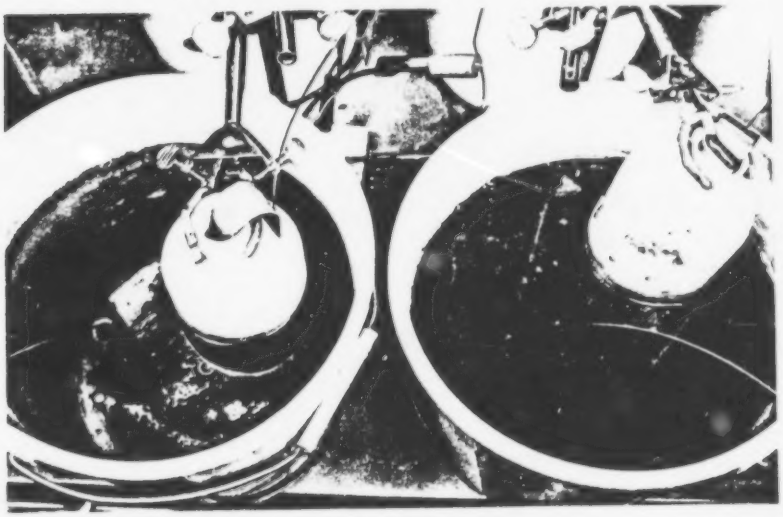

Figure 6: Two test cells, on the left before the test and on the right during test, when copious ferrous and ferric corrosion products clouded the anolyte.

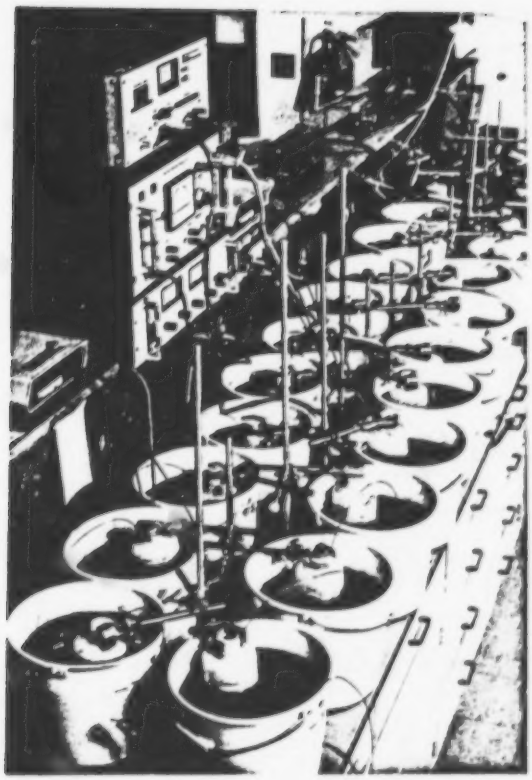

Figure 7: Twenty two test cells in series with associated power supplies.

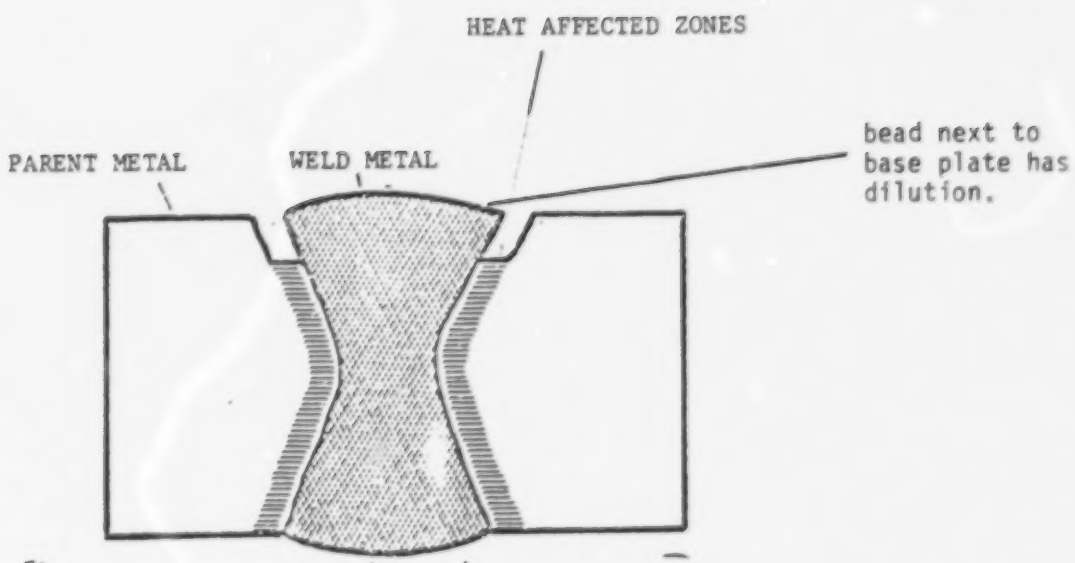

Figure 8: Composite representation of various test samples representing parent metal-weldment combination.

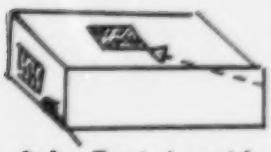

Figure 9a) Test Location = cross section.

Figure 9b) Test location plane along rolling direction

Figure 9: The test locations and specimen configuration.

9a. - cross-section
9b. - side surface, i.e., rolling plane
9c. - test specimen after assembly in holder.

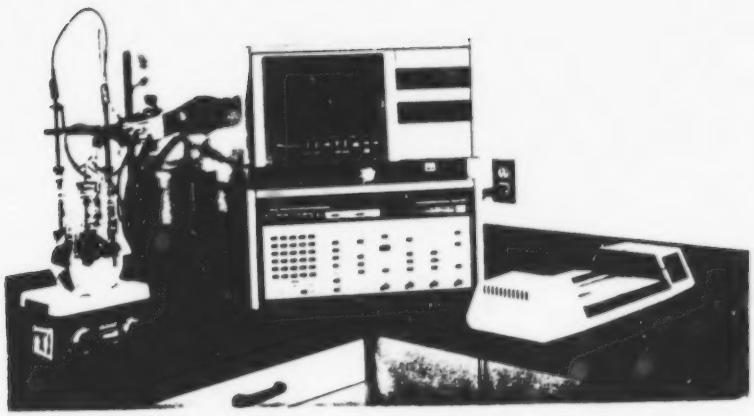

Figure 10: A view of Model 351-1 EGG-PAR corrosion monitoring system together with corrosion cell that was used for potentiostatic tests.

A - PAR model 273 Potentiostat/galvanostat
B - Microprocessor
C - Recorder
D - Glass cell containing test electrode, counter and reference electrodes, and N_2-gas inlet and outlet.

WELD METAL CORROSION
ANODIC DISSOLUTION TEST

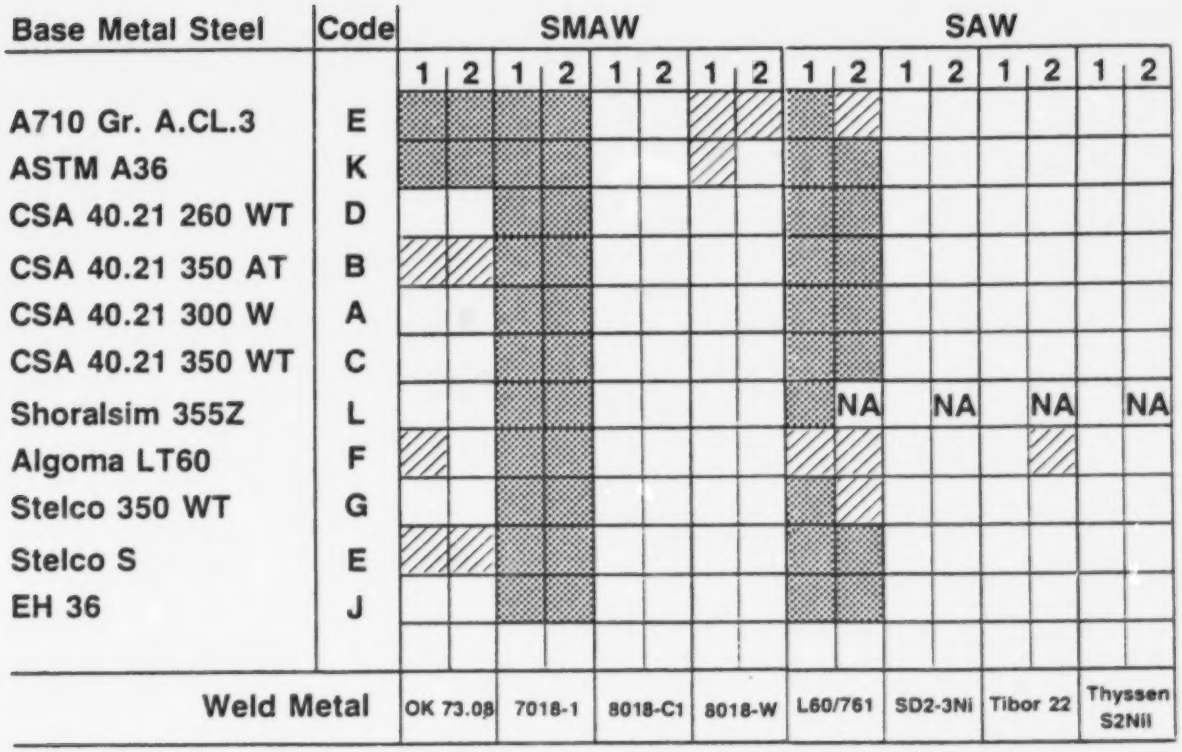

Figure 11: Preferential attack of weld metal as judged by the depth of attack.

HEAT AFFECTED ZONE CORROSION
ANODIC DISSOLUTION TEST

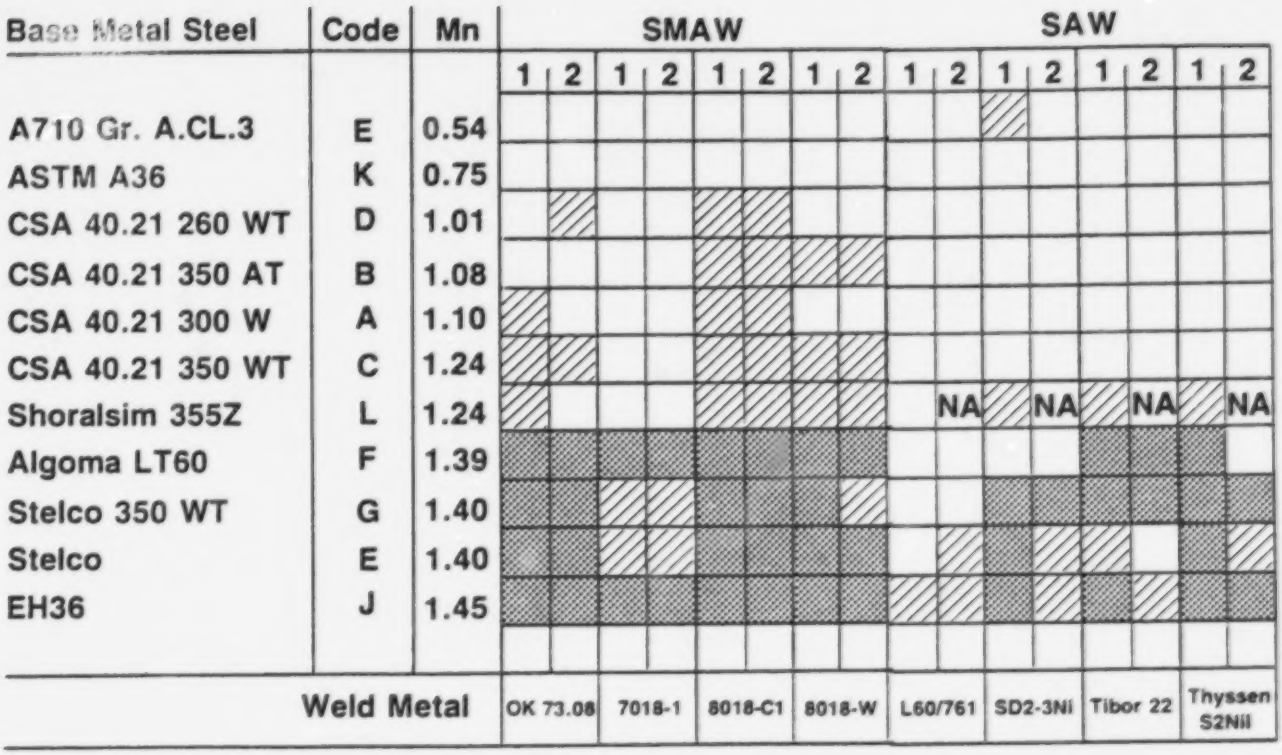

Figure 12: Preferential heat affected zone attack as judged by the depth of attack.

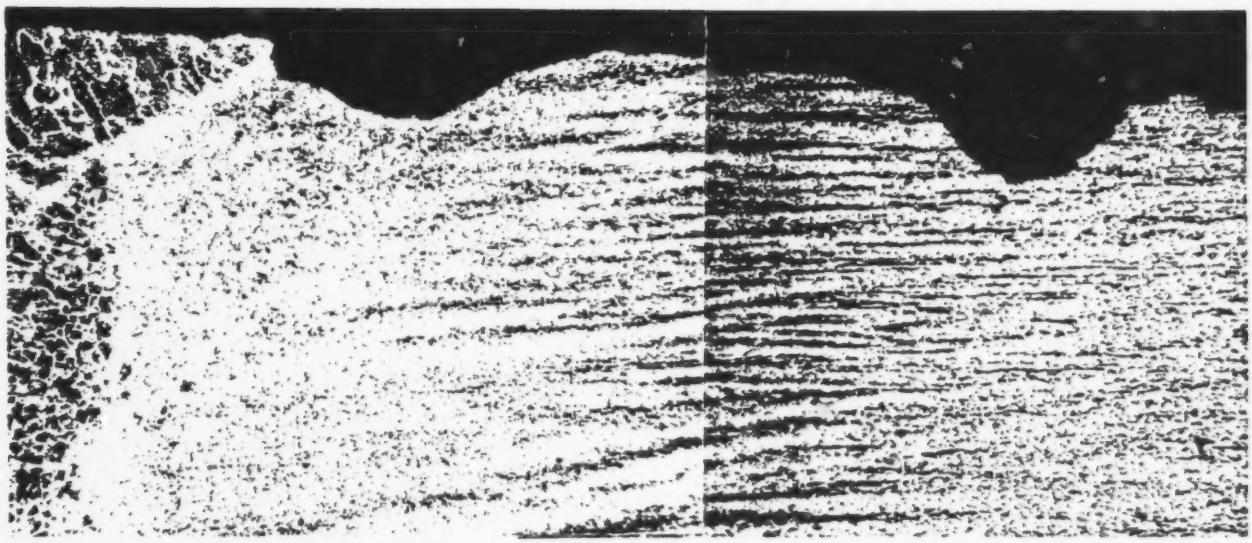

Figure 13: Photomicrograph of Stelco 350 WT butt weld specimen G41 (welded with OK 73.08 at 1.2 kJ/mm heat input) after anodic dissolution. Note preferential attack of supercritical (coarse grain) region and subcritical region of the HAZ. Neg. 8995, 8997; Mag X 50; Etch 2% nital.

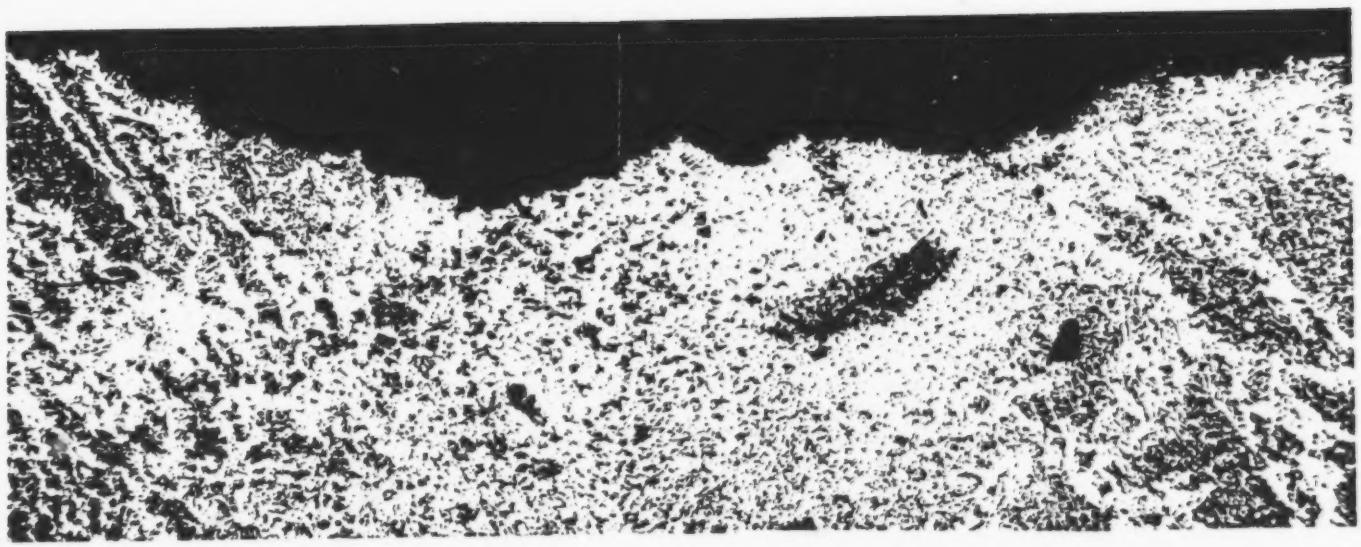

Figure 14: Photomicrograph of butt weld specimen G52 (Stelco 350 WT welded with L60/761 at 4.0 kJ/mm) after anodic dissolution test. Note preferential attack of supercritical (coarse grain) region and subcritical region of the HAZ. Neg. 9669, 9670; Mag X 50; Etch 2% nital.

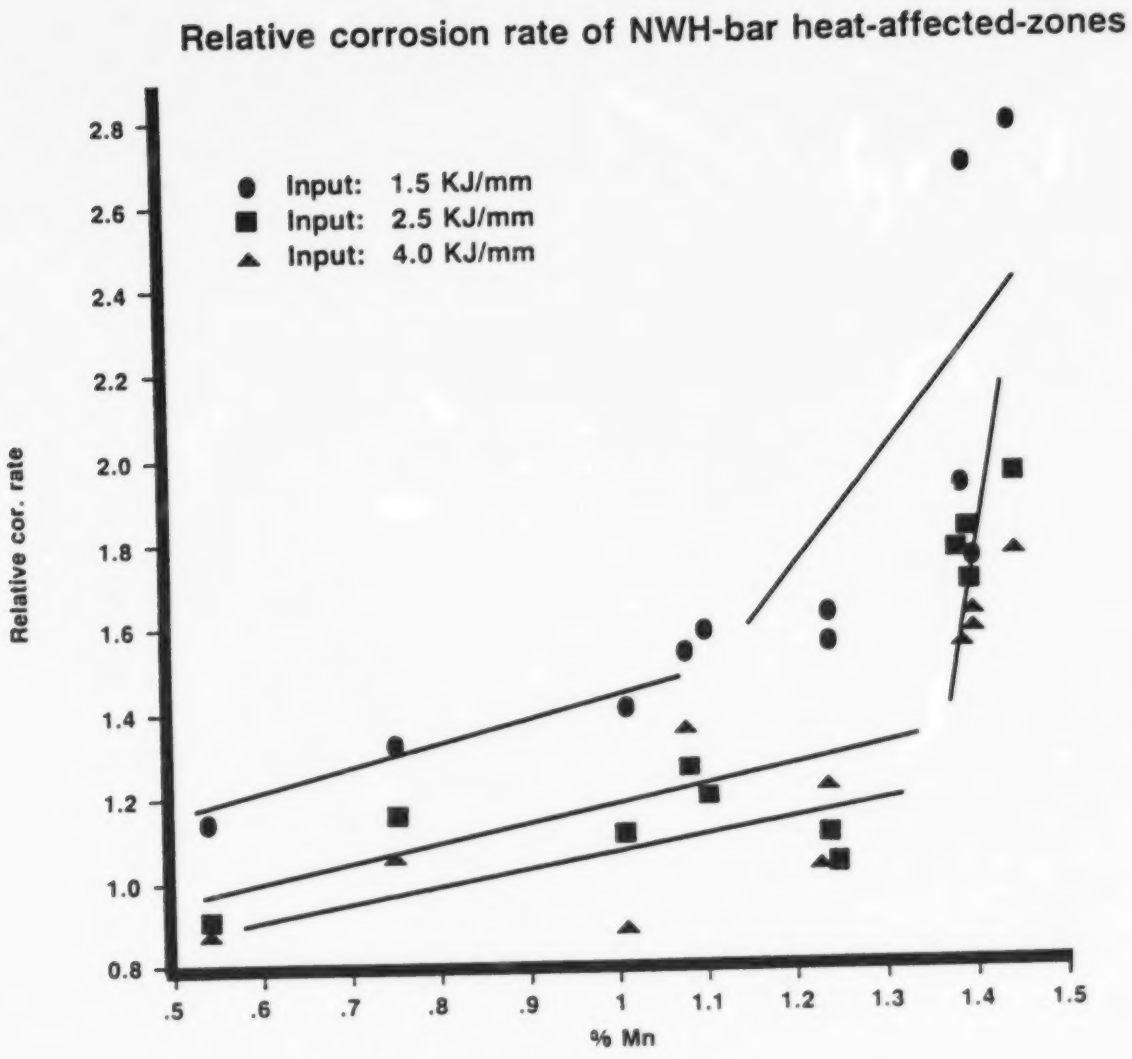

Figure 15: Relative corrosion rate of NWH bar heat affected zones increased with manganese content and were higher at lower heat inputs.

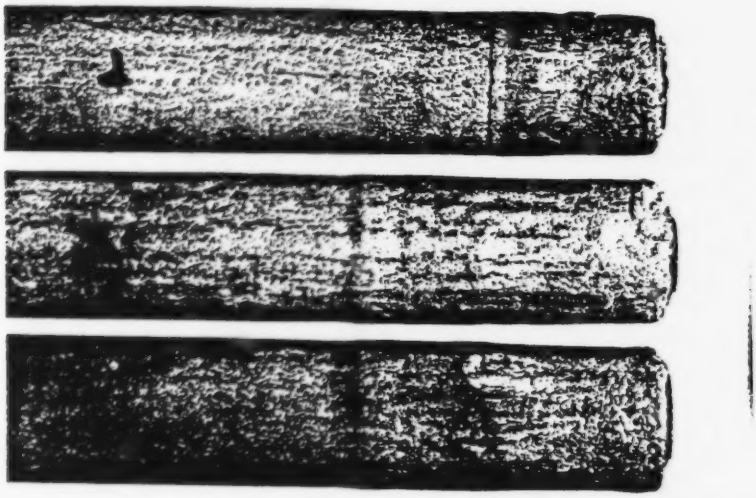

a) A710, 0.54%Mn

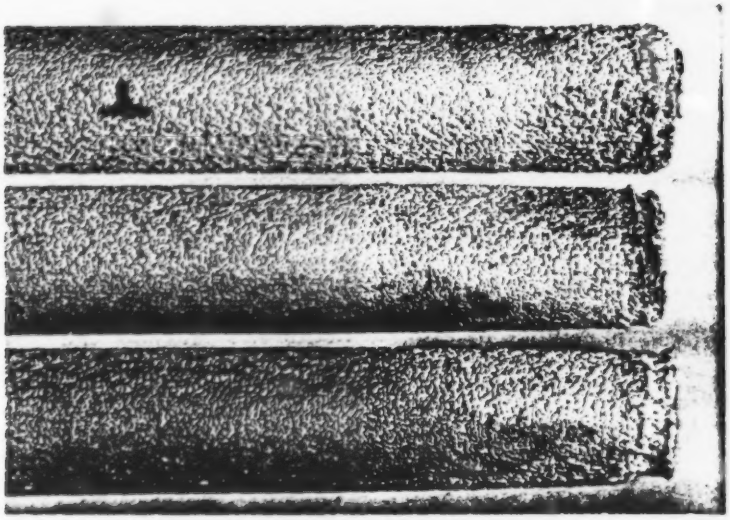

b) A36, 0.75%Mn

Figure 16 (a) thru (k)

Figure 16: NWH-bar specimens for each base plate after anodic dissolution tests. Each figure shows bars with equivalent heat-inputs 1.5, 2.5 and 4.0 kJ/mm (top, middle, bottom)

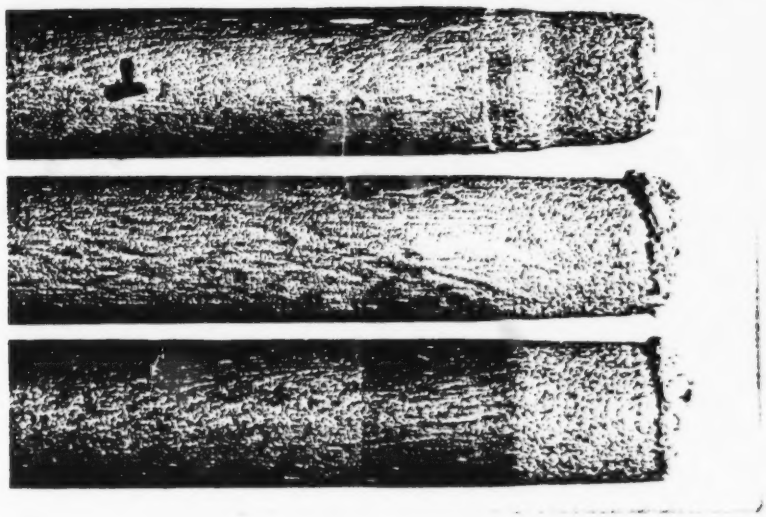

c) E260WT, 1.01%Mn

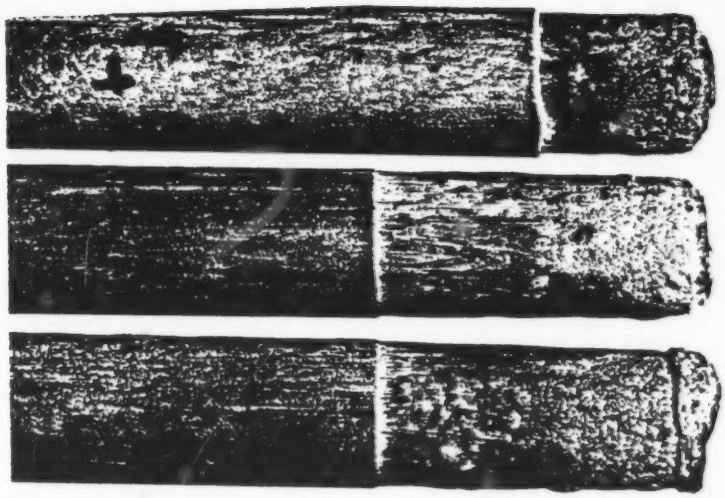

d) 350AT, 1.08%Mn

Figure 16-2

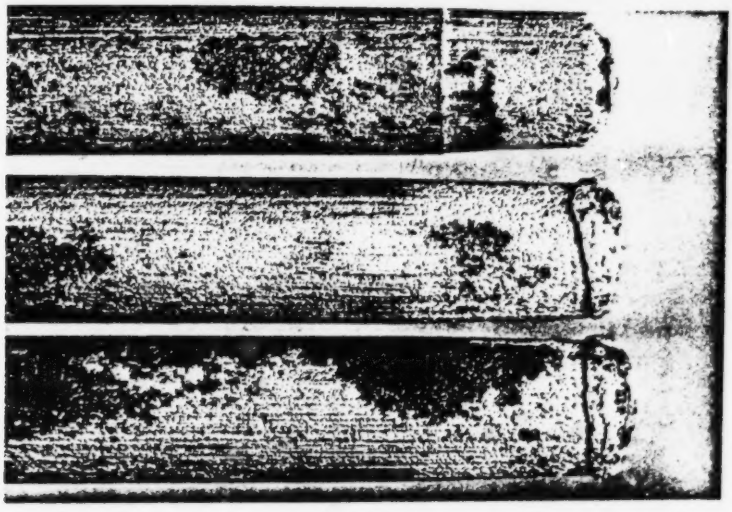

e) 300W 1.10%Mn

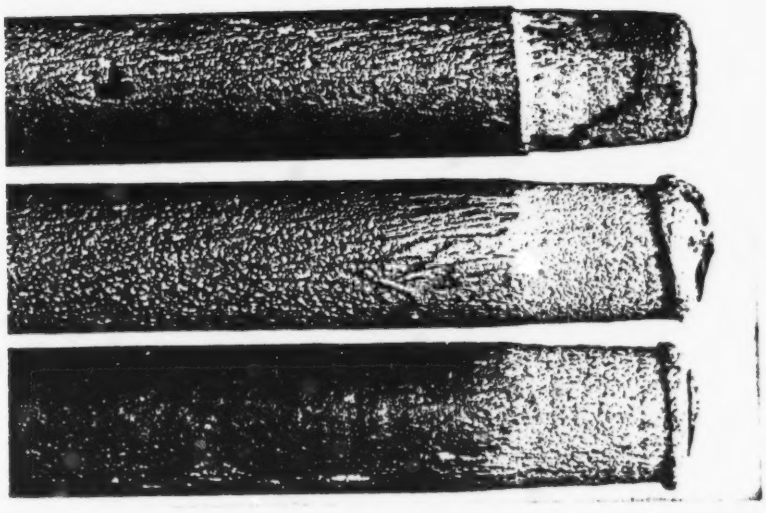

f) Algoma 350WT, 1.24%Mn

Figure 16-3

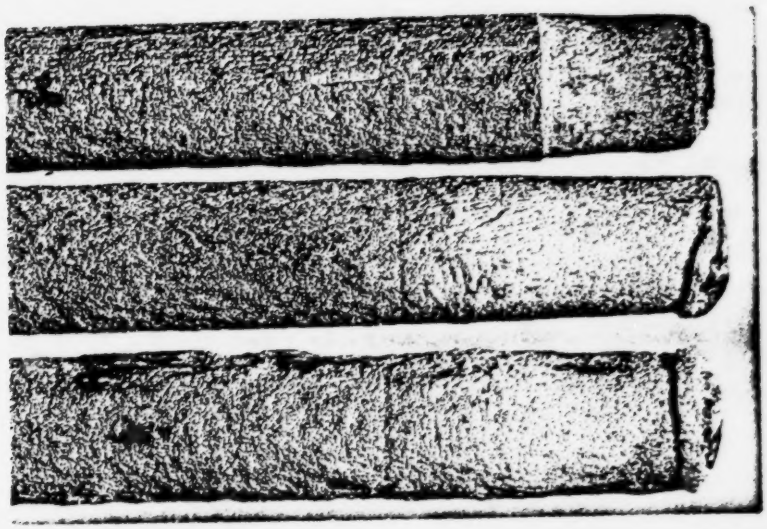

g) 355Z, 1.24%Mn

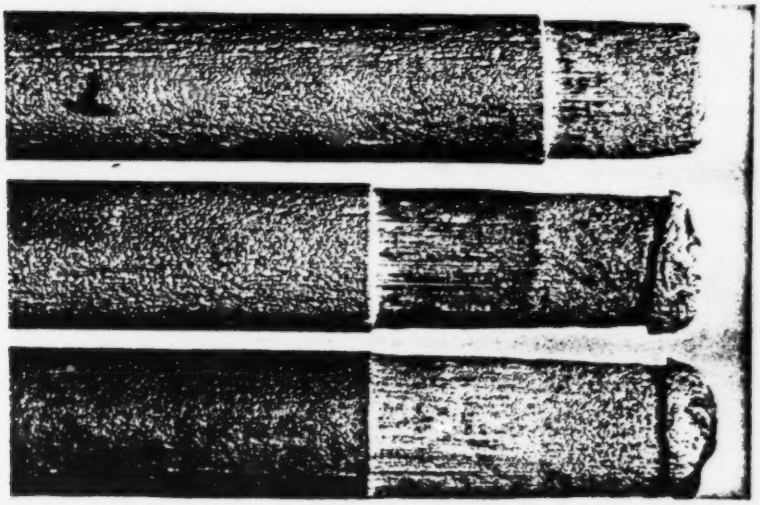

h) LT60, 1.39% Mn

Figure 16-4

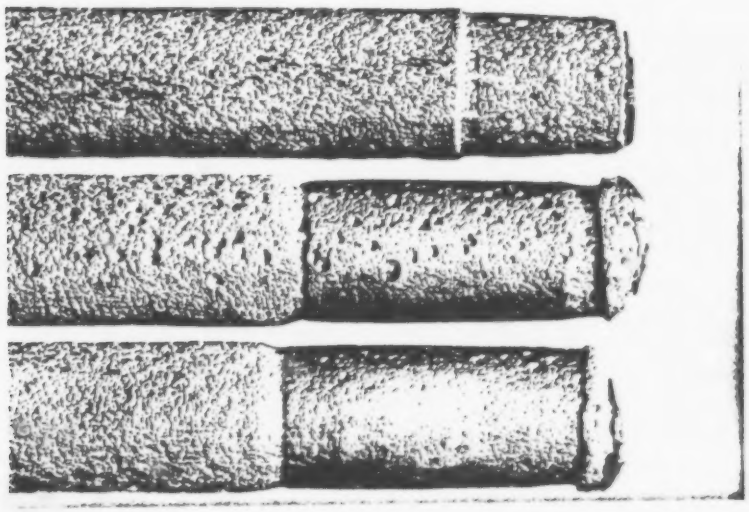

i) Stelco 350WT, 1.40%Mn

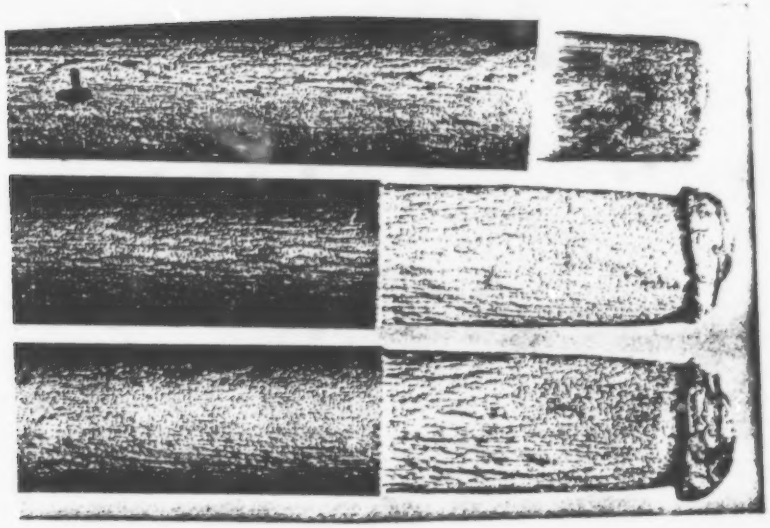

j) Stelco S, 1.40%Mn

Figure 16-5

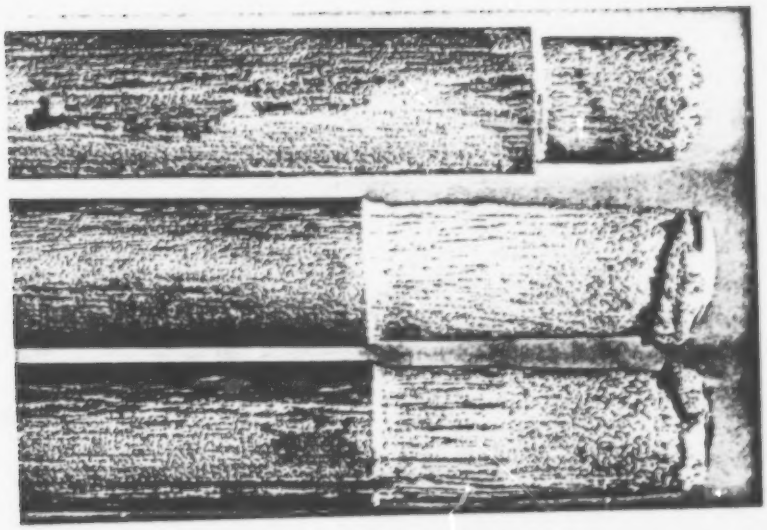

k) EH36, 1.45%Mn

Figure 16-6

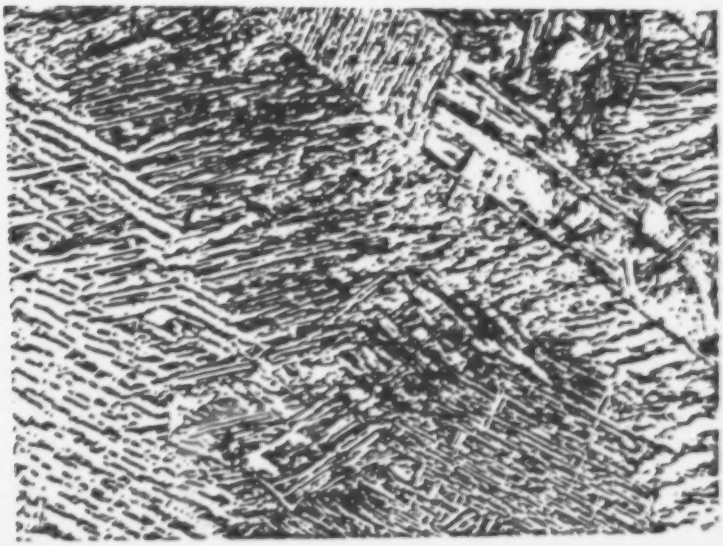

a) simulated HI = 1.5 kJ/mm, coarse grained HAZ.
Neg. 9008; Mag X 500; Etch 2% nital.

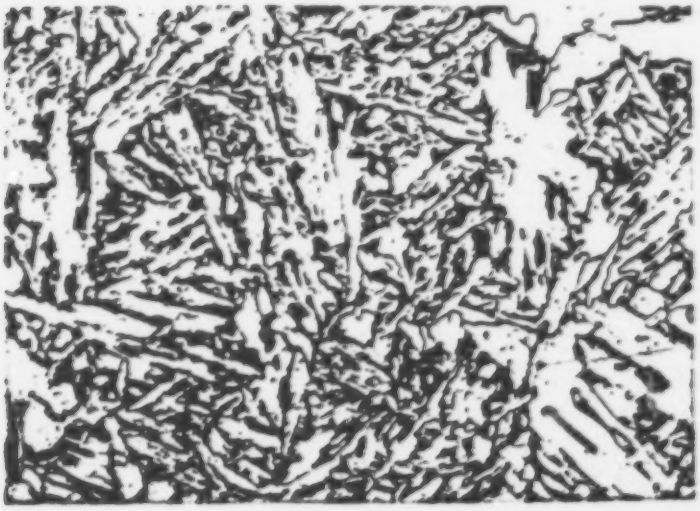

b) simulated HI = 4.0 kJ/mm, coarse grained HAZ.
Neg. 9007; Mag X 500; Etch 2% nital.

Figure 17: Microstructure of NWH Bar for Steel CR after anodic dissolution tests

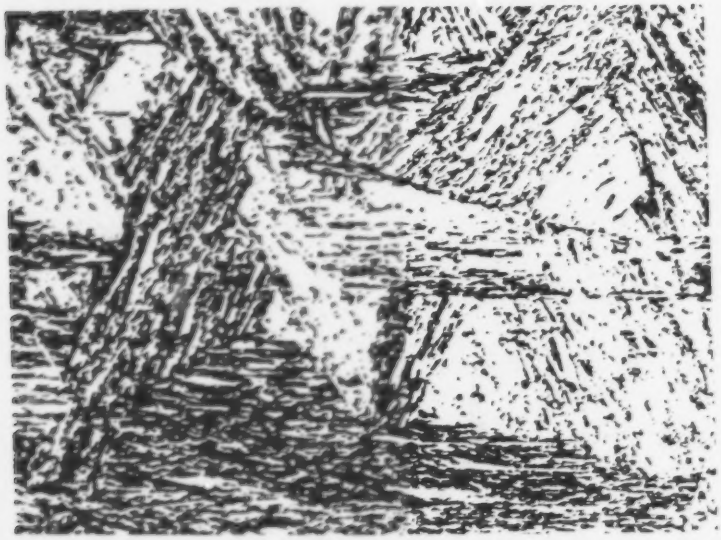

a) simulated HI = 1.5 kJ/mm, coarse grained HAZ
Neg. 9000; Mag X 500; Etch 2% nital.

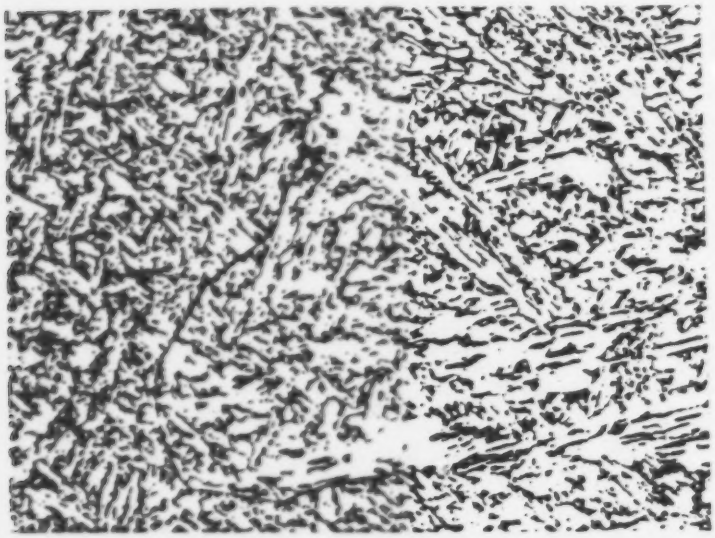

b) simulated HI = 4.0 kJ/mm, coarse grained HAZ.
Neg. 8999; Mag X 500; Etch 2% nital.

Figure 18: Microstructure of NWH Bars for Steel E after anodic dissolution tests

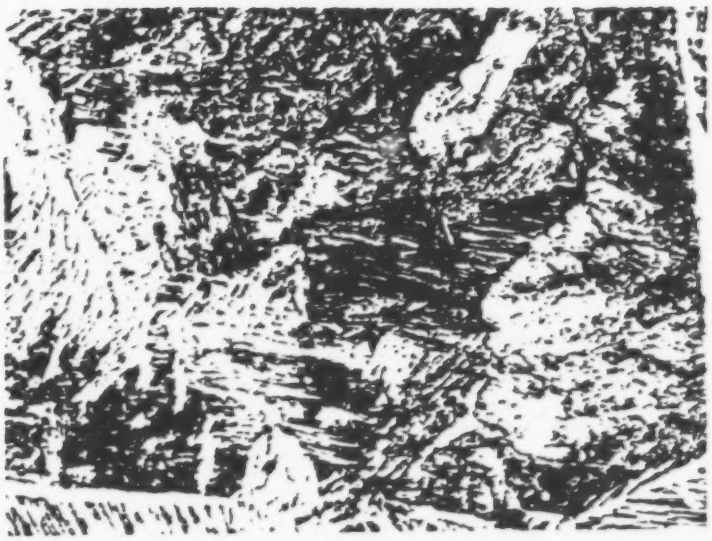

a) simulated HI = 1.5 kJ/mm, coarse grained HAZ.
Neg. 9002; Mag X 500; Etch 2% nital.

b) simulated HI = 4.0 kJ/mm, coarse grained HAZ.
Neg. 9001; Mag X 500; Etch 2% nital.

Figure 19: Microstructure of NWH Bars for Steel K after anodic dissolution tests

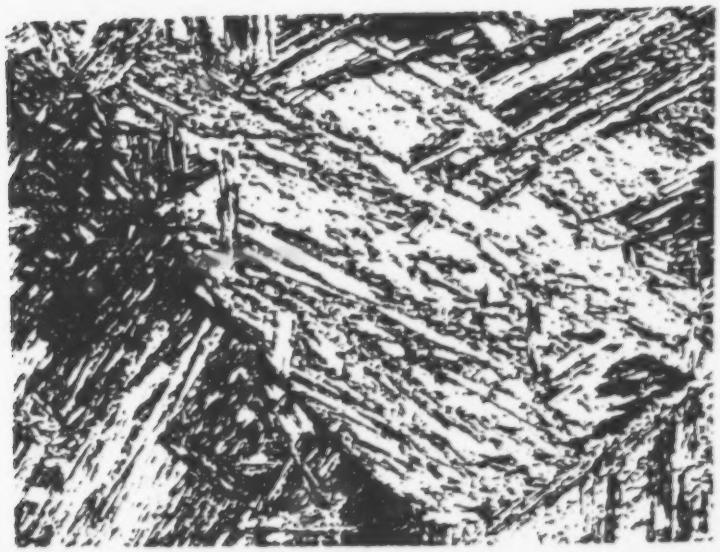

a) simulated HI = 1.5 kJ/mm, coarse grained HAZ.
Neg. 9005; Mag X 500; Etch 2% nital.

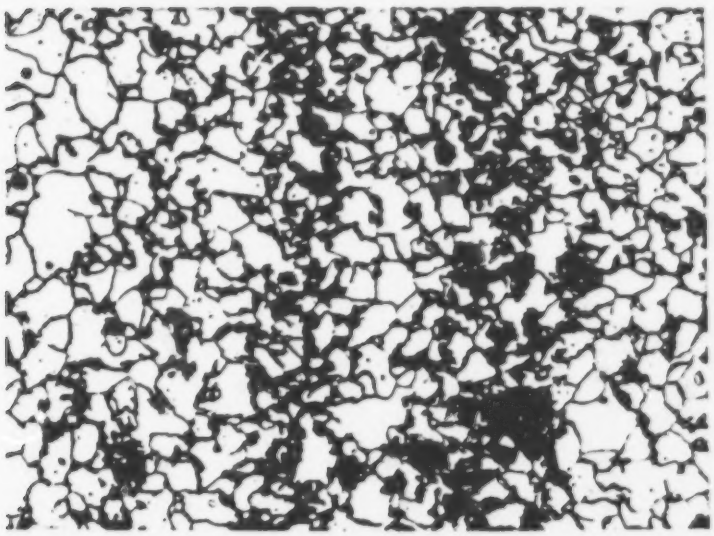

b) simulated HI = 1.5 kJ/mm, subcritical HAZ.
Neg. 9006; Mag x 500; Etch

Figure 20: Microstructure of NWH bars for steel F after anodic dissolution tests

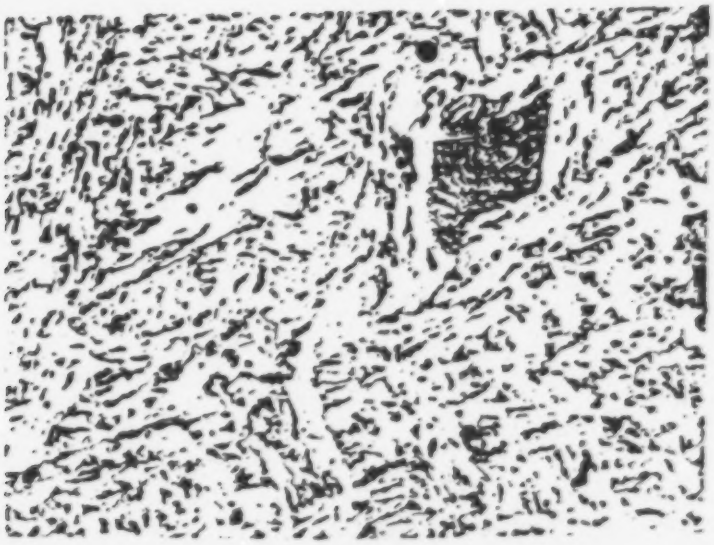

c) simulated HI = 4.0 kJ/mm, coarse grained HAZ.
Neg. 9003; Mag X 500; Etch 2% nital.

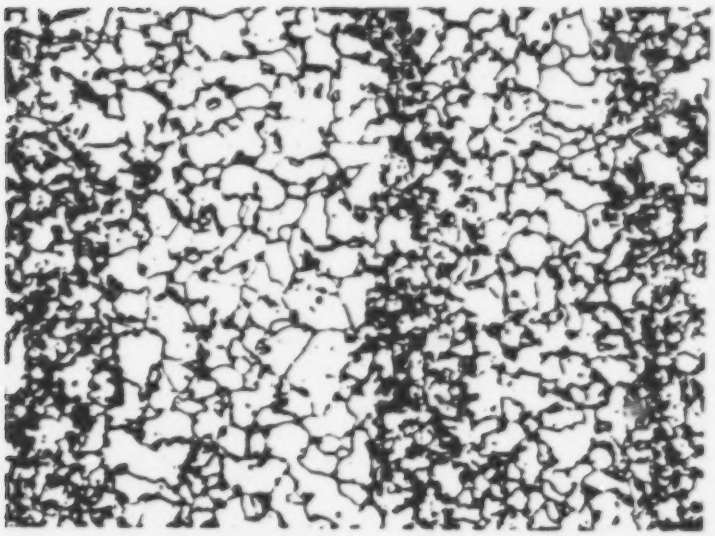

d) simulated HI = 4.0 kJ/mm, subcritical HAZ.
Neg. 9004; Mag. X 500; Etch 2% nital.

Figure 20: Microstructure of NWH bars for Steel F after anodic dissolution tests

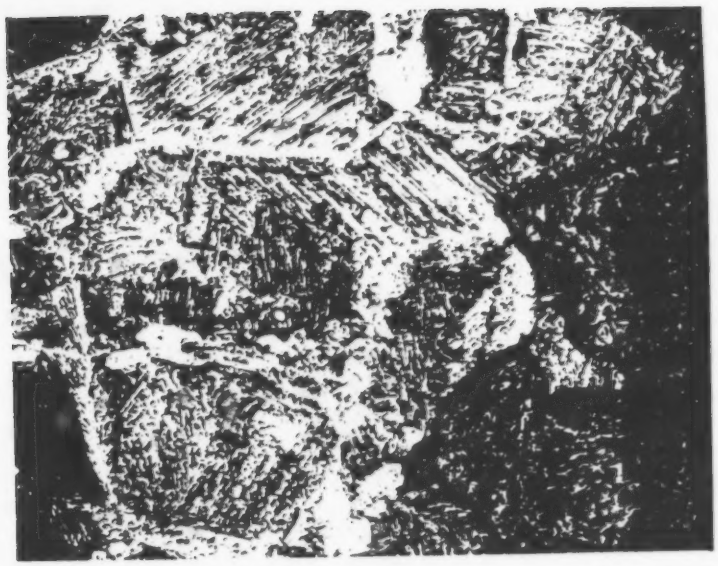

Figure 21: Noren Weld Hardened Bar for Steel K at low heat input. Note the non-uniform corrosive attack. Neg. 8998; Mag X 100; Etch 2% Nital.

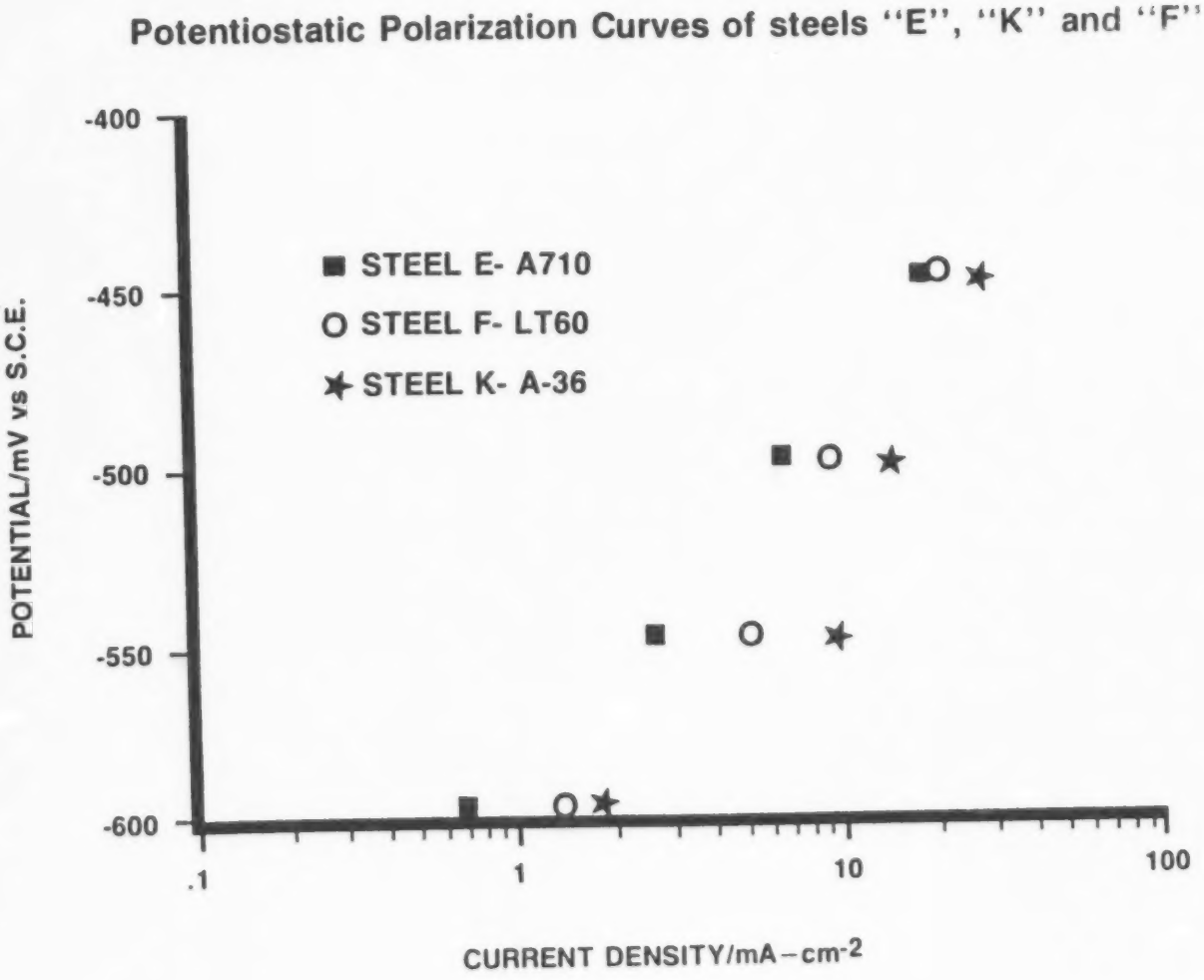

Figure 22a: Potentiostatic polarization curves of steels E, K and F in 3.5% NaCl solution. Transverse cross sections were tested.

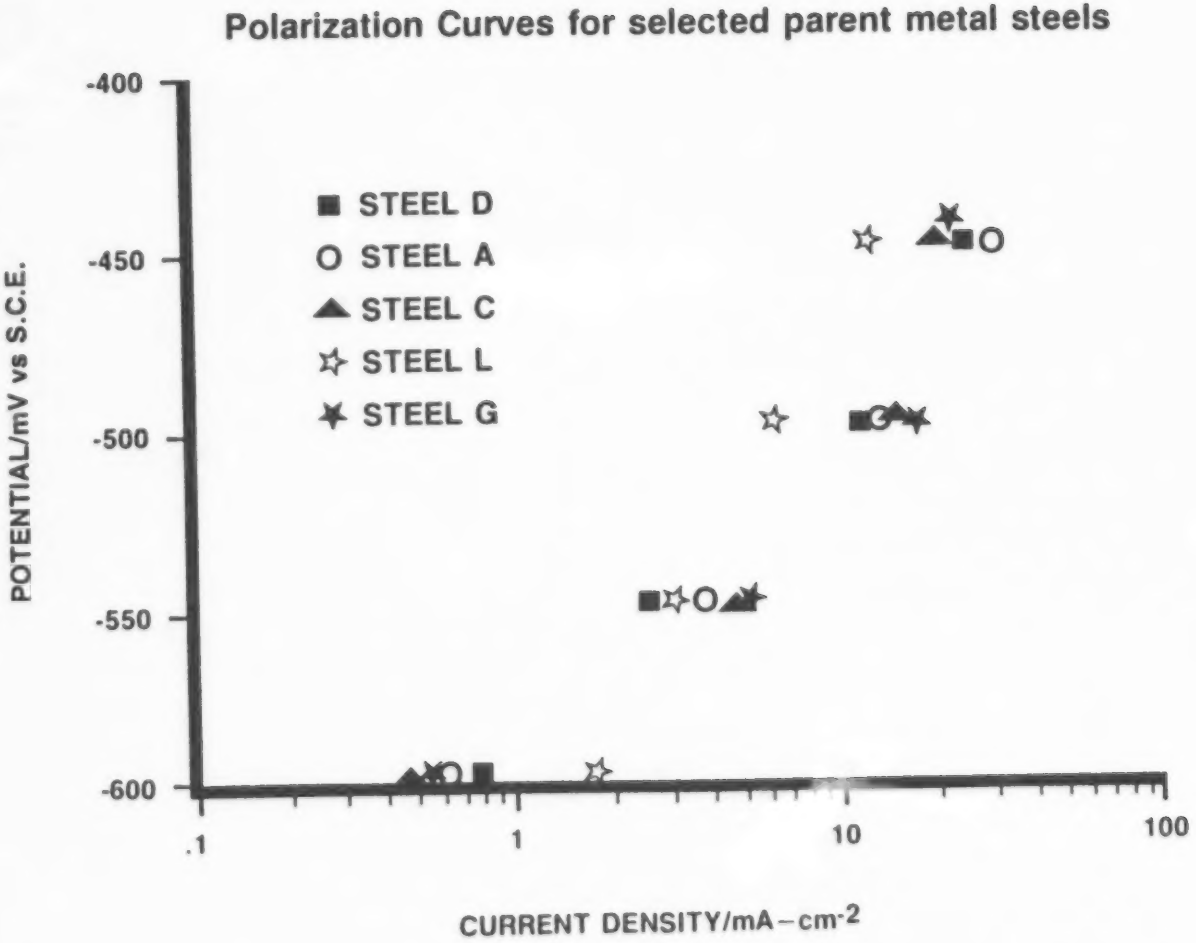

Figure 22b: Potentiostatic polarization curves of steels D, A, C, L and G in 3.5% NaCl solution. Transverse cross sections were tested.

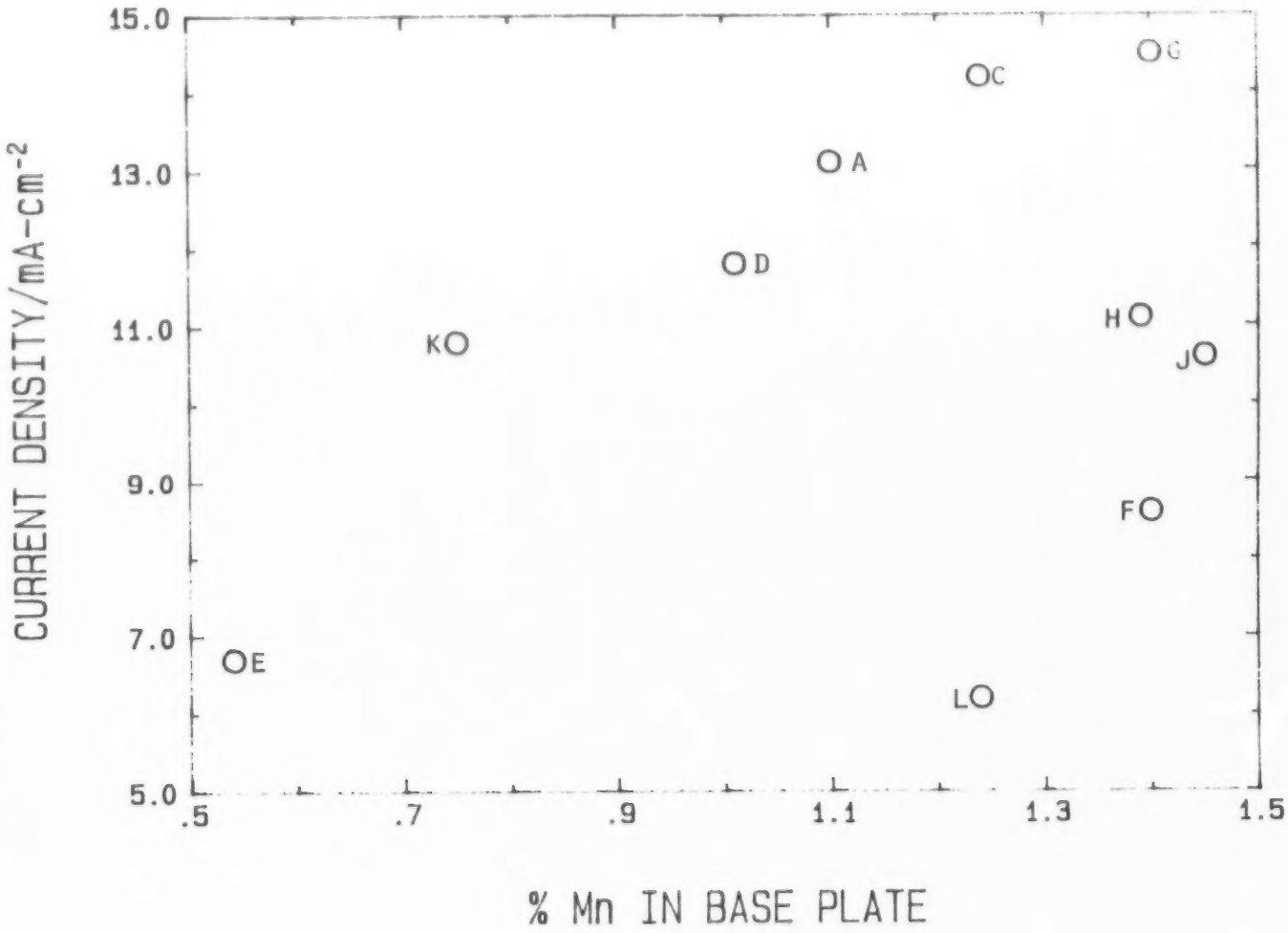

Figure 23: Current densities at -500 mV vs base plate manganese content. The current densities were measured at rolling planes, i.e. side surfaces of specimens.

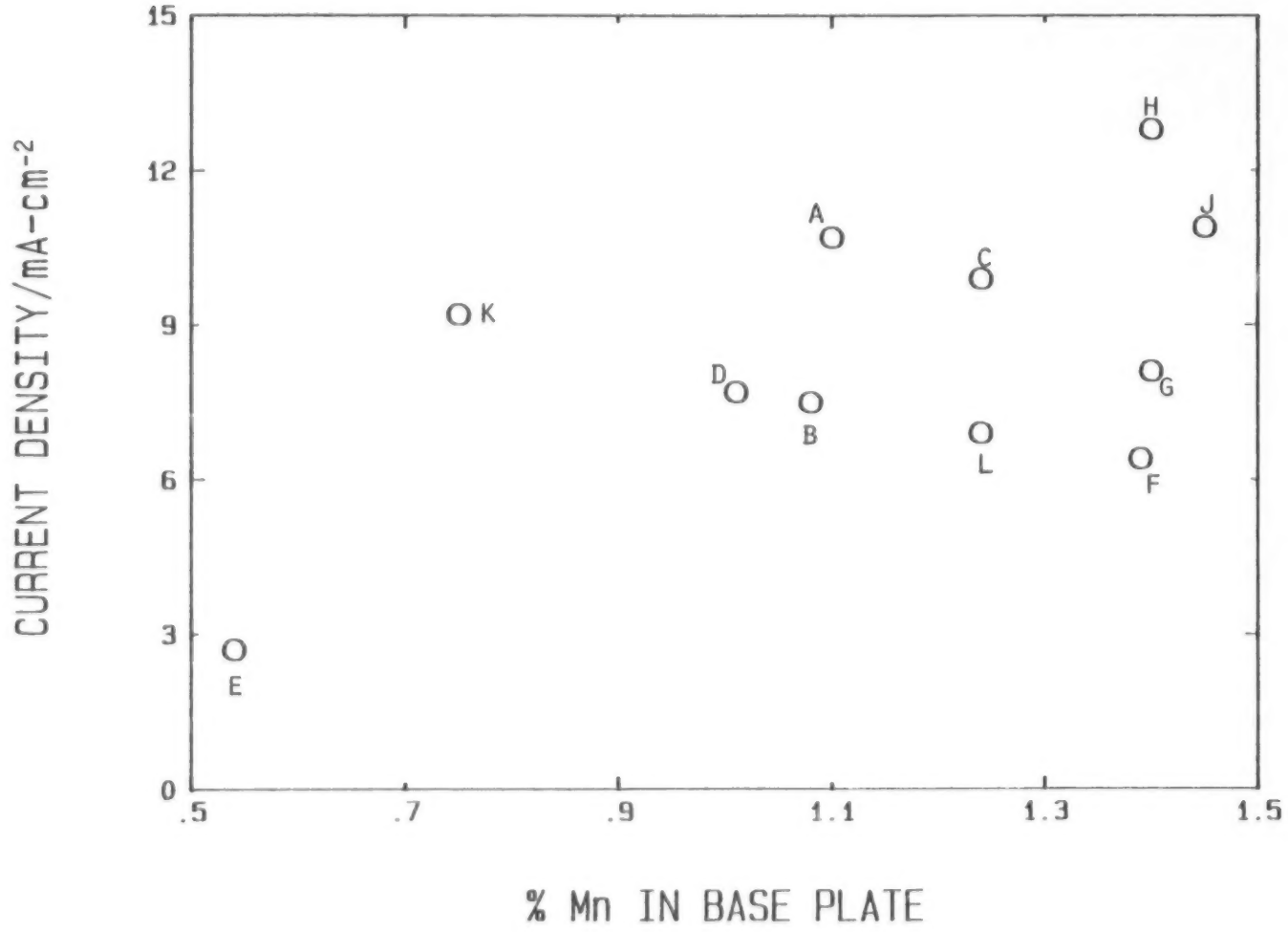

Figure 24: Current densities at -500 mV vs base plate manganese content. The current densities were measured at the cross-sectional surfaces.

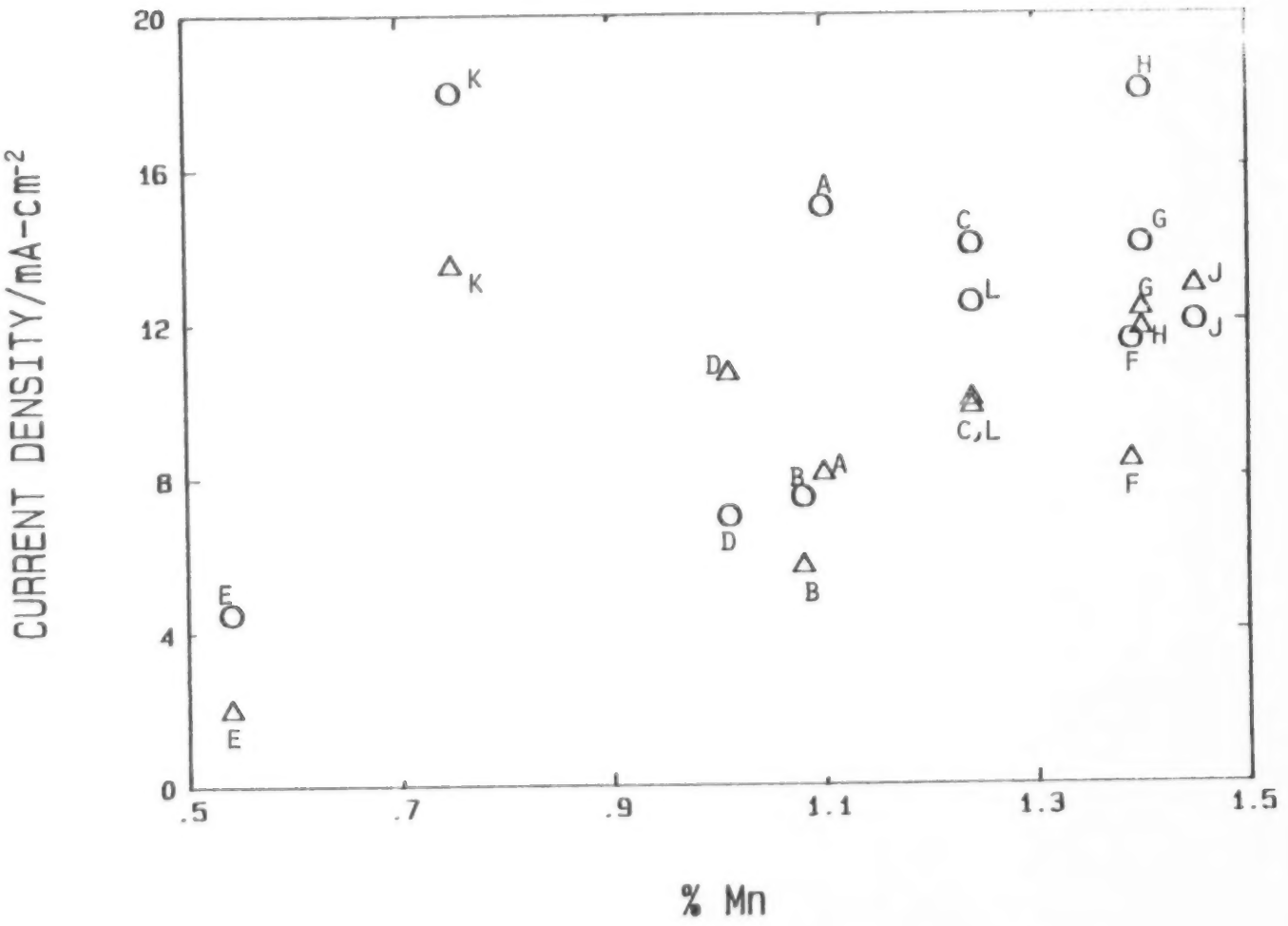

Figure 25: Current densities of Gleeble simulated HAZ's at -500 mV vs % Mn in corresponding base plate steels. Heat inputs: o - 1.2 and Δ - 4.0 kj/mm.

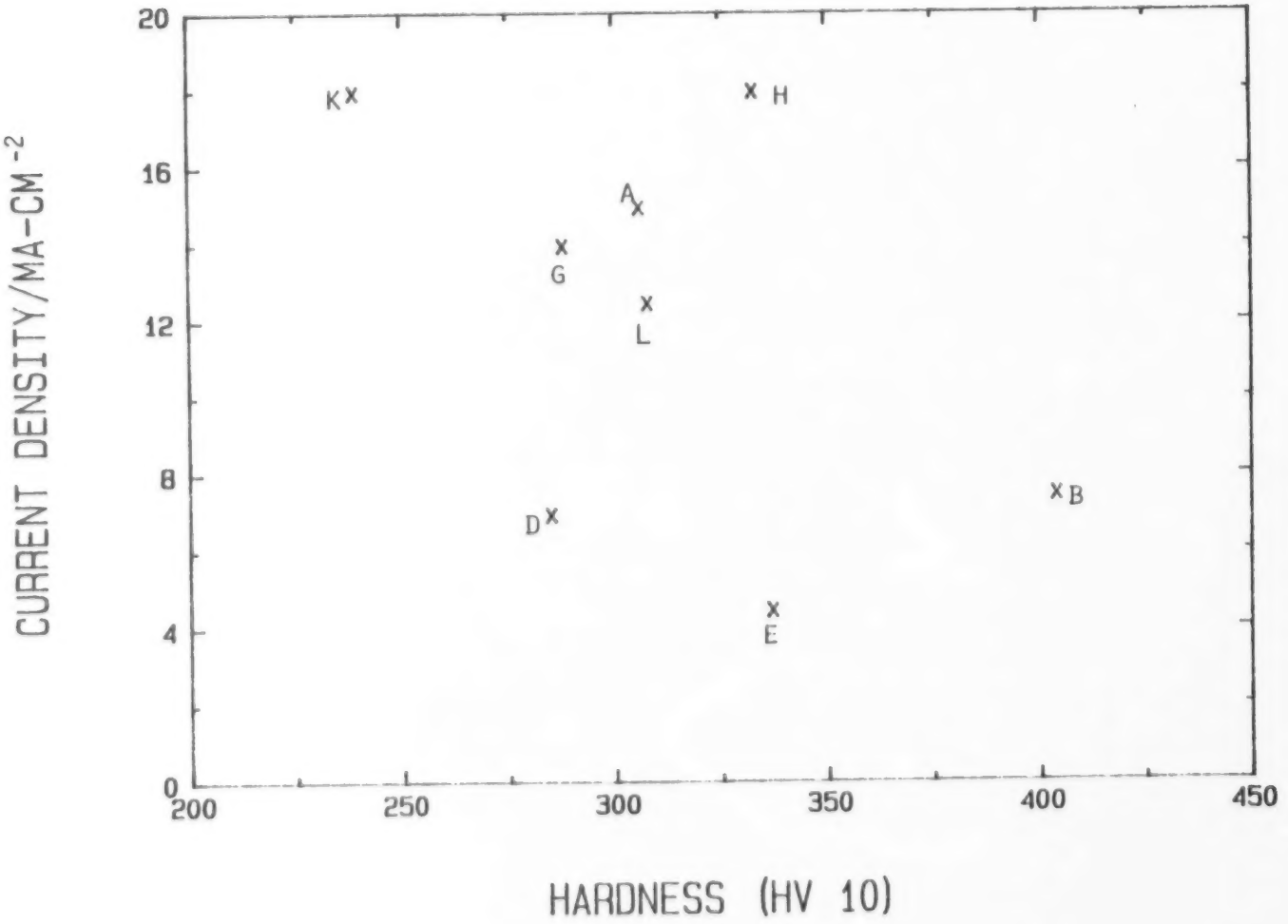

Figure 26: Current densities at -500 mV vs hardness of Gleeble simulated heat affected zones. Heat input 1.2 kJ/mm.

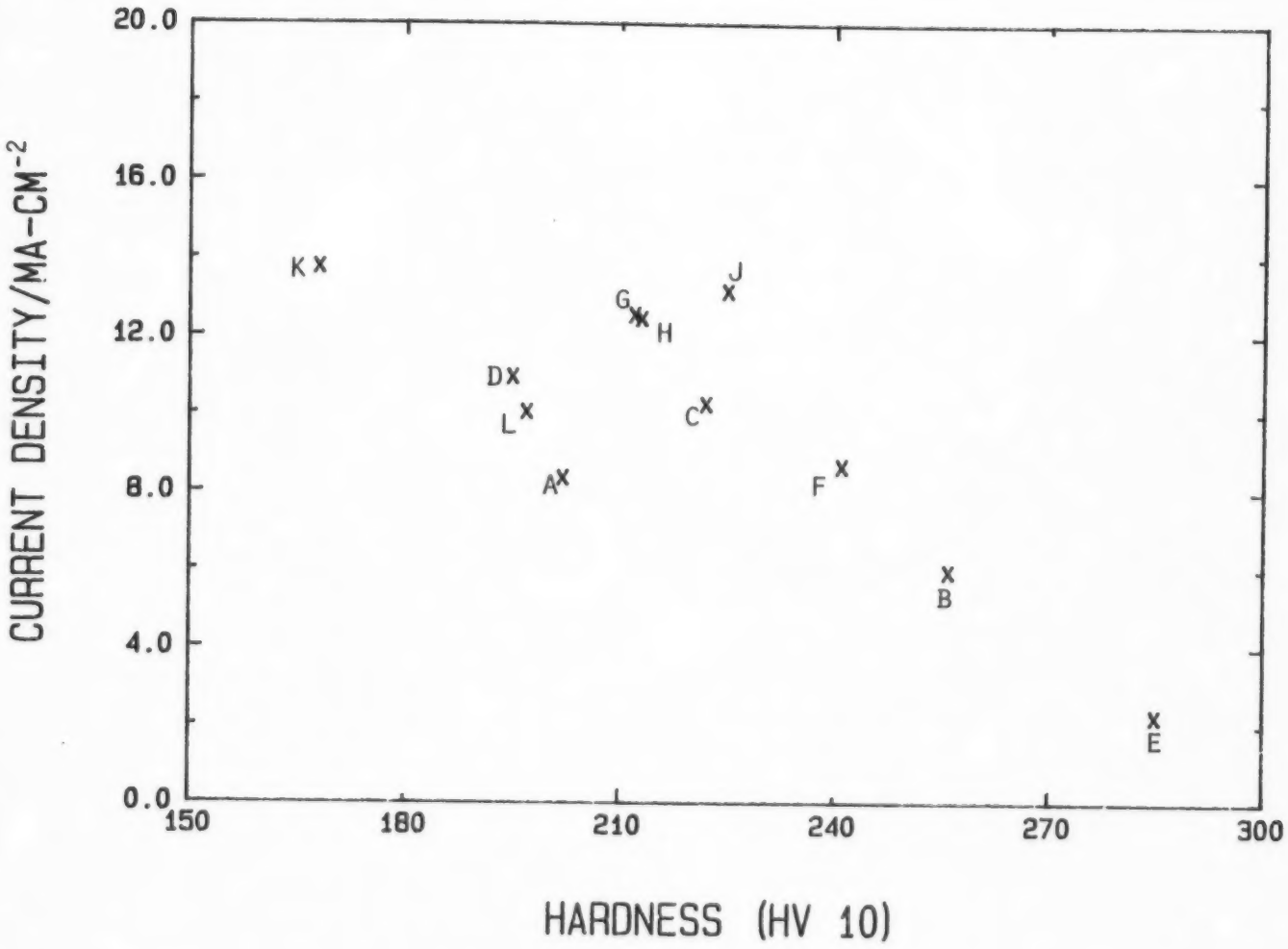

Figure 27: Current densities at -500 mV vs hardness of Gleeble simulated heat affected zones. Heat input 4.0 kJ/mm.

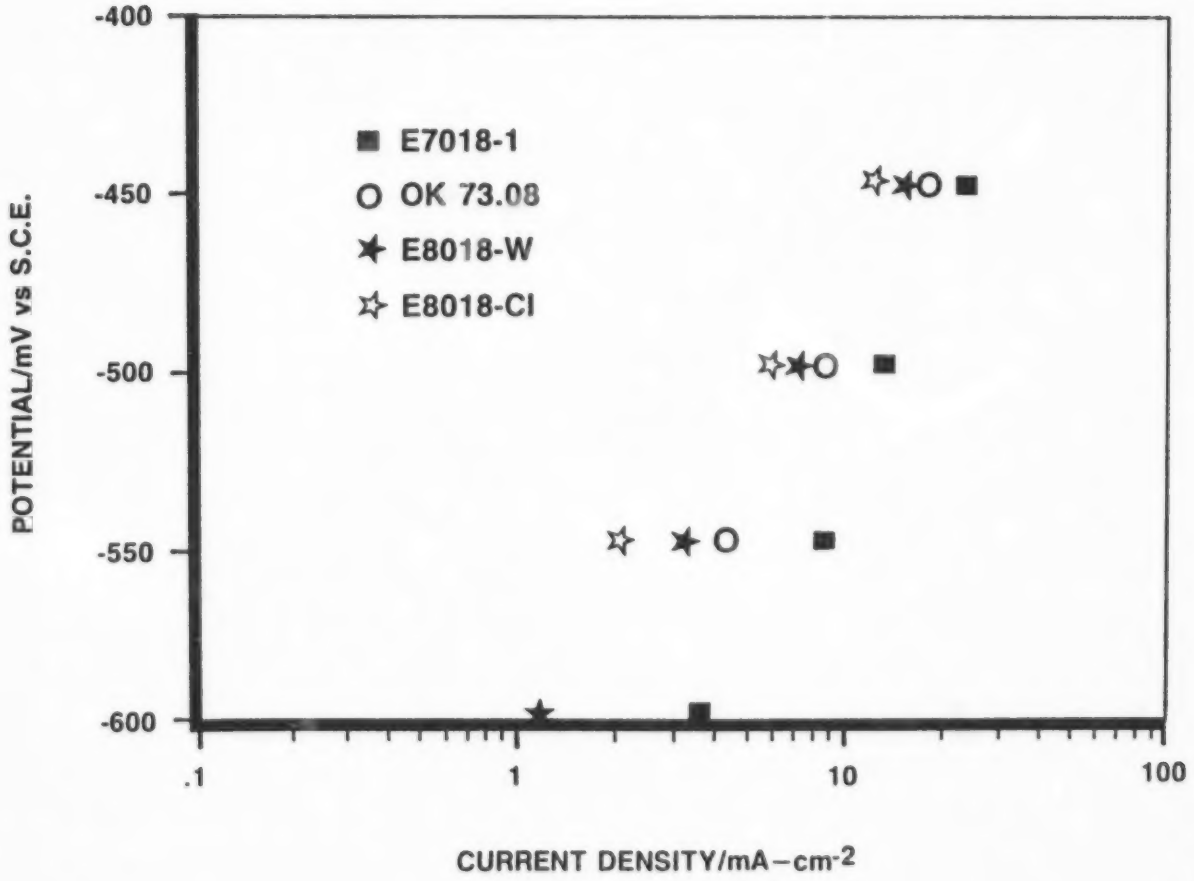

Figure 28: Potentiostatic anodic polarization curves for SMAW (Shielded Metal Arc Welding) consumables deposited at 1.2 kJ/mm.

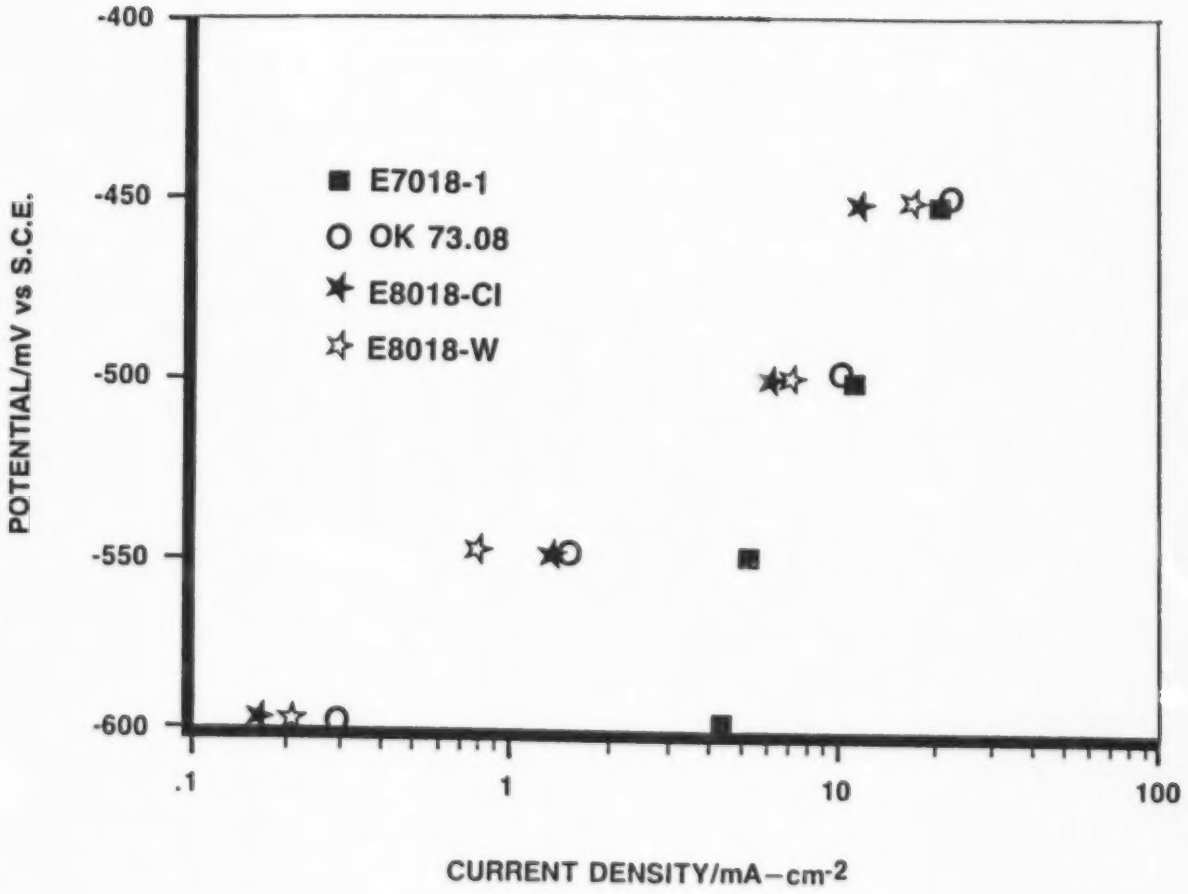

Figure 29: Potentiostatic anodic polarization curves for SMAW consumables deposited at 2.5 kJ/mm.

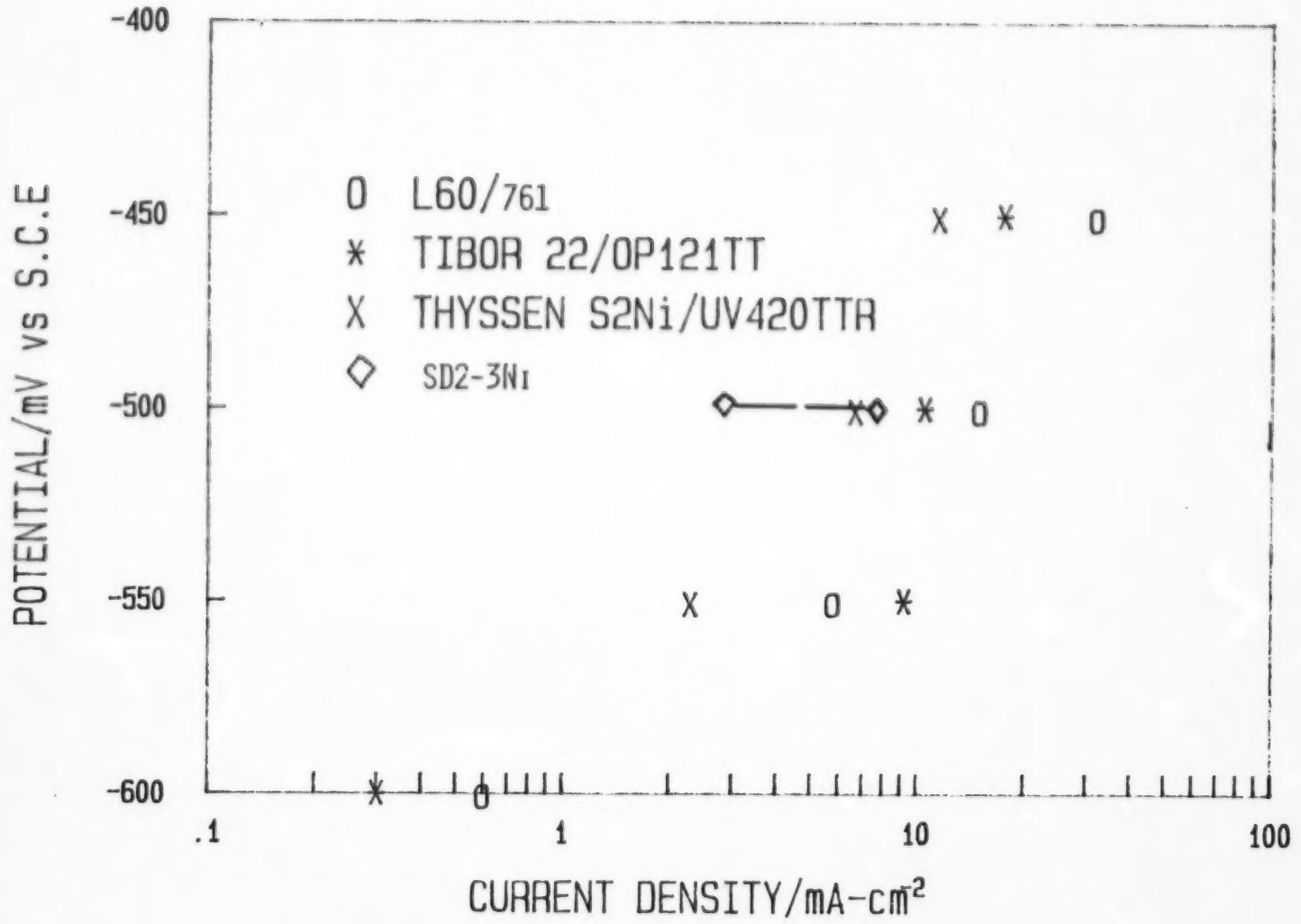

Figure 30: Potentiostatic anodic polarization curves for SAW consumables deposited at 2.5 kJ/mm.

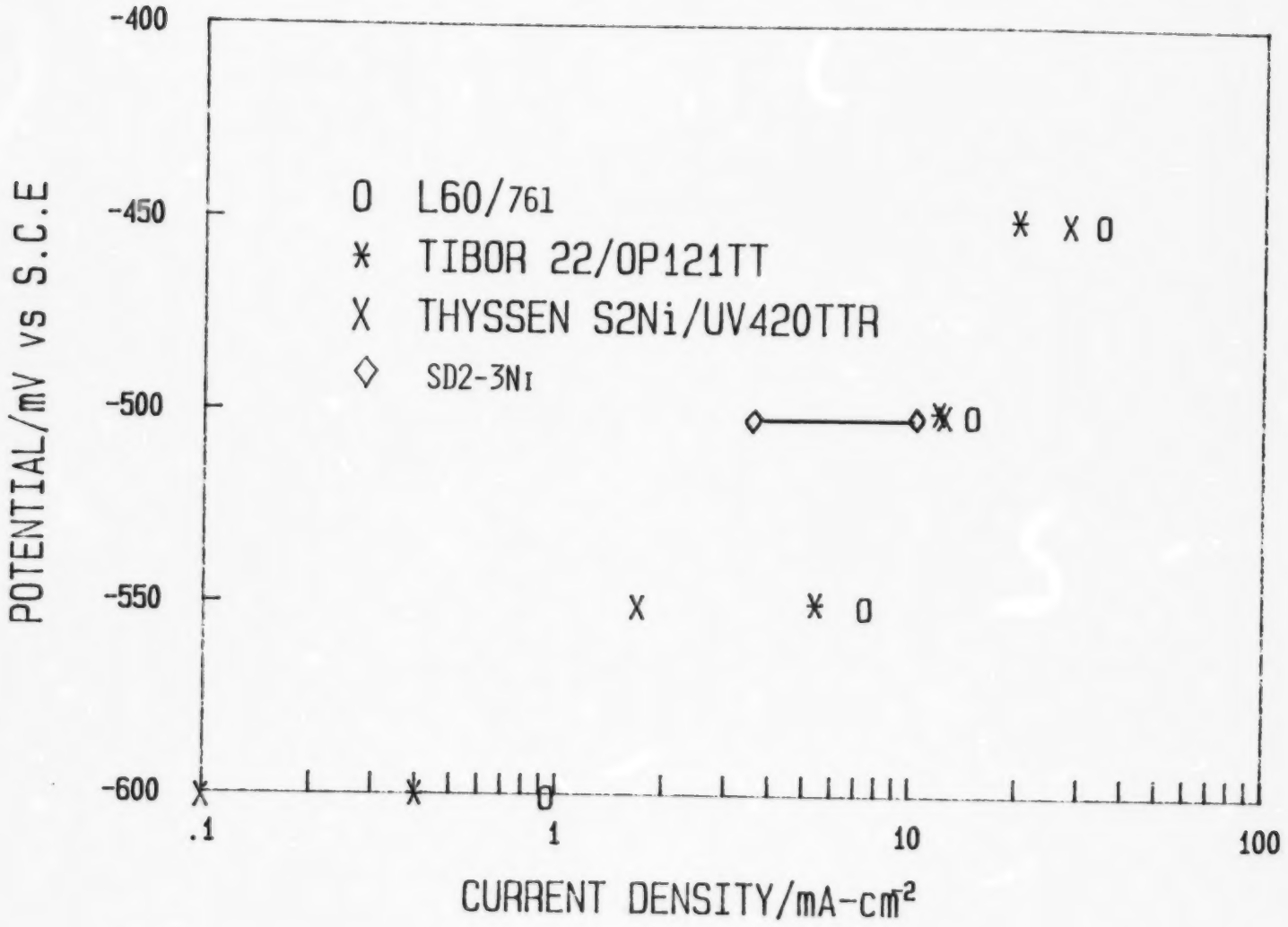

Figure 31: Potentiostatic anodic polarization curves for SMAW consumables deposited at 4.0 kJ/mm

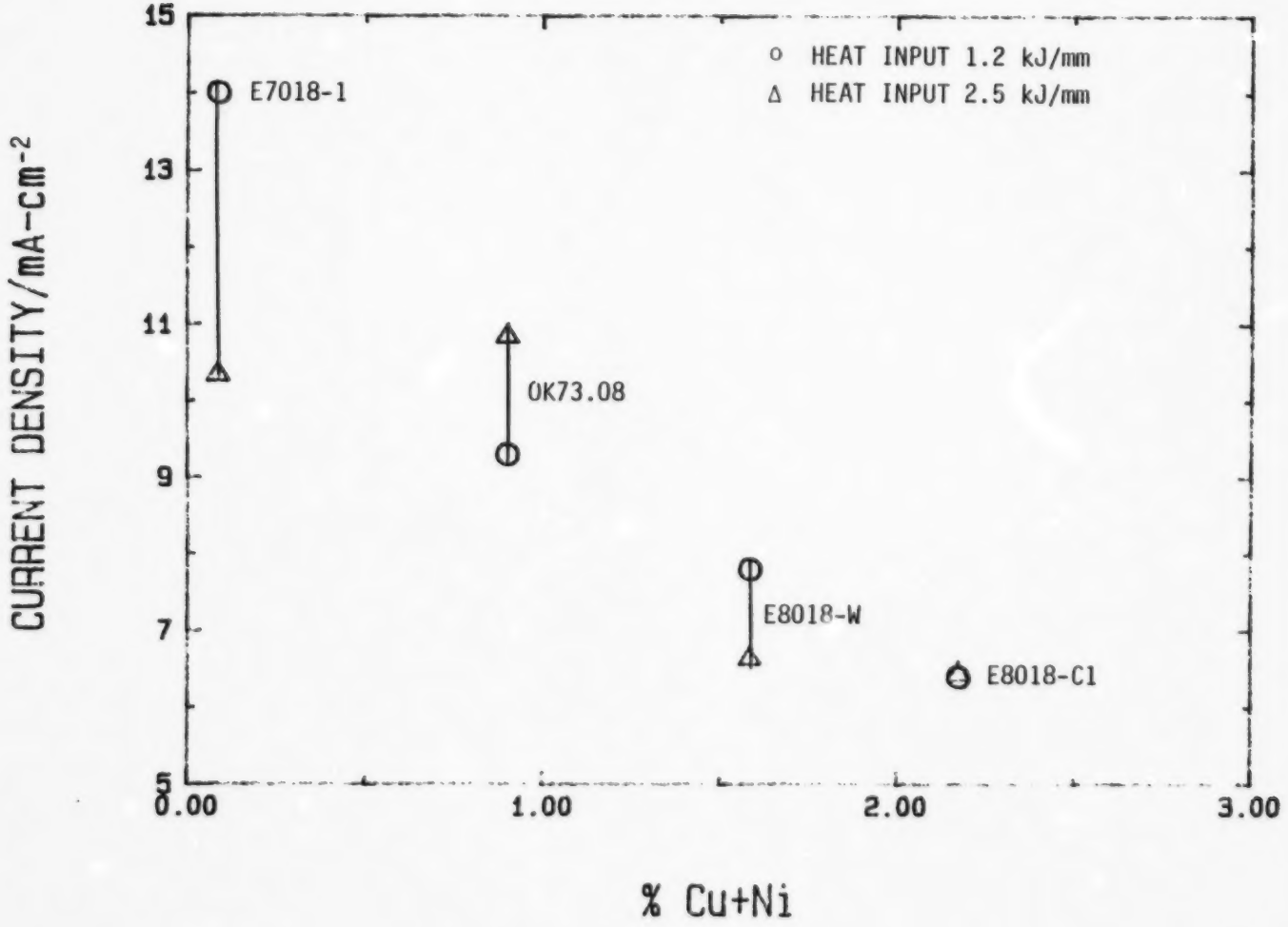

Figure 32: Current density at -500 mV vs %Cu+Ni plots for SAW consumables.

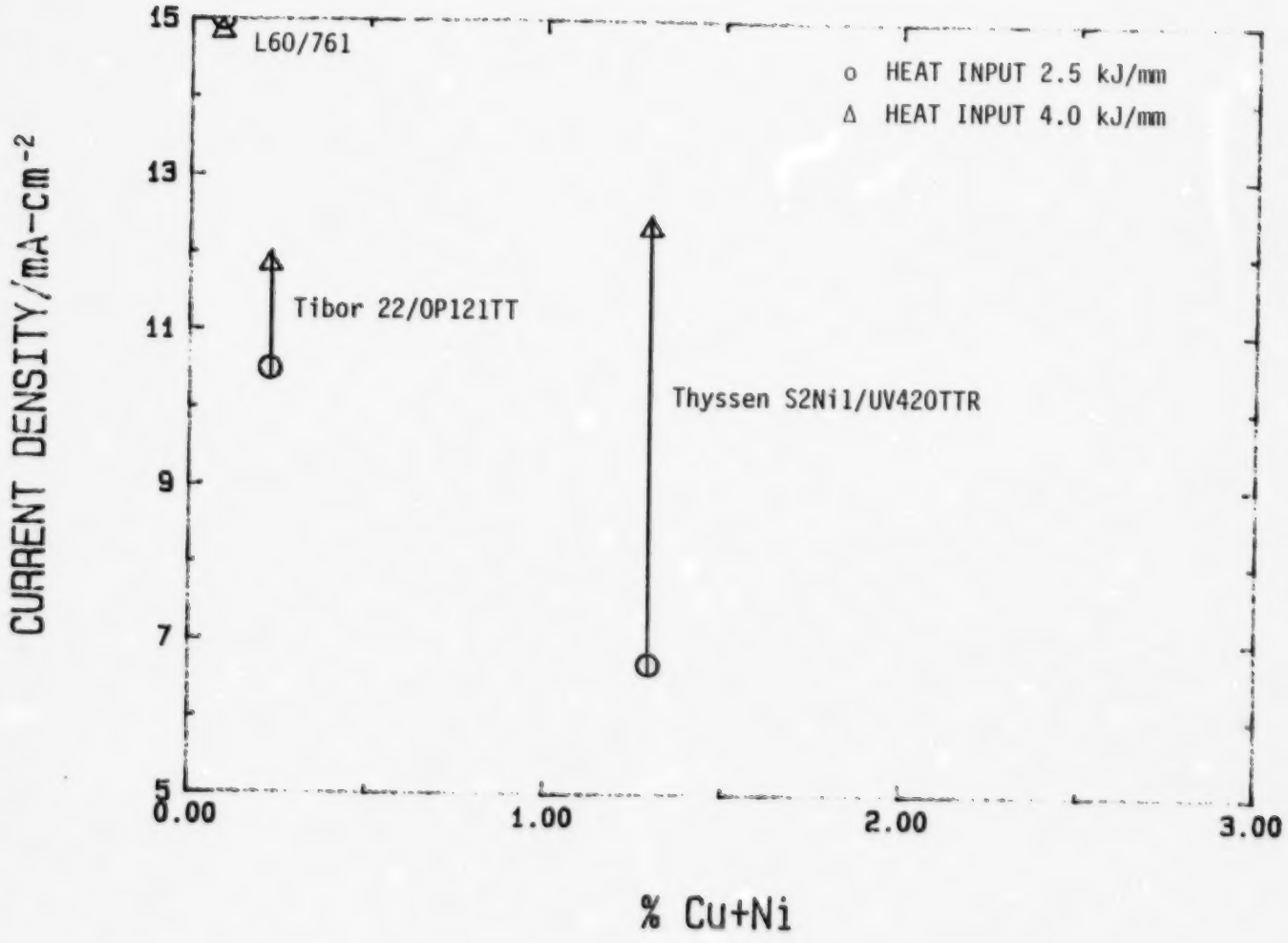

Figure 33: Current density at -500 mV vs %Cu+Ni plots for SAW consumables.

APPENDIX I

Table I: Depth of Weld Metal Attack

Table II: Depth of Heat Affected Zone Attack

APPENDIX I

TABLE I

DEPTH OF WELD METAL ATTACK - ANODIC DISSOLUTION TESTS ON BUTT WELDS

Anodic dissolution tests in stagnant 3.5% sodium chloride solutions exposed to air at room temperature. Current density - 0.88 mA/cm2.

Heat Inputs: 1) SMAW Consumables - Low (1) - 1.2 } kJ/mm
High (2) - 2.5 }

2) SAW Consumables - Low (1) - 2.5 } kJ/mm
High (2) - 4.0 }

Depths of attack exrpessed in μm.

Base Metal Steel	Code	SMAW								SAW							
		1		2		3		4		5		6		7		8	
		1	2	1	2	1	2	1	2	1	2	1	2	1	2	1	2
A710	E	520	460	920	860	<100			600	640	200			160			
ASTM A36	K	420	360	1110	840			260	120	430	650						
CSA G40.21 260WT	D			840	440					660	540						
CSA G40.21 350AT	B	260	240	740	300	140	40	200	180	780	300						
CSA G40.21 300W	A			460	300					720	620						
CSA G40.21 350WT	C			460	380					400	440						
Shoralsim 355Z	L			440	500					760							
Algoma LT60	F			760	780					260	300						
Stelco 350 WT	G			720	420					520							
Stelco	H			360	380					880	540						
Kawasaki EH36	J			660	400					760	780						

WELD METAL	OK73.08	7018-1	8018-C1	8018-W	L60/761	SD2-3Ni	Tibor22	Thyssen S2Ni1
Manganese	1.16	1.40	0.91	0.96	1.85	0.95	1.01	1.16
Silicon	0.37	0.37	0.31	0.38	1.12	0.27	0.17	0.22
Copper	0.35	0.04	0.03	0.19	0.07	0.09	0.17	0.04
Nickel	0.55	0.05	1.92	1.40	0.02	2.79	0.06	1.23
Molybdenum	-	-	0.01	0.03	-	0.11	0.24	-

APPENDIX I

TABLE II

DEPTH OF HEAT AFFECTED ZONE ATTACK - ANODIC DISSOLUTION TESTS ON BUTT WELDS

Conditions as in Table I of this Appendix.

Base Metal Steel	Code	Mn	SMAW								SAW							
		kJ/mm	1.2				2.5				2.5				4.0			
		Weld:	1	2	3	4	1	2	3	4	5	6	7	8	5	6	7	8
A710	E	0.54							< 100			100						
ASTM A36	K	0.75			160				160			120	160	110			50	20
CSA G40.21 260WT	D	1.01	< 100		140	180	120		160	220		100	100	100		100	100	100
CSA G40.21 350AT	B	1.08										100	< 100	< 100			< 100	
CSA G40.21 300W	A	1.10	240		280	80	160		120	80		80	100	120		60	60	
CSA G40.21 350WT	C	1.24	180		360	220	200		320	340		280	160			160	140	
Shoralsim 355Z	L	1.24	200		500	180			280			140	240	120				
Algoma LT60	F	1.39	360		400	180	400			400			340	500		100	300	
Stelco 350 WT	G	1.40	240		220	340	560		440	220		500	280	320		340	520	280
Stelco	H	1.40	380		480	240	100		500	400		500	260	340		180		240
Kawasaki EH36	J	1.45	500		540	500	400		560	380		320	460	380		260	240	380

APPENDIX II

Optical macrographs of the as-corroded transverse sections of previously machined ends of butt weld specimens after anodic dissolution

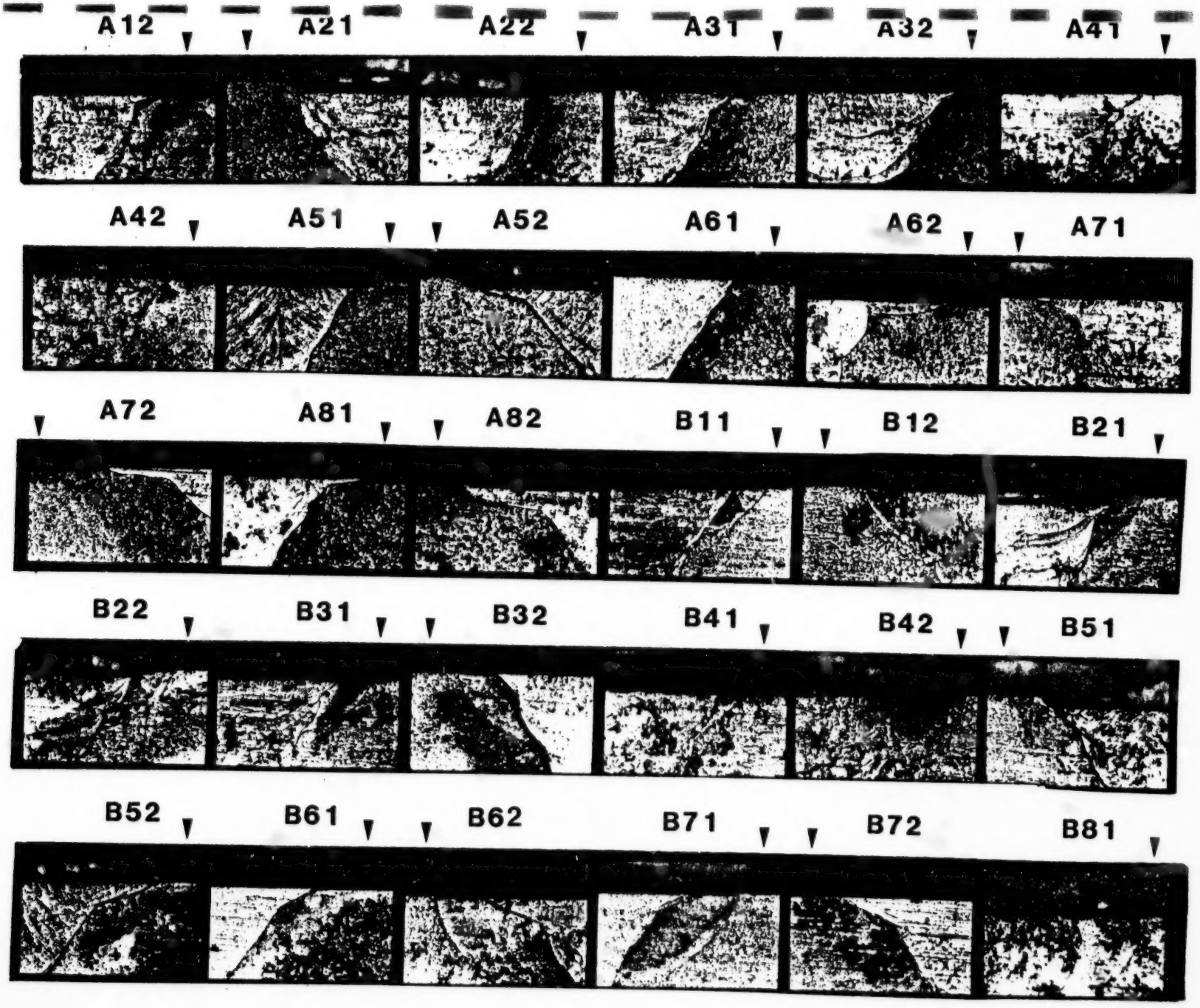
A12
A21
A22
A31
A32
A41
A42
A51
A52
A61
A62
A71
A72
A81
A82
B11
B12
B21
B22
B31
B32
B41
B42
B51
B52
B61
B62
B71
B72
B81

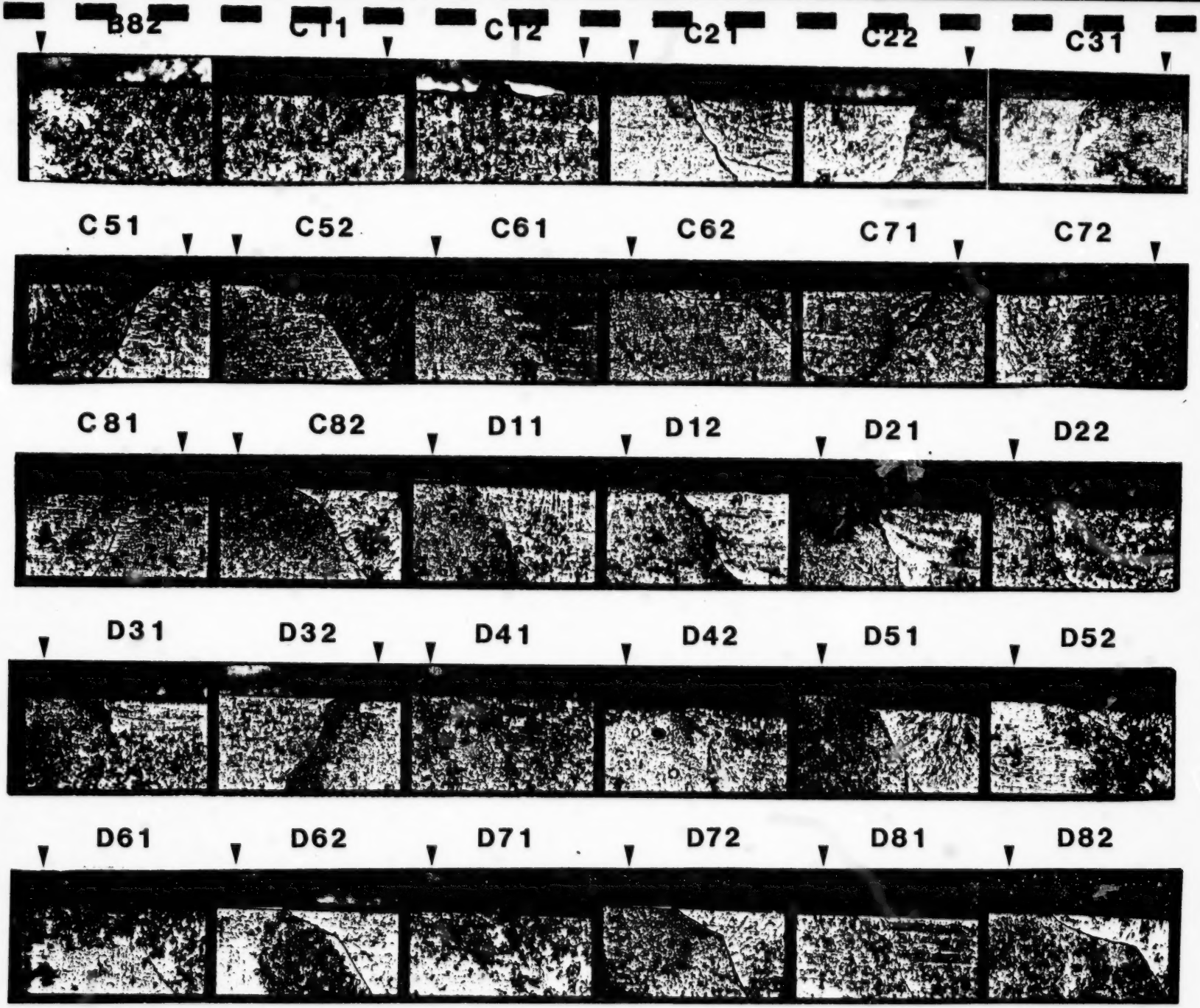
B82
C11
C12
C21
C22
C31
C51
C52
C61
C62
C71
C72
C81
C82
D11
D12
D21
D22
D31
D32
D41
D42
D51
D52
D61
D62
D71
D72
D81
D82

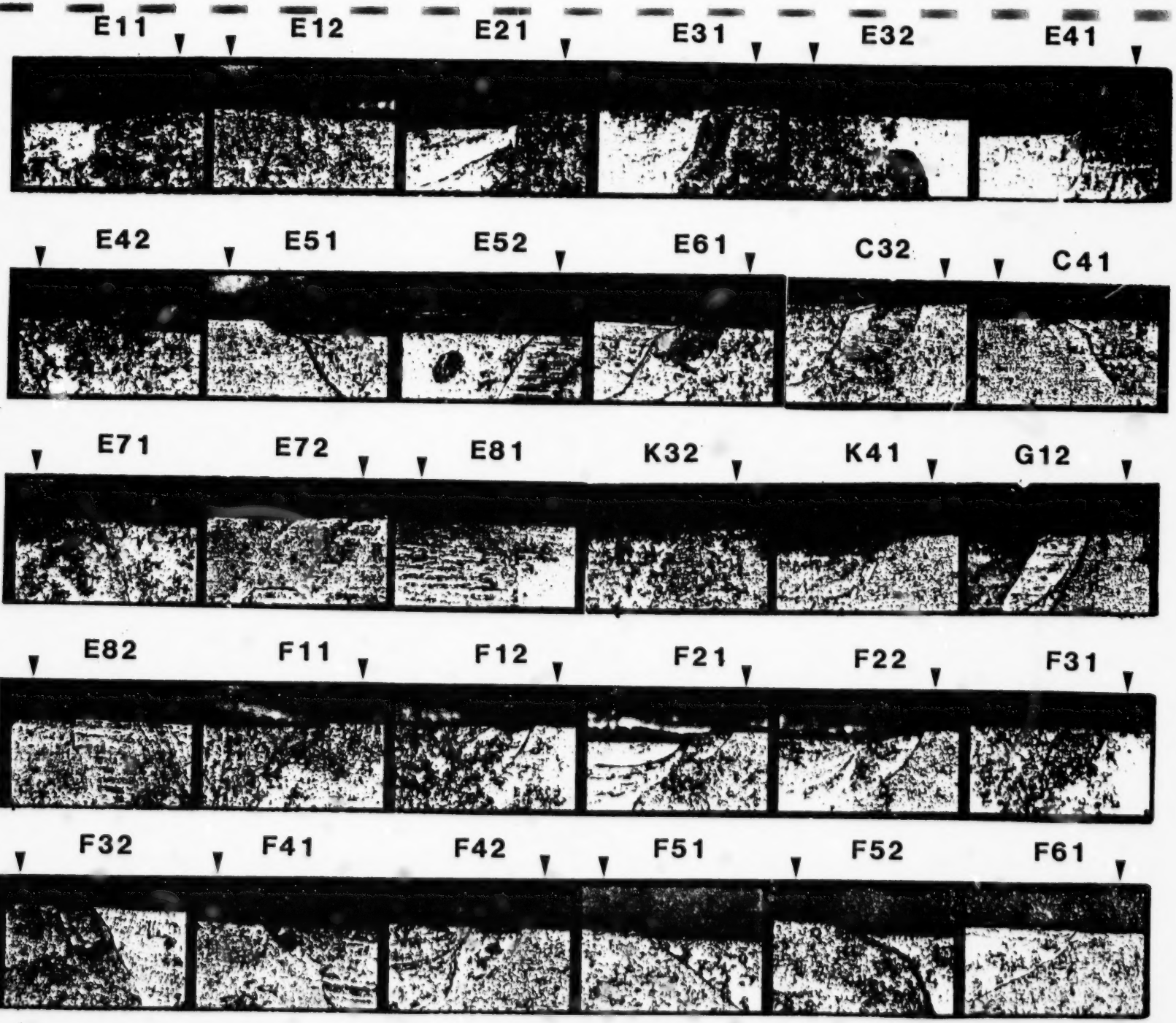
E11
E12
E21
E31
E32
E41
E42
E51
E52
E61
C32
C41
E71
E72
E81
K32
K41
G12
E82
F11
F12
F21
F22
F31
F32
F41
F42
F51
F52
F61

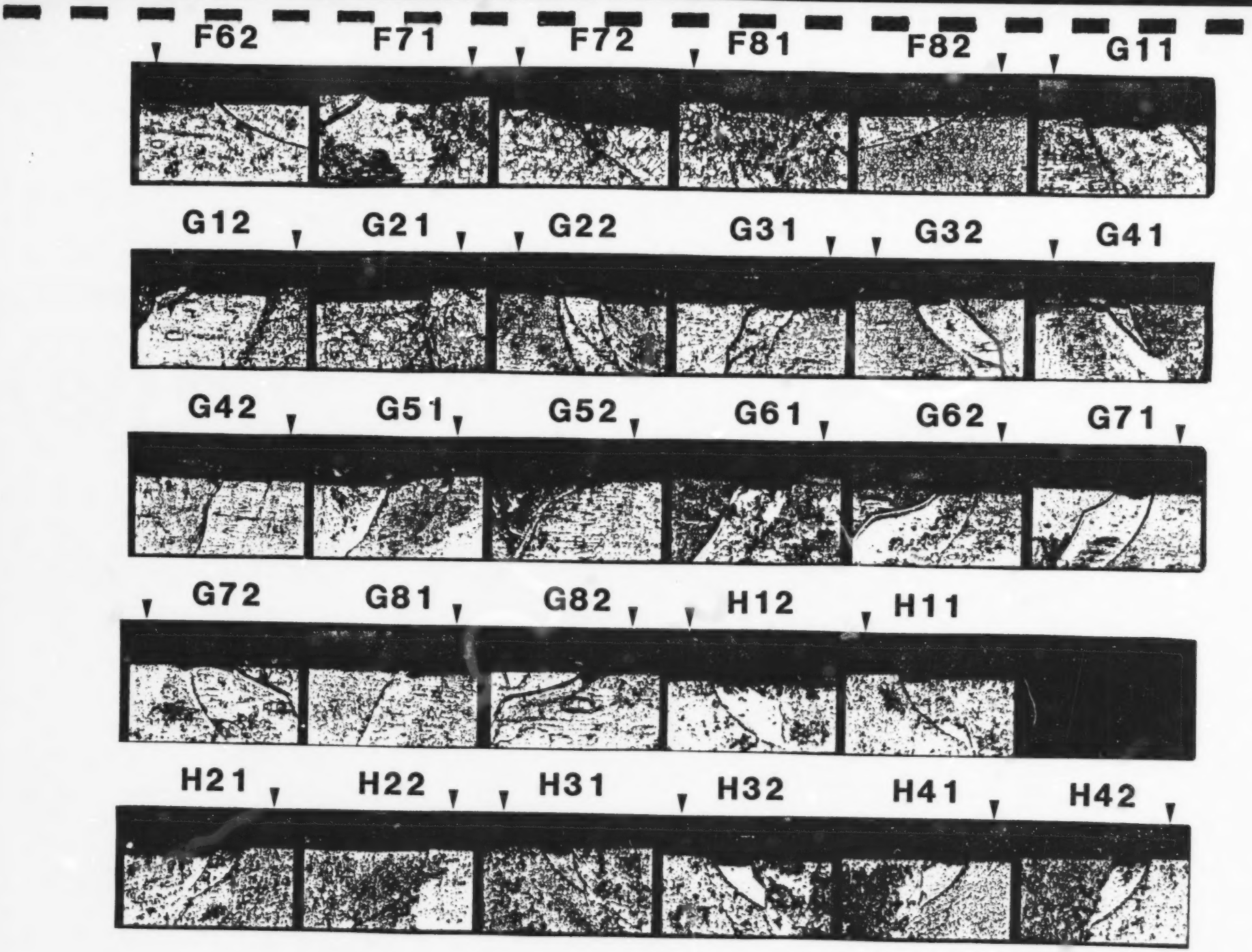
F62
F71
F72
F81
F82
G11
G12
G21
G22
G31
G32
G41
G42
G51
G52
G61
G62
G71
G72
G81
G82
H12
H11
H21
H22
H31
H32
H41
H42

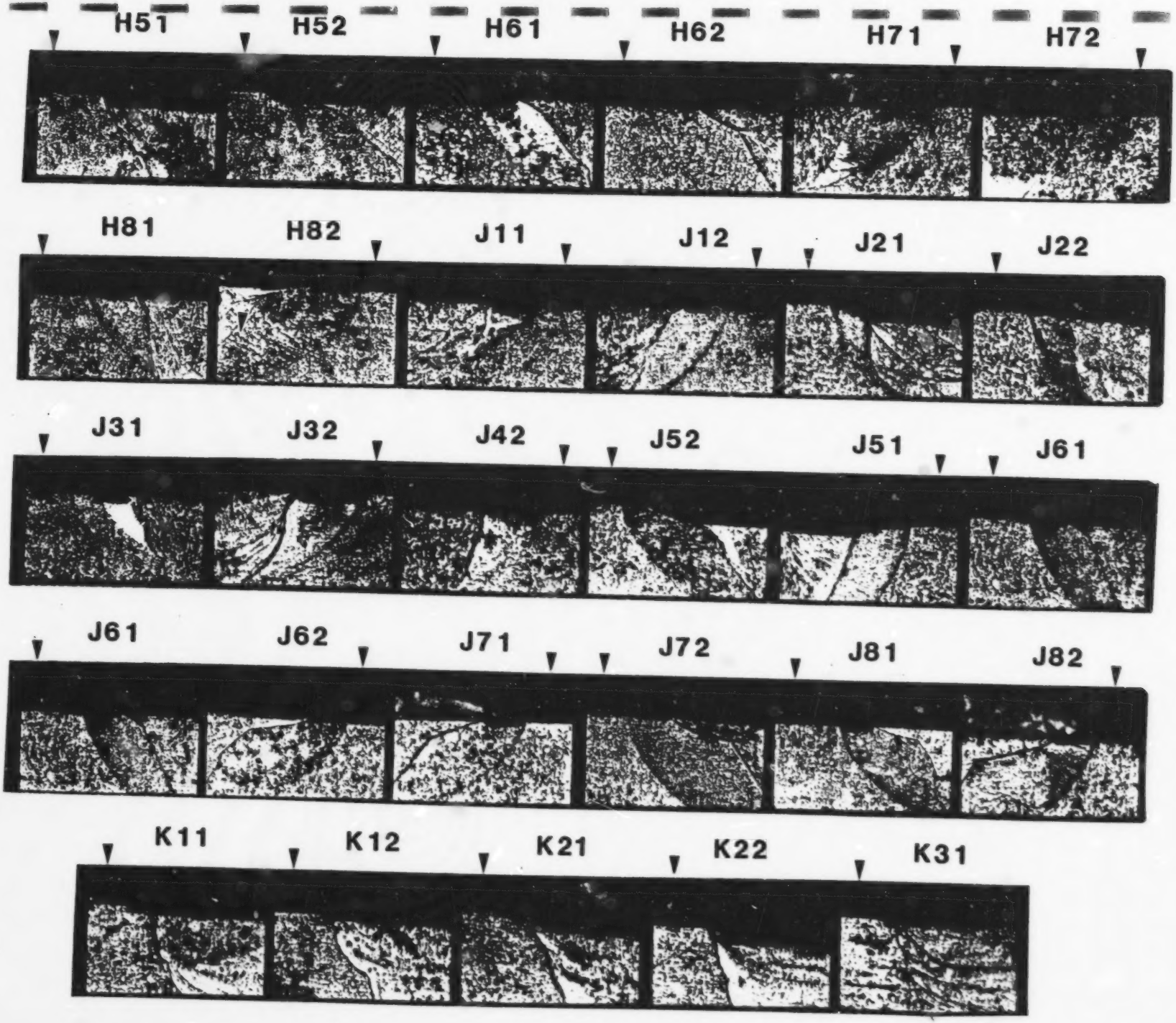
H51
H52
H61
H62
H71
H72
H81
H82
J11
J12
J21
J22
J31
J32
J42
J52
J51
J61
J61
J62
J71
J72
J81
J82
K11
K12
K21
K22
K31

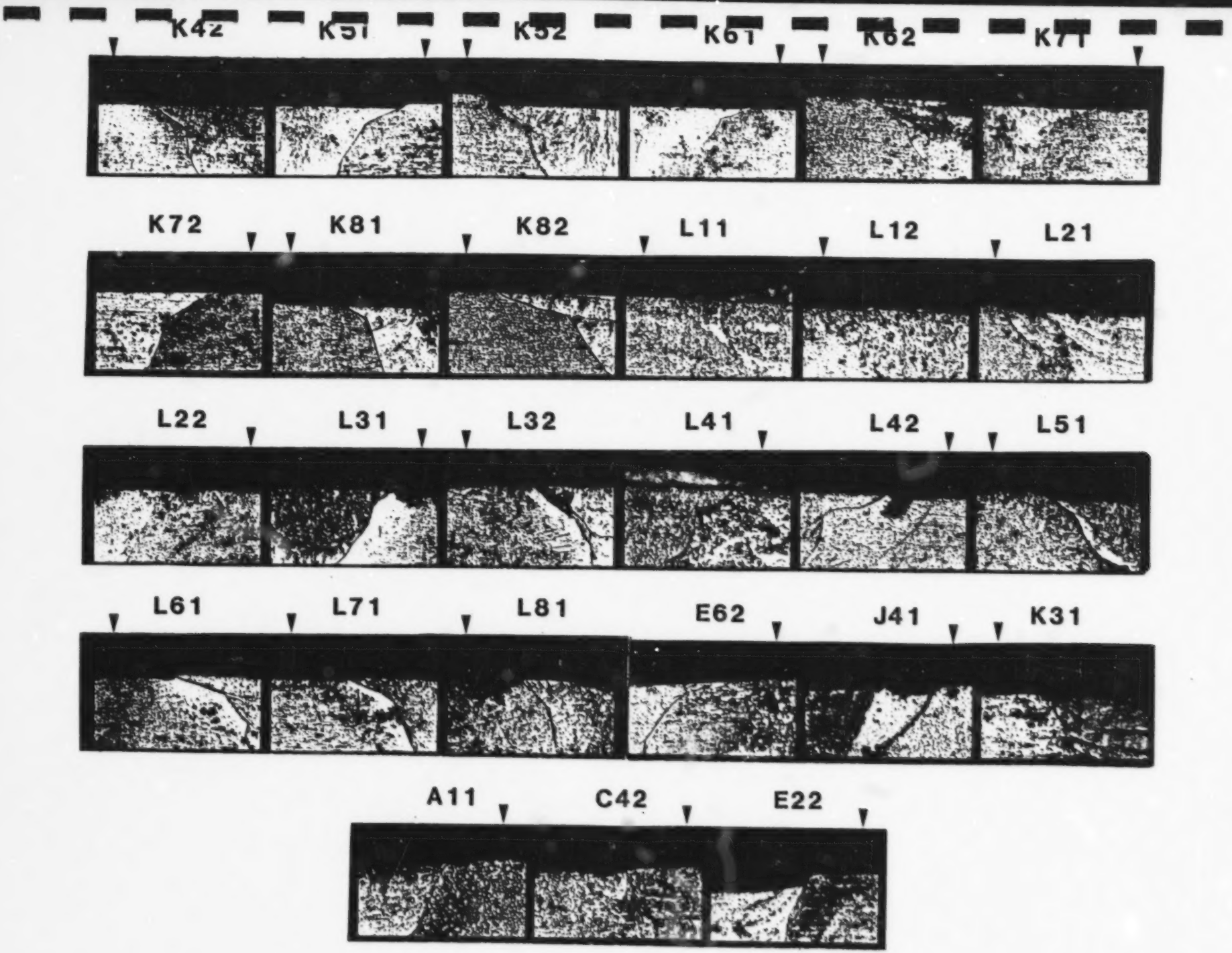
K42
K51
K52
K61
K62
K71
K72
K81
K82
L11
L12
L21
L22
L31
L32
L41
L42
L51
L61
L71
L81
E62
J41
K31
A11
C42
E22

APPENDIX III

A. Justification, method of regression analyses and results

B. Table showing current ratios, ΔMn, ΔSi, ΔCr, ΔCu, and ΔNi values at low and high heat inputs

C. Regression analyses plots - current ratio vs ΔMn, ΔSi, ΔCu, ΔNi and ΔCr at low and high heat inputs (two figures)

APPENDIX III

REGRESSION ANALYSES OF CURRENT RATIO DATA: POTENTIOSTATIC TESTS

A. Justification, Method of Regression Analyses and Results

As has been described in the introduction, initial attempts to reduce preferential corrosion of weld metal relied on alloying elements like Ni and Cu. When the problem shifted to the heat-affected zone, the focus changed to the level in the base plate as the key factor with the objective of specifying steel and weld metal chemistry such that both zones have matching corrosion resistance, and the probability of preferential corrosion is minimized, one needs to look at the two chemistries together.

The first effort in this direction was made by Inoue and his workers[9] who related the degree of preferential corrosion to difference in base plate and weld metal copper and nickel contents, and suggested the following empirical relationship:

$$\text{Degree of preferential corrosion} = 0.38 - 3.8\,(\Delta Cu) + 1.1\,(\Delta Ni) \qquad (1)$$

where ΔCu, ΔNi } difference of Cu or Ni between base-plate and weld metal

These authors did not state the level of correlation of this equation. Their corrosion assessments were rather qualitative, either by visual observations or a measurement of thickness at one location using a micrometer.

This equation was tested with present by plotting the current ratios vs 3.8 (ΔCu) + 1.1 (ΔNi) but the correlation was rather poor. With the desirability of the particular objective in mind, and inspite of the limited range in which certain elements were present, further attempts were continued by plotting the current ratio (R) data at low (R_I) and high (R_{II}) heat inputs vs ΔMn + ΔSi + ΔCr + ΔCu + ΔNi (where for example ΔMn = % Mn in base plate - % Mn in weld metal), and performing a multi-linear regression analysis. The current ratios of $R_{HAZ/WM}$ and ΔMn, ΔSi, ΔCr, ΔCu and ΔNi values shown in the table of this Appendix. At low and high heat inputs, the following empirical relationships with 70% correlation co-efficients were noted:

Low Heat Input

$$R^*_I = 1.14+0.03\ \Delta Mn+0.13\ \Delta Si-0.75\ \Delta Cr-0.19\ \Delta Cu-0.45\ \Delta Ni \qquad (2)$$

High Heat Input

$$R^*_{II} = 0.92+0.32\ \Delta Mn-0.24\ \Delta Si-0.12\ \Delta Cr+0.23\ \Delta Cu-0.27\ \Delta Ni \qquad (3)$$

(*High values of R imply HAZ corrosion in preference to weld metal corrosion).

Noting the obvious limitations of the data base for the regression analysis, the following can be inferred from these equations:

i) the intercepts i.e., 1.14 and 0.92 are marginally different in equations 5 and 6.

ii) for identical base plate and weld metal composition in regard to Mn, Si, Cu, Ni, Cr, the equations suggest slight HAZ corrosion at the low heat input, and slight weld metal corrosion at high heat input.

iii) for a given weld metal composition,

- increase in base plate Mn leads to increased HAZ preferential corrosion susceptibility.
- increase in base plate Ni and Cr contents lead to decrease in HAZ preferential corrosion susceptibility.
- the effect of Si and Cu are not uniform at the low and high heat inputs, and possibly confounded by the presence of Mo.
- the equations would also imply the same for weld metal preferential corrosion, given a constant base plate composition.

The above relationships are graphically shown in Figures 1 and 2 of this Appendix. A better relationship with high degree of reliability could be established only after thorough studies with base-plate and consumables having systematic, carefully controlled variations in chemical composition.

APPENDIX III

TABLE SHOWING CURRENT RATIOS, ΔMn, ΔSi, ΔCr, ΔCu AND ΔNi AT LOW AND HIGH HEAT INPUTS

PRIORITY	0	1	2	3	4	5	99
SET	I2	dMn	dSi	dCr	dCu	dNi	I1
73-08	0.31	-0.62	-0.08	0.635	0.85	0.34	0.48
7018	0.31	-0.86	-0.08	0.66	1.165	0.84	0.32
8018C1	0.52	-0.27	-0.01	0.675	1.174	-1.26	0.7
8018W	0.44	-0.42	-0.09	0.455	1.015	-0.51	0.58
L60/761	0.16	-1.31	-0.83	0.655	1.135	0.87	0.23
Tibor	0.19	-0.47	0.12	0.605	1.035	0.83	0.33
Thyssen	0.18	-0.62	0.07	0.665	1.135	-0.34	0.51
73-08	1.45	-0.41	-0.34	-0.055	-0.32	-0.53	1.93
7018	1.45	-0.65	-0.34	-0.03	-0.005	-0.03	1.29
8018C1	2.4	-0.06	-0.27	-0.015	0.004	-2.13	2.81
8018W	2.05	-0.21	-0.35	-0.235	-0.155	-1.38	2.31
L60/761	0.93	-1.1	-1.09	-0.035	-0.035	0	1.1
Tibor	1.13	-0.26	-0.14	-0.08	-0.135	-0.04	1.54
Thyssen	1.09	-0.41	-0.19	-0.025	-0.035	-1.21	2.4
73-08	0.81	-0.15	-0.14	-0.045	-0.34	-0.54	0.73
7018	0.81	-0.39	-0.14	-0.02	-0.025	-0.04	0.5
8018C1	1.35	0.2	-0.06	-0.005	-0.016	-2.14	1.09
8018W	1.14	0.05	-0.15	-0.225	-0.175	-1.39	0.9
L60/761	0.74	-0.84	-0.89	-0.025	-0.055	-0.01	0.6
Tibor	0.9	0	0.06	0.105	-0.155	-0.055	1.16
Thyssen	0.87	-0.15	0.01	-0.015	-0.055	-1.22	1.33
73-08	0.6	-0.08	-0.05	0.315	-0.05	0.02	0.81
7018	0.6	-0.32	-0.05	0.34	0.265	0.52	0.54
8018C1	1	0.27	0.02	0.355	0.274	-1.58	1.17
8018W	0.85	0.12	-0.06	0.135	0.115	-0.83	0.96
L60/761	0.41	-0.77	-0.8	0.335	0.235	0.55	0.44
Tibor	0.49	0.07	0.15	0.285	0.135	0.51	0.63
Thyssen	0.47	-0.08	0.1	0.345	0.235	-0.66	0.99
73-08	1.1	-0.06	-0.18	-0.055	-0.34	-0.54	1.61
7018	1.1	-0.3	-0.18	-0.03	-0.025	-0.04	1.07
8018C1	1.82	0.29	-0.11	-0.015	-0.016	-2.14	2.34
8018W	1.54	0.14	-0.19	-0.235	-0.175	-1.39	1.92
L60/761	0.57	-0.75	-0.93	-0.035	-0.055	-0.01	1.2
Tibor	0.69	0.09	0.02	-0.085	-0.155	-0.05	1.15
Thyssen	0.66	-0.06	-0.03	-0.025	-0.055	-1.22	1.79
73-08	1.12	0.08	-0.14	-0.025	-0.3	-0.48	1.51
7018	1.12	-0.16	-0.14	0	0.015	0.02	1
8018C1	1.86	0.43	-0.06	0.015	0.024	-2.08	2.19
8018W	1.58	0.28	-0.15	-0.205	-0.135	-1.33	1.78
L60/761	0.7	-0.61	-0.89	-0.005	-0.015	0.05	0.82
Tibor	0.84	0.23	0.06	-0.055	-0.115	0.01	1.18
Thyssen	0.81	0.08	0.01	0.005	-0.015	-1.16	1.84
73-08	1.04	0.08	0.05	0.015	-0.053	-0.386	1.34
7018	1.04	-0.16	0.05	0.04	0.262	0.114	0.89
8018C1	1.73	0.43	0.12	0.055	0.271	-1.986	1.95
8018W	1.46	0.28	0.04	-0.165	0.112	-1.236	1.54
L60/761	0.68	-0.61	-0.7	0.035	0.232	0.144	0.74
Tibor	0.83	0.23	0.25	-0.015	0.132	0.104	1.07
Thyssen	0.8	0.08	0.2	0.045	0.232	-1.066	1.66

Current ratios at low and high heat inputs are low I(1) and high I(2). Heat inputs - low 1.2 (SMAW) and 2.5 (SAW) kJ/mm; high 2.5 (SMAW) and 4.0 (SAW) kJ/mm.

APPENDIX III - TABLE CONTINUED

73-08	0.93	0.23	-0.09	0.105	-0.2	-0.4	1.24
7018	0.93	-0.01	-0.09	0.13	0.115	0.1	0.82
8018C1	1.55	0.58	-0.02	0.145	0.124	-2	1.8
8018W	1.31	0.43	-0.1	-0.075	-0.035	-1.25	1.47
L60/761	0.59	-0.46	-0.84	0.125	0.085	0.13	0.68
Tibor	0.71	0.38	0.11	0.075	-0.015	0.09	0.98
Thyssen	0.69	0.23	0.06	0.135	0.085	-1.08	1.52
73-08	1.2	0.24	-0.08	-0.065	-0.1	-0.3	1.51
7018	1.2	0	-0.08	-0.04	0.215	0.2	1
8018C1	2	0.59	-0.01	-0.025	0.224	-1.9	2.19
8018W	1.69	0.44	-0.09	-0.245	0.065	-1.15	1.79
L60/761	0.85	-0.45	-0.83	-0.045	0.185	0.23	0.88
Tibor	1.03	0.39	0.12	-0.095	0.085	0.19	1.27
Thyssen	1	0.24	0.07	-0.035	0.185	-0.98	1.97
73-08	1.41	0.24	-0.08	-0.065	-0.35	-0.28	1.94
7018	1.41	0	-0.08	-0.04	-0.035	0.22	1.29
8018C1	2.35	0.59	-0.01	-0.025	-0.026	-1.88	2.81
8018W	1.99	0.44	-0.09	-0.245	-0.185	-1.13	2.31
L60/761	0.82	-0.45	-0.83	-0.045	-0.065	0.25	1.03
Tibor	0.99	0.39	0.12	-0.095	-0.165	0.21	1.49
Thyssen	0.95	0.24	0.07	-0.035	-0.065	-0.96	2.31
73-08	1.13	0.29	0.08	-0.055	-0.21	-0.53	1.34
7018	1.13	0.05	0.08	-0.03	0.015	-0.03	0.86
8018C1	1.88	0.64	0.15	-0.015	0.114	-2.13	1.88
8018W	1.59	0.39	0.07	-0.235	-0.045	-1.38	1.54
L60/761	0.93	-0.4	-0.67	-0.035	0.075	0	0.83
Tibor	1.13	0.44	0.28	-0.08	-0.025	-0.04	1.19
Thyssen	1.09	0.29	0.23	-0.025	0.075	-1.21	1.85

Regression Output: **Current Ratios at Low Heat Input**

Constant	1.1420460
Std Err of Y Est	0.3510644
R Squared	0.6837023
No. of Observations	77
Degrees of Freedom	71

X Coefficient(s) 0.032226 0.1257828 -0.75044 -0.19038 -0.43534 0.118398

Regression Output: **Current Ratios at High Heat Input**

Constant	0.9238669
Std Err of Y Est	0.2825580
R Squared	0.6950597
No. of Observations	77
Degrees of Freedom	71

X Coefficient(s) 0.315420 -0.239639 -1.12573 0.228945 -0.26832 0.118398

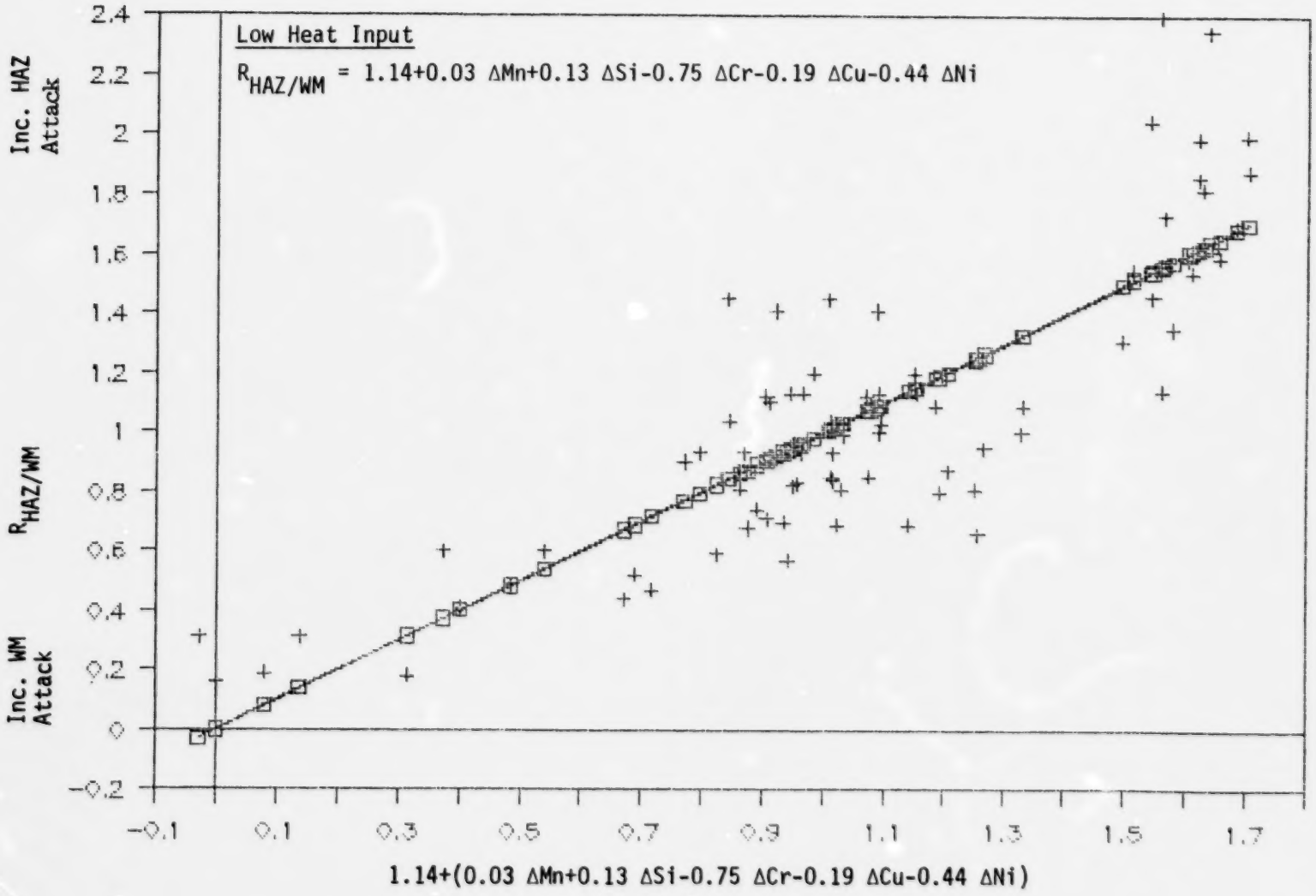
Low Heat Input
$R_{HAZ/WM}$ = 1.14+0.03 ΔMn+0.13 ΔSi-0.75 ΔCr-0.19 ΔCu-0.44 ΔNi
Inc. HAZ Attack
$R_{HAZ/WM}$
Inc. WM Attack
2.4
2.2
2
1.8
1.6
1.4
1.2
1
0.8
0.6
0.4
0.2
0
-0.2
-0.1
0.1
0.3
0.5
0.7
0.9
1.1
1.3
1.5
1.7
1.14+(0.03 ΔMn+0.13 ΔSi-0.75 ΔCr-0.19 ΔCu-0.44 ΔNi)

Figure 1

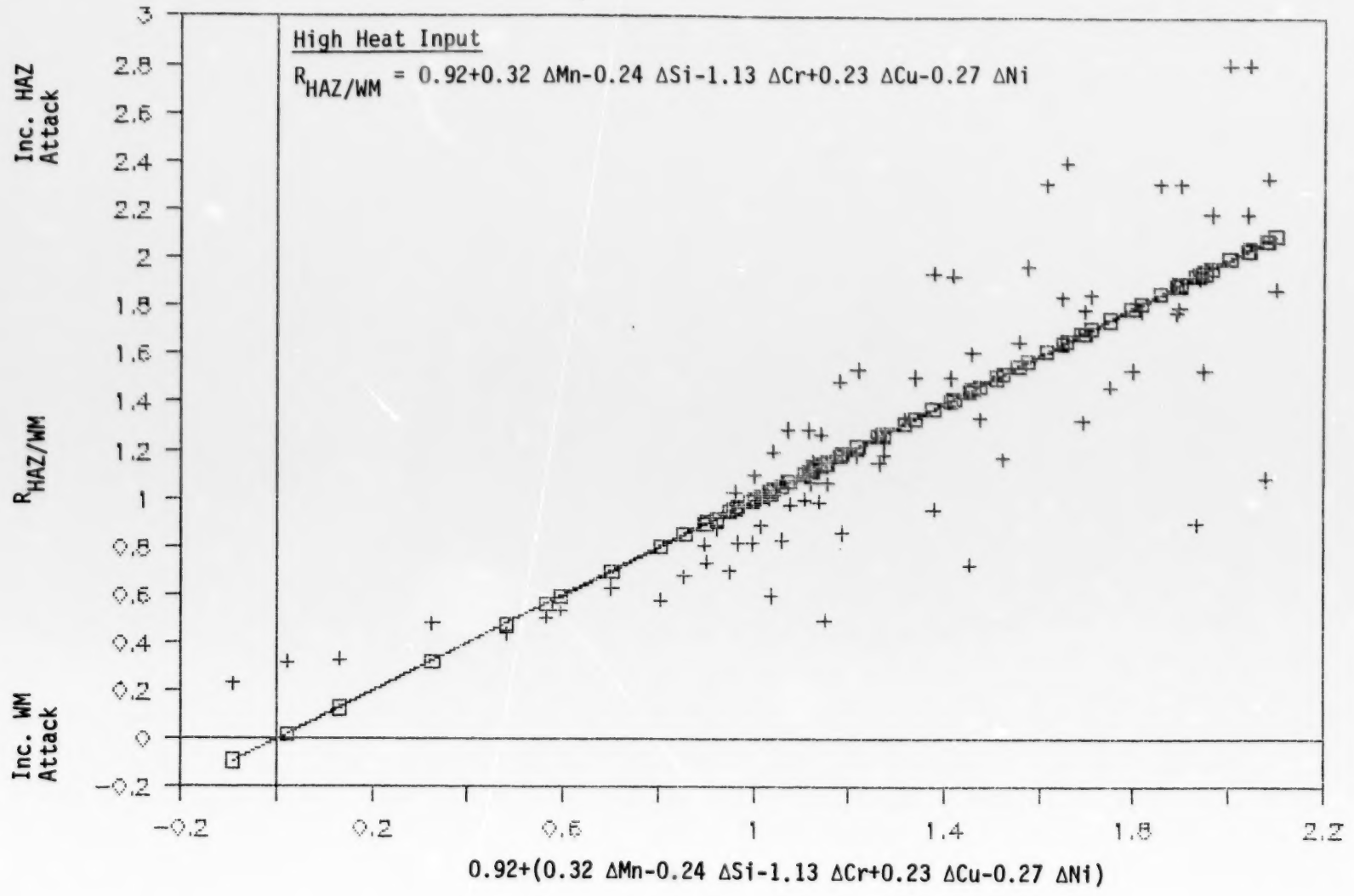
High Heat Input
$R_{HAZ/WM}$ = 0.92+0.32 ΔMn-0.24 ΔSi-1.13 ΔCr+0.23 ΔCu-0.27 ΔNi
Inc. HAZ Attack
Inc. WM Attack
$R_{HAZ/WM}$
3
2.8
2.6
2.4
2.2
2
1.8
1.6
1.4
1.2
1
0.8
0.6
0.4
0.2
0
-0.2
-0.2
0.2
0.6
1
1.4
1.8
2.2
0.92+(0.32 ΔMn-0.24 ΔSi-1.13 ΔCr+0.23 ΔCu-0.27 ΔNi)

Figure 2